Department of Chemical Engineering

Multi-scale Modelling and Optimization Study on the Thermal Management of SOFC

Shi Tang

This thesis is presented for the Degree of
Doctor of Philosophy
of
Curtin University

August 2016

Declaration

To the best of my knowledge and belief this thesis contains no material previously published by any other person except where due acknowledgement has been made.

This thesis contains no material which has been accepted for the award of any other degree or diploma in any university.

Acknowledgements

I would like to express my thanks to my supervisor, Prof. Moses O.Tade, for supporting me to complete this thesis throughout my PhD program, who gave me great expertise, patience, and understanding. Without his encouragement and guidance, this work is impossible to be completed.

In particular, I would like to thank my co-supervisor, Dr. Amirpiran Amiri, who has made numerous valuable comments on my studies, provided professional feedbacks toward problems in my research, and gave me patient guidance in technical writing. I would like to extend my thanks to my co-supervisor, Dr. Periasamy Vijay, for his support and advice throughout my candidature. I would like to express my thanks to our research group member, Mike Akpughe, who provided me the supports for experimental data.

My special thanks go to China Scholarship Council (CSC) and Curtin International Postgraduate Research Scholarship (CIPRS), who provide scholarship and support this research work.

I would also like to thank my dear family and friends for their love, support and encouragement throughout the years

Abstract

SOFC (Solid Oxide Fuel Cell) is considered as a promising technology to resolve the current limitation of energy sources and environmental pollution problems. However, it still faces the challenges for practical applications and commercialization. In this area, the thermal management is one of the critical problems that need more efforts for debottlenecking and enhancement. To overcome the mentioned challenges, a deeper understanding of the thermal behavior of the SOFC is essential. This can be achieved through rigorous mathematical modelling and numerical simulations. Due to the wide spectrum of time and length scales of predominant phenomena involved in SOFC process, this thesis employs the multi-scale modelling and optimization approach to study the thermal behavior of the SOFC stack and propose effective thermal management strategies for the SOFC.

A cell level model for a multi-layer SOFC surrounded by a constant temperature furnace is presented based on TSR (tank-in-series reactor) methodology, which offers salient features such as simplicity and flexibility, in addition to reliability. A set of V-I characteristics data is used for parameter adjustment followed by model verification against two independent sets of data. The Model results show a good agreement with practical data, offering a significant improvement compared to reduced models. This model is found to be flexible enough to simulate the distributed thermal behaviors in the multi-layer structure that is basic for the further thermal management analysis. Besides, the distributed thermal behavior analysis within the multi-later structure is carried out, which gives better insights for the thermal management purpose.

The validated numerical model described above is integrated and extended to the stack level to allow further studies at commercial scale. The current study explores the effects of operating variables on the temperature gradient in a multi-layer SOFC

stack and presents a trade-off optimization. Three promising approaches were numerically tested via a model-based sensitivity analysis. Initially, usage of the excess air is critically assessed, while large efficiency reducing will be induced. Subsequently, the adjustment of inlet gas temperatures is introduced as a complementary methodology to reduce the efficiency loss due to application of excess air. The last approach, regulation of the oxygen fraction in the cathode coolant stream, as a strategy to reduce the negative effect of excess air with enhancing the stack efficiency, is examined from both technical and economic viewpoints. The advantages and disadvantages of each approach are presented through the above analysis, while the potential feature achieved by combining them is also showed. Finally, a multi-objective optimization calculation is conducted to find an operating condition in which the efficiency and temperature gradient of the stack are maximum and minimum, respectively.

Since SOFC is a device that would be applied in an integrated plant, the thermal analysis was extended to the SOFC system to further seek the challenges and opportunities for thermal management goals. The exergy evaluation was emphasised to evaluate the influence of various strategies on system performance. Temperature profiles as well as thermal, electrical and total efficiencies were estimated for each analysis. In order to conduct this analysis at plant scale initially, the analysis was carried out via a simple flowsheet approach presented in literature. Since different criteria, associated with different levels of SOFC system, must be met simultaneously for the thermal management purposes, a more detailed system model was also used to overcome the limitation of the simple system model. This model offers distributed profiles inside stack along with plant-wide mass and energy balances. Four tactics, including excess air flowrate, oxygen concentration in cathode inlet, anode off-gas recycling, and cathode off-gas recycling, were tested. The effects of each tactic on the exergy losses are also assessed. None of these strategies offers

perfect results for thermal management in all levels. Each one has positive and negative sides that are discussed in details.

In conclusion, this study proposed a validated multi-layer model which is adequate for the thermal management study inside the cell/ stack, based on which, the deeper insights are provided for the thermal management purpose. The parametrical sensitive analysis and the multi-objective optimization conducted on stack level provide the potential solutions for the improved thermal management of SOFC. Finally, the study concerning SOFC thermal behaviors in different levels is conducted. Based on the study, system operating conditions for the improved thermal management of SOFC system in multi-scale can be proposed.

Publications of this thesis

1. **S. Tang**, A. Amiri, P. Vijay, M.O. Tadé, Development and validation of a computationally epicient pseudo 3D model for planar SOFC integrated with a heating furnace, Chemical Engineering Journal 290 (2016) 252-262.

2. A. Amiri*, **S. Tang***, P. Vijay, M.O. Tadé, Planar Solid Oxide Fuel Cell Modeling and Optimization Targeting the Stack's Temperature Gradient Minimization, Industrial & Engineering Chemistry Research 55 (2016) 7446-7455.) . Copyright (2016) American Chemical Society

*: **Co-first Author**

3. Poster Presentation:

S. Tang, A. Amiri P. Vijay, M.O. Tadé, Thermal Management Study of Planar SOFC by a Computational Approach, at EMN meeting on fuel cells, Energy Materials Nanotechnology, 23-27 May, 2016, Jeju, South Korea

Table of Content

Declaration I

Acknowledgements II

Abstract III

Publications of this thesis VI

List of Tables..... XI

List of Figures..... XIII

Chapter 1

Introduction

1.1 Background and motivation.....2

1.1.1 Significance of fuel cell 2

1.1.2 SOFC (Solid Oxide Fuel Cell) technology and applications 4

1.1.3 Literature review and research gaps.....10

1.2 Purpose and the contributions of this study.....15

1.3 Thesis Outline:.....17

References:.....19

Chapter 2

Development and Validation of a Computationally Efficient Pseudo 3D Model for Planar SOFC Integrated with a Heating Furnace †

Statement of Contribution to Co-authored Published Paper ..26

2.1 Introduction 27

2.2 Experimental set up and procedure 30

2.3 Layered-TSR modelling framework 32

2.3.1 Model structure 32

2.3.2 Model development.....37

2.3.3 Parameter adjustment and model validation 38

2.4 Results and discussion 41

2.4.1 Demonstration of the model improvement 42

2.4.2 Thermal comparison of adiabatic and non-adiabatic operations.....44

2.4.3 Model-based design of experiments 53

2.5 Conclusions 57

Nomenclature.....58

References: 61

Chapter 3

Planar Solid Oxide Fuel Cell Modelling and Optimization Targeting the Stack's Temperature Gradient Minimization[†]

Statement of Contribution to Co-authored Published Paper ..67

3.1 Introduction 68

3.2 Modelling 70

The Stack subcomponents and model framework 70

3.3 Results and discussions 74

3.3.1 Temperature gradients in two dimensions 74

3.3.2 Sensitivity analysis 77

3.3.2.1 Strategy #1: excess air flow 78

3.3.2.2 Strategy #2: adjustment of the gases' temperature difference at cell's inlet (ΔT_{in}) 81

3.3.2.3 Strategy #3: utilization of the oxygen-enriched air 84

3.5 Multi-objective optimization 89

3.6 Conclusions 94

Nomenclature 95

References: 97

Chapter 4

Exergy Analysis and Thermal Management at System Scale

4.1 Introduction 102

4.2 Energy and exergy estimation 106

4.3 Exergy analysis for a SOFC system with a simple model ... 109

4.3.1 Model description and flowsheet 109

4.3.2 Simulation results 111

4.3.2.1 Model validation 111

4.3.2.2 Exergy analysis 112

4.4 Thermal management study on SOFC system with a comprehensive model. 114

4.4.1 Model description and flowsheet 114

4.4.2 Simulation Results 116

4.4.2.1 System performance evaluation for a basis case 116

4.4.2.2 Parameter studies of the thermal behaviours 119

4.4.2.2.1 Air flow rates (Scenario #1) 120

4.4.2.2.2 Oxygen concentration in fresh cathode gas (Scenario #2) 122

4.4.2.2.3 Anode recycling ratio (Scenario #3) 124

4.4.2.2.4 Cathode recycling (Scenario #4) 126

4.5 Conclusions: 128

Nomenclature 129

References: 131

Chapter 5

Conclusions and Recommendations

5.1 Conclusions 136

5.2 Recommendations 138

Appendix I

Permission of Reproduction from the Copyright Owner.....140

List of Tables

Chapter 1

Table 1.1: Types of fuel cells [6] 5

Chapter 2

Table 2.1: Model parameters mostly compatible with the experimental settings 31

Table 2.2: Operating conditions 32

Table 2.3: Governing and constitutive equations for layers [15, 20–21] 36

Table 2.4: Error function values for two models at different temperatures.....41

Table 2.5: Voltage losses under different operating conditions.....43

Chapter 3

Table 3.1: Equations for temperature evaluation.....73

Table 3.2: Operating conditions used for SOFC stack simulation 75

Table 3.3: Stack performance fed with different oxygen concentration cathode 86

Table 3.4: Economic calculation results……88

Table 3.5: Manipulating variables and their ranges 91

Table 3.6: Optimization designed with different schemes 91

Table 3.7: Optimization results for different points of the Pareto front, labelled in Figure 3.6, for basis case (Basis), optimized case 1 (OC 1) and optimized case 2 (OC 2)…… 93

Chapter 4

Table 4.1: Comparison of studies for the SOFC system concerning exergy analysis and detailed stack characters.....105

Table 4.2: Calculating results in comparison with published data. 111

Table 4.3: Simulation input parameters [24] 112

Table 4.4: Operating conditions for the basis case 116

Table 4.5: Simulation results for the system thermal behaviors at different air flowrates.....120

Table 4.6: Simulation results for the system thermal behaviors at different oxygen concentration in fresh cathode gas 122

Table 4.7: Simulation results for the system thermal behaviors at anode recycling ratio 125

Table 4.8: Simulation results for the system thermal behaviors with cathode recycling.....128

List of Figures

Chapter 1

Figure 1.1: World energy consumption by regions from 2011-2040 (above); world energy consumption annual change in average (below). (based on the data in Ref.1) 3

Figure 1.2: World energy consumption (based on data in Ref.1) 3

Figure 1.3: A system of SOFC fed by integrated biomass gasifier. (adapted from Ref. [8]).....6

Figure 1.4: Tubular SOFC structure.....8

Figure 1.5: Planar SOFC structure 8

Figure 1.6: Flow configurations for planar SOFC 9

Figure 1.7: Schematic of the thesis structure and organization. 18

Chapter 2

Figure 2.1: Schematic of the experimental set up. 30

Figure 2.2: Schematic of the model's layers.....35

Figure 2.3: The results of parameter adjustment at 1053 K.....40

Figure 2.4: Model validation at 1083 K.....40

Figure 2.5: Model improvement demonstration at: (a) 1033 K, (b) and 1083 K.....43

Figure 2.6: Heat transfer distributions: (a) adiabatic condition ("simple model"), (b) adiabatic condition ("improved model"), (c) non-adiabatic condition ("comprehensive model"). 46

Figure 2.7: Temperature distributions: (a) adiabatic condition ("simple model"), (b) adiabatic condition ("improved model"), (c) non-adiabatic condition ("comprehensive model") 48

Figure 2.8: OCV and Voltage losses captured through different modelling approaches. Voltage losses are summation of ohmic and activation losses shown by A for "simple model", B for "improved model", and C for "comprehensive model" all under same operating conditions**.**.....52

Figure 2.9: Overpotentials' ratio (activation-to-ohmic) for adiabatic and non-adiabatic operations.....53

Figure 2.10: Furnace temperature required to active a particular average cell temperature (1170 K) under different fuel and air flow rates. 55

Figure 2.11: Estimation of PEN temperature based of furnace temperature and fuel and air flows: (a) different air flow rates, (b) different fuel and air flow rates (constant flows' ratio) 56

Chapter 3

Figure 3.1: Schematic diagram of SOFC stack model (adapted from Ref. 22). 72

Figure 3.2: Temperature profiles and maximum temperature differences between the "hottest" and "coldest" cells embedded inside a stack and operating under adiabatic and non-adiabatic conditions with basis operating conditions.....76

Figure 3.3: (a) Effect of excess air flow on stack's average temperature and temperature gradient elements; (b) Effect of excess air flow on temperature gradient and efficiency; (c) Stack's efficiency versus stack's temperature gradient regulated by applying excess air ($F_{H_2} = 900 ml/\min$).....80

Figure 3.4: (a) Temperature gradient of stack with different ΔT_{in} ($i = 5245\, A/m^2$); (b) Total temperature gradient of stack with different $\Delta T_{in;}$ (c) Stack efficiency achieved under different temperature gradient in varied operating condition ($F_{H_2} = 900 ml/\min$). 83

Figure 3.5: Stack temperature gradient and efficiency achieved under different

cathode flowrates with different oxygen concentration applied in cathode gas ($F_{H_2} = 900 ml/\min$) 85

Figure 3.6: Trade–off between efficiency and temperature gradient; Pareto points for basis case and optimization trials ($F_{H_2} = 900 ml/\min$).....91

Chapter 4

Figure 4.1: Schematic illustration of process unit in plant 108

Figure 4.2: AspenPlus simple SOFC system model flowsheet (adapted from Ref. 24) 109

Figure 4.3: Exergy share of the input for the plant 113

Figure 4.4: Schematic multi-scale model structure (adapted from [21-22] 115

Figure 4.5: Energy balance of the system calculated in energy (top) and exergy (bottom).....117

Figure 4.6: Process flowsheet for a SOFC stack system. The rectangular boxes with arrows show the exergy loss in each process, the oval boxes with arrows show the ratio of exergy loss and the input exergy into the system, the rectangular boxes without arrows show the system input and output. 119

Figure 4.7: Ratio of the exergy losses to the total exergy input for different air flow rates 121

Figure 4.8: Ratio of the exergy losses to the total exergy input for different oxygen concentration in cathode 124

Figure 4.9: Ratio of the exergy losses to the total exergy input for different anode recycling ratio 126

Figure 4.10: SOFC system flowsheet modification for simulation of cathode recycle stream. The rectangular boxes with arrows show the exergy loss in each process, the oval boxes with arrows show the ratio of exergy loss and the input exergy into the

system, the rectangular boxes without arrows show the system input and output...127

Chapter 1

Introduction

1.1 Background and motivation

1.1.1 Significance of fuel cell

Energy and environmental issues are becoming two vital global challenges nowadays. The situation is becoming more severe with the increasing energy demand due to the growth in population and the acceleration of the global industrial revolution. According to the World Energy Outlook presented in Figure 1.1, an increase of 50.8% in energy consumption of the world would be expected from 2011 to 2040, with an annual increasing rate of approximately 1.7% on average [1].

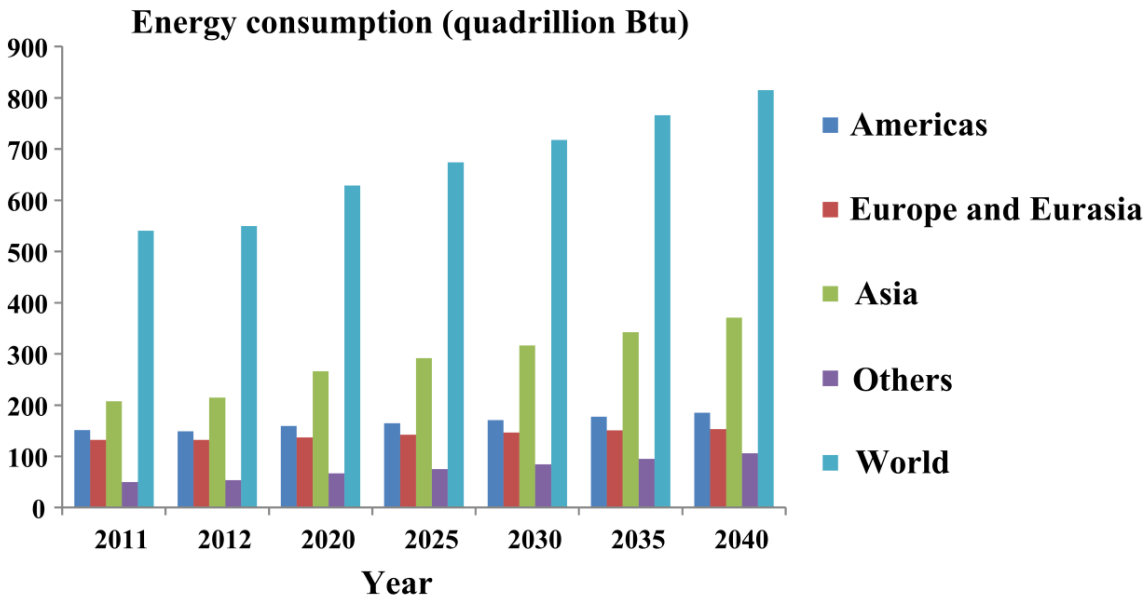

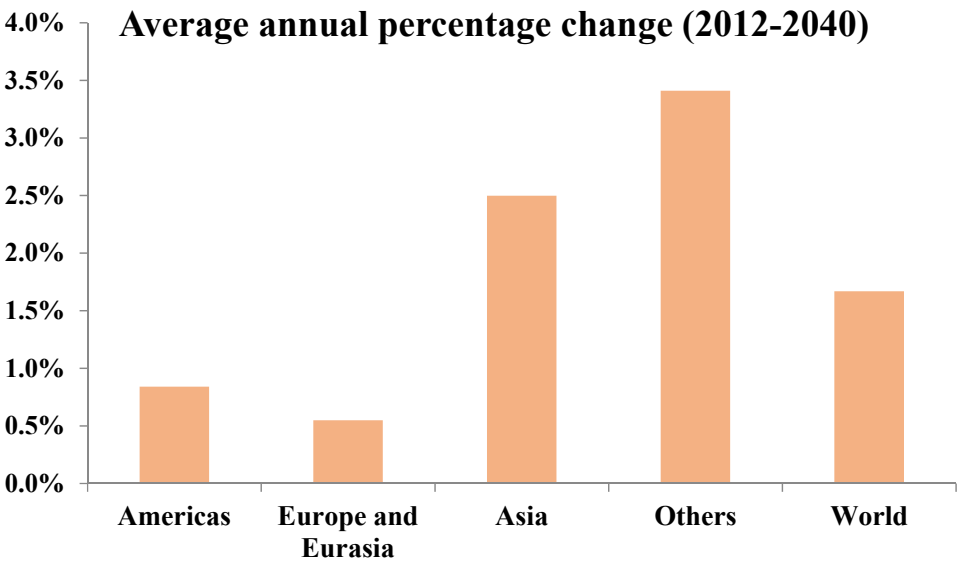

Figure 1. 1: World energy consumption by regions from 2011-2040 (above); world energy consumption annual change in average (below). (based on the data in Ref.1)

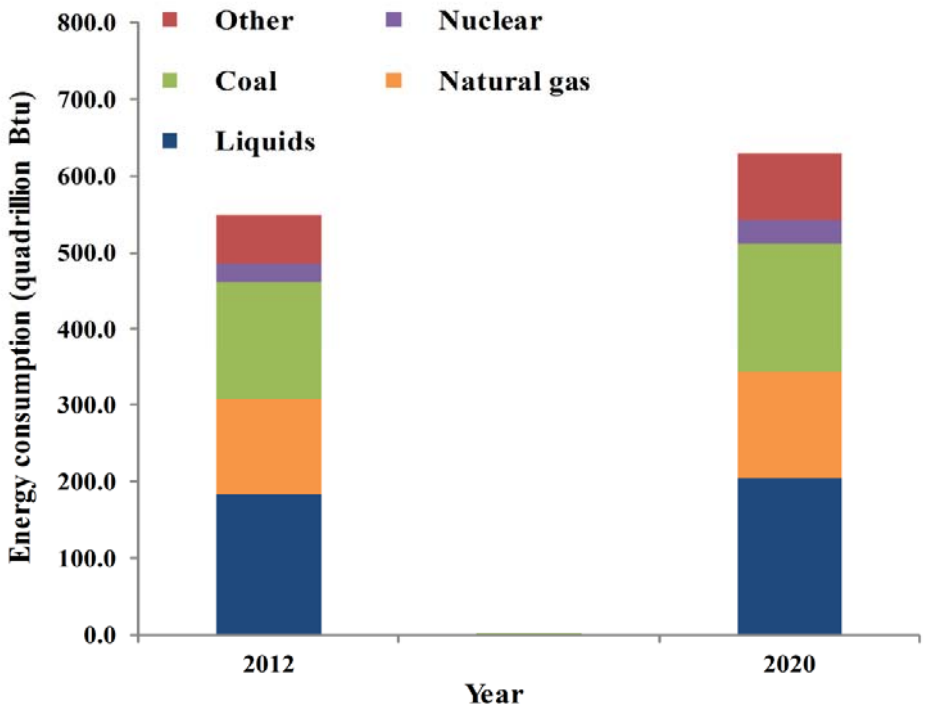

Figure 1. 2: World energy consumption (based on data in Ref.1)

So far, fossil fuels (oil, natural gas, and coal) still play a major role as the world's energy sources. As the Figure 1.2 shows, up to 83% of the world's energy sources are made up of non-renewable resources, which will eventually face the problem of exhaustion. Besides, these fuels need to be transferred into thermal energy for the first step in the practical application, and then transferred into mechanical energy or electrical power. In view of this, the system will be limited by the Carnot Cycle leading to relatively lower efficiency that is normally lower than 33% [2]. Moreover, the emissions during combustion of these fuels, such as nitrogen oxide (NOx) and sulfur oxide (SOx), form the main atmospheric pollutants. These justify the urgent requirement for technologies that provide highly efficient and clean energy sources.

Fuel cells technology is one of the answers as it can precisely meet the current requirement for the energy sources [3] and [4]. Unlike the traditional way of electricity generation that comply with the certain thermal cycles, the fuel cell utilizes the electrochemical process and converts the chemical energy into electrical energy directly. Thus, it gets rid of the limitation of Carnot cycle, resulting in a higher efficiency. Additionally, the reaction product is just water, resulting in much lower pollution compared with other traditional power generation methods [5].

1.1.2 SOFC (Solid Oxide Fuel Cell) technology and applications

The main types of fuel cells that are currently used include: AFC (Alkaline Fuel Cell), DMFC (Direct Methanol Fuel Cell), PCFC (Protonic Ceramic Fuel Cell), PAFC (Phosphoric Acid Fuel Cell), PEMFC (Proton Exchange Fuel Cell), MCFC (Molten Carbonate Fuel Cell), SAFC (Sulfuric Acid Fuel Cell), and SOFC (Solid Oxide Fuel Cell). Based on different working temperatures and the fuels that are used, the classification of fuel cells are illustrated in Table 1. 1 [6], in which, AFC, DMFC, PAFC, SAFC, PEMFC are the low temperature fuel cells; while MCFC,

SOFC, PCFC work at mid-to high temperatures.

Table 1. 1: Types of fuel cell [6]

Fuel cell type	Electrolyte	Operating temperature	Fuel
PEM	Polymer, proton-exchange membrane	50~80 °C	Methanol or impure pure hydrogen from hydrocarbons
SAFC	Sulfuric acid	80~90 °C	Alcohol or less pure hydrogen
AFC	Potassium hydroxide	50~200 °C	Pure hydrogen or hydrazine
DMFC	Polymer	60~200 °C	Methanol
PAFC	Phosphoric acid	160~210 °C	Hydrogen
MCFC	Molten salt	630~650 °C	Hydrogen carbon monoxide, natural gas, propane, marine diesel
PCFC	Thin membrane of barium cerium oxide	600~700 °C	Hydrocarbons, hydrogen
SOFC	Ceramic as stabilized zirconia and doped perovskite	600~1000 °C	Natural gas or propane

Among different of fuel cells, SOFC is considered as the most attractive one [7]. Compared with low working temperature fuel cells, such as PEMFC, it can avoid precious metal as the catalyst and eliminate the CO poisoning of the electrodes. Besides, the high operating temperature allows internal reforming and gives large flexibility in fuel selection, such as the biomass, natural gases, coal gases, or other hydrocarbons. More importantly, it offers possibilities for the utilization of the exhaust gases and heat recycling through a hybrid system with steam turbine or gas

turbine, etc., such as shown in Figure 1.3. These combination systems can increase the whole efficiency of the electricity power system, and reduce the pollution to the environment [9].

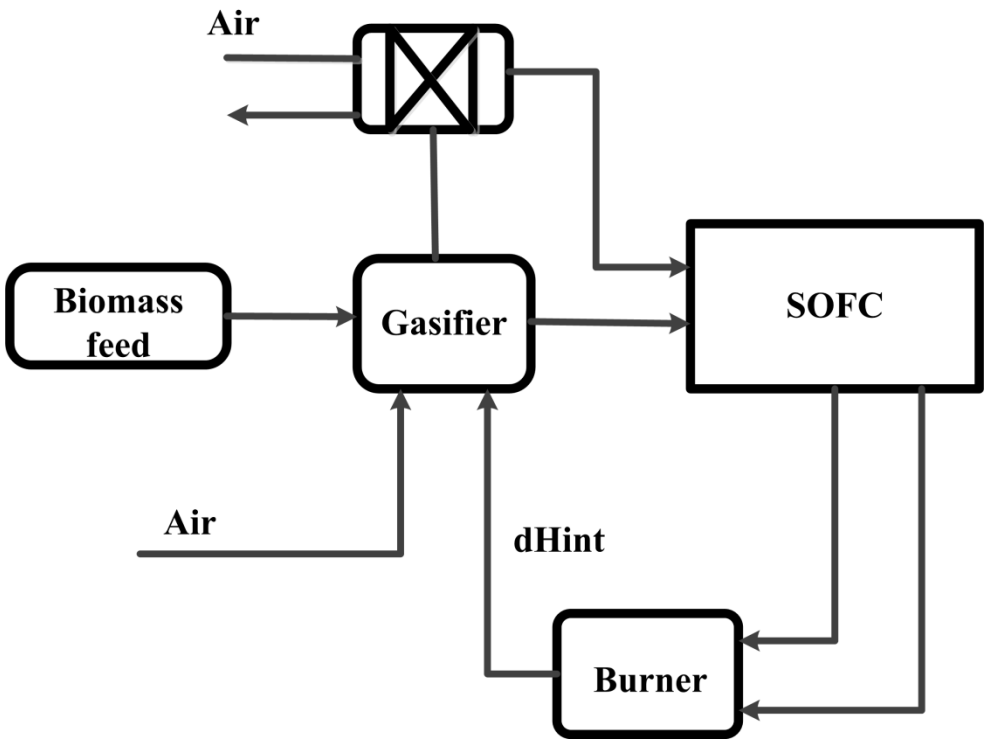

Figure 1. 3: A system of SOFC fed by integrated biomass gasifier. (adapted from Ref. [8])

Compared with other fuel cells with high operating temperature, such as MCFC, it even avoids the corrosion of electrodes in fuel cells, since the electrolyte of the SOFC is solid. Besides, the SOFC system has higher power density and lager range of electricity generation capacity as well, compared with other fuel cells. The SOFC's can be applied to the large-scale power station, or in small-scale applications. Especially for the CHP (Combined heat and power) application for remote communities, SOFC is considered as the best candidate among all types of fuel cells [10], [11], and [12].

There are two main typical designs for SOFC configurations currently, which are tubular and planar SOFCs. The tubular configuration is shown in Figure 1.4. Two tubes are mainly included, which are called the cell tube and guidance/ injection tube, respectively. The outer surface and inner surface of the cell tube forms the anode and cathode respectively, between which, solid oxide electrolyte is lied. Air is injected from the guidance tube into the cell tube and passes through the cathode, while fuel flows through the anode on the other side of the cell tube. The advantage of tubular SOFC is the diversity in fuel selection. However, much higher Ohmic losses are incurred compared with the planar type. For the planar SOFC, the compartments are assembled as shown in Figure 1.5. It is mainly constructed of a positive-electrolyte-negative electrode (PEN), top/bottom interconnects, and gas channels. Air and fuel can pass through channels of interconnects. Additionally, three different flow configuration designs can be used for the planar SOFC, co-flow, counter-flow, and cross-flow, as illustrated in Figure 1.6. Multiple cells can be stacked in series to construct a SOFC stack, and higher power can be generated. The high power density is the most prominent advantage of the planar configuration. Besides, the simplicity in manufacturing and the associated low manufacturing costs are also the benefits compared to the tubular SOFC. However, the biggest challenge for the planar structure is the stresses generated in the structure due to the large cell area and nonhomogeneous temperature distribution [13].

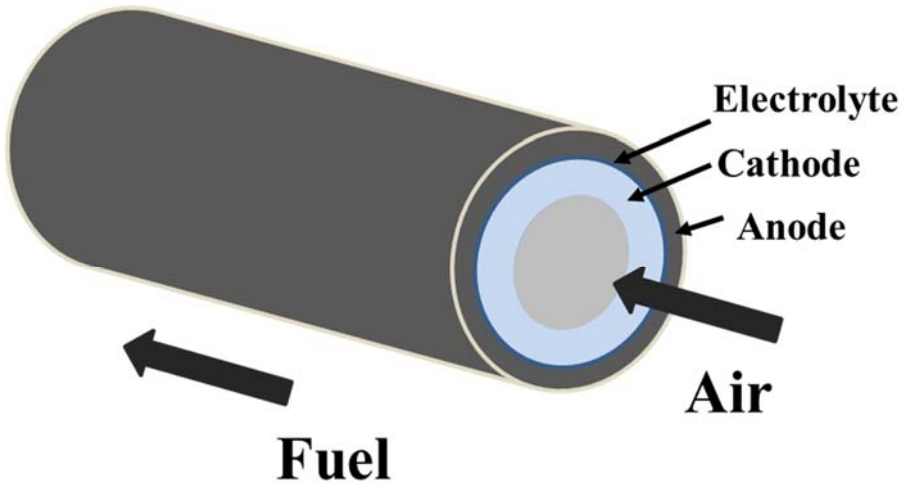

Figure 1. 4: Tubular SOFC structure

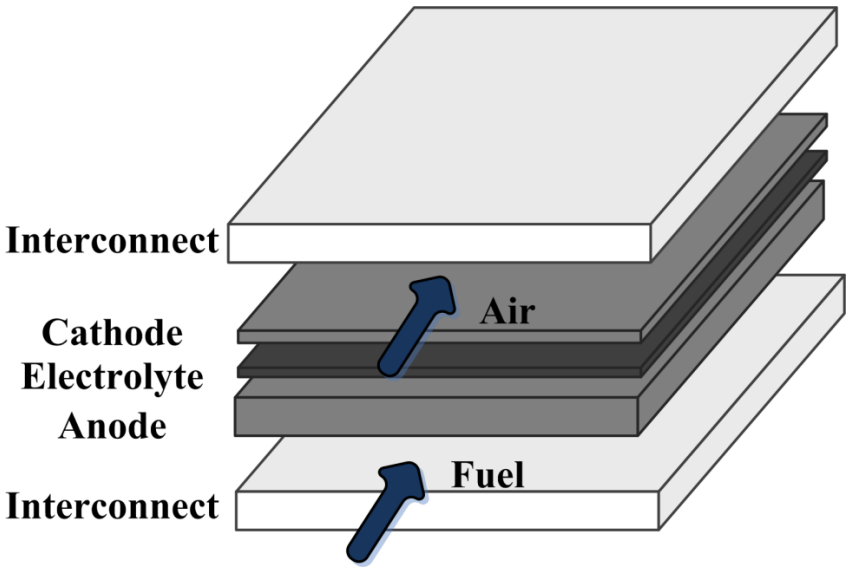

Figure 1. 5: Planar SOFC structure

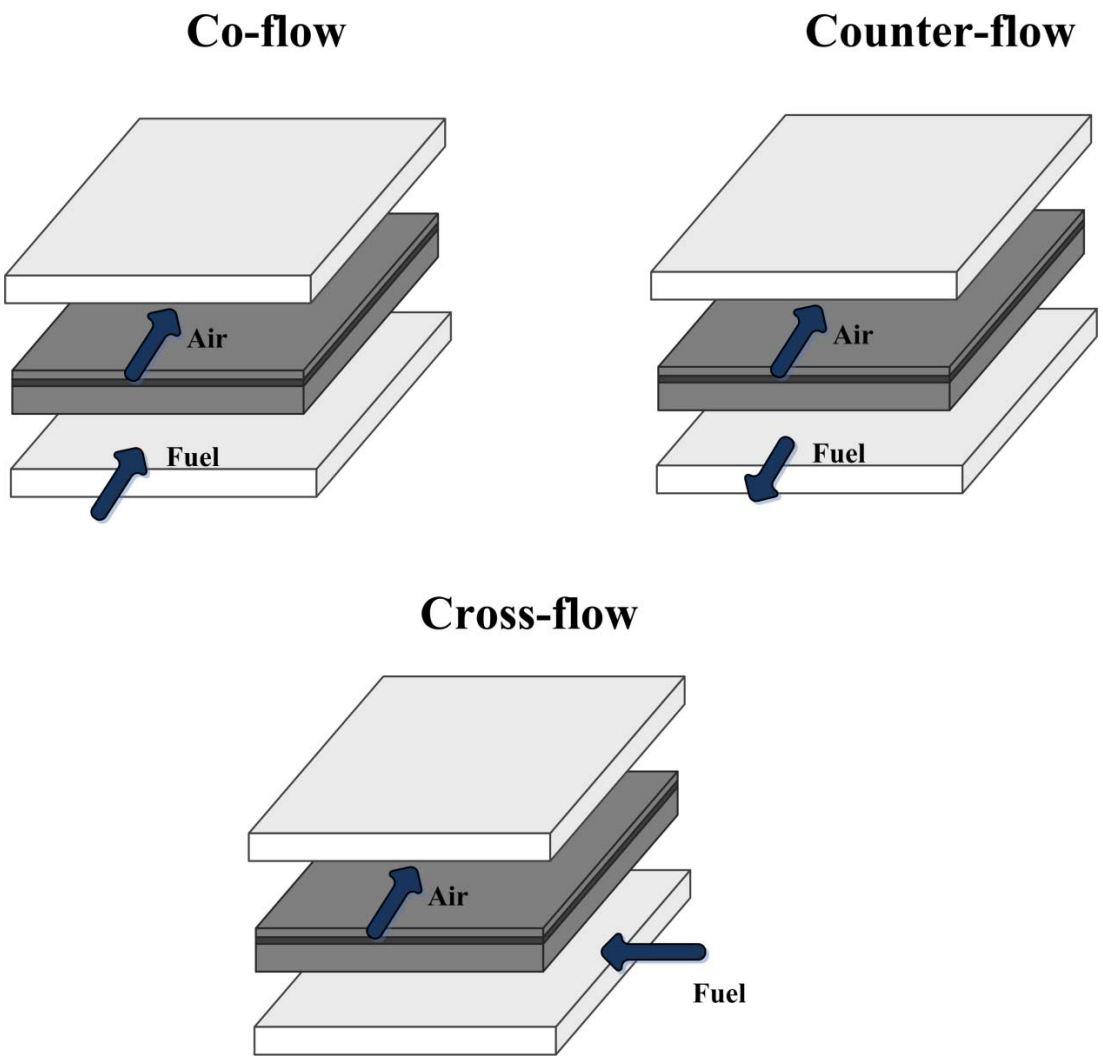

Figure 1. 6: Flow configurations for planar SOFC

Until now, the commercialization of the SOFC faces lots of obstacles, such as the high operation costs, long system trial cycle, under desired operation performances, etc. [14] and [15]. It is claimed in Ref. [16] that the main technical barriers in SOFC technology include the low thermal resistance, complexity caused by fuel reforming, insufficiency in SOFC efficiency and fuel utilization.

As SOFC benefits from the advances brought by the high temperature, it also suffers from the vital problems caused by the same high operating temperature [17], [18], and [19]. The most vital challenge is the thermal stresses generated in SOFC. During

the SOFC operation, the process of heat transfer, mass transfer and the electrochemical dynamics are highly coupled. Accordingly, the internal flow field, temperature field and the electric field are highly mal-distributed [18]. Thus, the uniformity of temperature distribution inside the SOFC, the mismatch of the thermal expansion coefficients on different materials for different compartments and other adverse phenomena are alleviated leading to the decline in the performance or other degradations. Two main approaches could be utilized for solving these problems; passive design based solution and active thermal management [16]. For the former, efforts are needed for new material or novel structure to increase the tolerance of large temperature gradients in the SOFC. While for the latter, more studies are required for the deeper understanding of the thermal behaviours, or optimization of thermal management in all respects of SOFC operation with the aim of controlling the temperature gradient in the SOFC. Energy conversion efficiency, up to 90% is predicted for a SOFC with heat recovery that can be achieved theoretically [4], and [20]. However, it is obvious that further developments are required for achieving this goal. The SOFC system efficiency is basically related to the cell or stack performance which are affected by cell/stack unit properties, such as the geometry, material, cell-to-cell connection in series, and also the operating conditions [16]. Thus, it is evident that the improvement of thermal management for a SOFC in all levels is urgently required.

1.1.3 Literature review and research gaps

Since the last two decades, large progress is achieved in the SOFC technologies through sustained research efforts. There are still many challenges that need solution. The computational models can play a crucial role in exploring the solutions for those challenges. It is relatively cheap in terms of time and money and can enable insights

that experiments cannot achieve [13], [18] and [19].

Until now, numbers of simulation models of SOFC have been reported (from 0D ~ 3D) in literature. The research objectives will decide the models that are chosen and developed for study [21]. For the purposes of system control, or other online diagnostic applications, lower dimensional (0D, 1D) models are more suitable due to the less computational time and their higher flexibility [21] and [22]. However, for the detailed analysis associated with cell or stack design, multi-dimensional models such as 2D and 3D models are necessary, since more detailed information will be needed. For the case of thermal study on a SOFC cell/ stack, a more detailed model which is capable of predicting the distributed temperature, mass, and other local distributions is required as an essential instrument.

The modelling study of Ferguson et al. [23] is considered as an outstanding work in the SOFC simulation in the early stages, and it is widely utilized. The 3D computational models they developed include the planar, tubular and cylindrical SOFC cell unit structures, by which, the distribution of voltage, temperature, reactants' concentration inside the SOFC are predictable. Besides, they compared the performance of a planar SOFC influenced by different flow configurations, the geometry of channel ribs, and electrolyte thickness. The results showed that the counter-flow configuration is most efficient for a planar SOFC. Yakabe et. al. [24] and [25] utilized the CFD (Computational Fluid Dynamic) tool, Star-CD, and created the 3D models which are capable of predicting the mass, temperature, voltage, current density fields inside the SOFC cell unit. Based on the distributed temperature results, principle thermal stress in SOFC structure were obtained by the FEA (Finite Element Analysis). Recknagle et. al. [26] developed a model using commercial software, Star-CD, combined with their own programing code to predict the fluid dynamic, current density, temperature distribution, and fuel utilization. They compared the impact of different flow configurations on the SOFC's performances.

Their research results showed that the most uniform temperature distribution is achieved by co-flow configuration. There are also noticeable dynamic simulation studies. Aguiar et. al. [27] and [28] created a dynamic model for an internal reforming anode-support SOFC. In their research in Ref.27, they implemented the mass, energy and electronic balance equations in their model, by which, the results for the dynamic response for voltage, power with the step change in current density under different operating conditions are achieved. And in their latter research [28], the control strategies study is conducted based on the dynamic model.

The computation time is a challenge for these higher dimensional models that usually employ the finite-volume method [29]. The prediction accuracy, tolerance, and computational budget are always required to be balanced for a simulation research. Besides, due to the limited sources of experimental data, measurement techniques, and the complexity of the multi-dimensional models, the models should be chosen very carefully according to the analysis purposes [21], [29] and [30]. It is also believed that the influence of simplifications of the models on the prediction accuracy is still not clear and the difference between simulation results and experimental data needs further understanding [13]. These gaps demand a reliable, delicate computational model with relevant validation for the thermal management study of a SOFC.

Regarding the thermal management of a SOFC, different researches have dealt with SOFC cell or system design. Some of them focus on the interconnects and the channels design. Huang et. al. [31] proposed different designs of interconnects and examined their influences on cell performance by experiments and simulation regarding the flow distribution and temperature distribution. The results showed that the improved design for interconnects can lead to more uniform flow distribution, and it will also lead to more homogeneous temperature distribution in the SOFC. Grondin et al. [32] investigated the influence of pin size and associated

cathode/interconnect contact area on the temperature gradient. Their results indicated that decreasing pin size and increasing the contact area are helpful in decreasing the temperature gradient as they will intensify the convective heat transfer at the cathode side.

Some researchers proposed different integrated designs of the SOFC system trying to solve the thermal problems of the cell/ stack. Jiang et al. [33] proposed a novel design of SOFC stack with injecting the fuel in different positions of the SOFC stack for the thermal management purpose. This novel structure allows the fuel introduced in the stack with controlled composition, pressure, velocities, and flowrates at the inlet to achieve the better thermal management across a SOFC stack. An inventive stacking arrangement of tubular SOFC was proposed by Lange et. al. [34]. In this structure, the electrical connection is located outside of the active area that can cool this high temperature area, which allows common materials to be used in this SOFC. As a result, lower operating temperature, less thermal stresses and longer life time can be achieved. Dilig et. al. proposed a SOFC stack design with heat pipe in Ref. [35]. The Planar SOFC stack is manufactured with the interconnects with the flat type heat pipe in it. Due to the super power of the heat transfer ability for the heat pipe, less extra air will be needed for cooling and a temperature gradient reduction can be achieved within this structure. Another SOFC configuration, single chamber SOFC, is also mentioned with regards to the thermal management considerations. Since lower operating temperature is required for this structure, around 300~ 600 °C [36].

There are also many studies that contribute to the temperature profiles of a SOFC in cell level, taking account the different features of SOFC including flow configuration, geometries, flow distributors, operating conditions, etc. Several investigations can be found for the thermal management of a SOFC stack, focusing on the influences of cell numbers, cell to cell variation, etc. However, more studies

are required for gaining a comprehensive understating of the temperature behaviour of the SOFC stack and the barriers in achieving homogeneous temperature profiles, methodologies for improving the SOFC performance with respect of thermal management. Regarding the impact of operating conditions on SOFC performance, many researchers mentioned that reducing the operating temperature is one of the solutions for achieving more uniform temperature distribution. However, the operating temperature or other parameters that influence the thermal behaviour have a strong impact on the electrochemical performance as well, which directly decides the stack efficiency. These multiple influences on the SOFC performance and the associated strategies should also be further studied.

Additionally, as a product to be applied in practice, the SOFC has to be used in a system, working together with all BOP (balance of plant). For the whole SOFC plant thermal management, besides the requirements of ensuring the cell/ stack is working within the required temperature range, the guarantee of a tolerant temperature gradient inside the stack, achieving the maximum system efficiency is also necessarily for the optimal thermal management in the system. There are numerous works studying different configurations of the SOFC system and the hybrid systems with the aim of maximising system efficiency. Some emphasized on the parametric studies. Palsson et al. [9] conducted the sensitive analysis of inlet temperature for fuel and turbine on the pressure and electrical efficiency in their SOFC-GT system. Lisbona et al. [37] investigated the electrical and thermal efficiency of a SOFC combined with heat and power system under different parameters. The parameters examined include the fuel utilization, gas temperature, anode off-gas recirculation rate, external pre-reforming and reaction extent. Their results pointed out that the pre-reforming degree is the only variable that would always increase the electrical efficiency. There are also many different configurations of SOFC hybrid systems studied in the literature. Granovskii et al. [38] proposed two possible SOFC-gas

turbine systems in their study. One is a SOFC hybrid system with gas turbine cycle that includes the steam generaion, while the other one involves the recycling of anode exhaust gases. The system performance is compared through energy and exergy analysis. Their results claimed that the former scheme is more favourable since it achieves higher power with high efficiency of fuel consumption. Four different hybrid SOFC-GT-biomass gasification system models are developed and studied by Toonssen et al. [39]. The energy analysis is conducted for the evaluation of the system scale performance. The study results indicate that highest electrical efficiency of 49.9% is achieved by the large scale system..

Most of the current thermal studies for a SOFC system in the literature are based on the simple SOFC model, while the detailed stack character is not considered within the SOFC system analysis and optimization study. However, the combined system and stack level performance requires parallel computation [40]. More parameter studies are necessary at each level of the SOFC and more importantly, the interaction between these levels must be studied, so as to obtain solutions for improved thermal management for a SOFC system.

The detailed literature review for different aspects are introduced in each of the following chapters (Chapter 2 ~ 4), with which, it can be observed that more efforts are required for the optimal thermal management of a SOFC in all levels, which also gives the motivation for this study.

1.2 Purpose and the contributions of this study

From the preceding discussions, it is clear that SOFC has great potential to be used in solving the energy problems that the world faces. However, the thermal management improvement of SOFC is one of the vital barriers to be overcome that

raise the requirements for both design and defining operating conditions of SOFC [40]. To overcome the challenges, a deeper understanding of the thermal behaviour of the SOFC is essential. The related parameter influences on the thermal behaviour of the SOFC would be helpful for design and operation. Therefore, this study aims to develop a complete reliable model for a planar SOFC according to the practical condition, with which further analyses can be performed. Achieving a more comprehensive understanding of the thermal behaviours inside the cell, stack as well as the system level is also a significant objective of this study. Based on the understanding of SOFC, the strategies for improved thermal management of SOFC will be provided. With these objectives, the main contributions of this thesis can be specified as:

- A validated model for Planar SOFC is developed and the improvement of prediction of this model can be observed.
- A deeper understanding of thermal management of a cell is achieved through the distributed analysis inside the cell.
- Temperature behaviors in both flowing and stacking directions of a multiple-layer SOFC stack are investigated.
- Three promising approaches are assessed on both temperature gradient and efficiency for a SOFC stack, with guidance provided for the improved thermal management.
- Through the multi-objective optimization, effective solutions for optimum SOFC performance are provided, and the improvement is achieved by application of the strategies proposed in this study.
- By utilization of the comprehensive system SOFC model, the thermal behaviors of both stack and system level and as well as the interactions between them are captured.
- 4 scenarios of system operation are provided. Deeper understanding of

exergy loss in the SOFC system is obtained through the sensitivity analysis with different scenarios. The results provide the direction for the system's operational design with enhanced total efficiency.

- Solutions for better thermal management for the SOFC system's operation considering both stack level and the system level can be formulated based on the results.

1.3 Thesis Outline:

Chapter 2 presents a layered-model for a SOFC cell in details that is developed according to the practical case. Besides, the experimental tests are introduced for the validation of this model. The comparison between experimental and simulation results are illustrated with the model prediction improvement analysis as well. Based on this model, a further distributed thermal analysis is also presented for the purpose of deeper understanding of thermal behaviours of SOFC. Additionally, the model-based test design for cell and heating furnace relations are presented.

In Chapter 3, the thermal study of stack level is conducted. Firstly, a SOFC stack model is developed based on the validated cell model. The temperature distribution and gradients are studied in two dimensions. Three strategies for different operating conditions are proposed and analyzed focusing on the thermal behaviours of the stack. An optimization study is conducted based on the sensitivity analysis results for obtaining effective solutions for the improved SOFC performance.

Subsequently, the system level thermal study is conducted in Chapter 4. With the aim of effectively using energy throughout the whole system, the exergy analysis is firstly conducted with a simple SOFC system model. Later a more comprehensive system model is introduced for the further analysis, with which, the thermal performance evaluation for both system and stack level is presented in detail. And

besides, four scenarios of system process operations with associated sensitivity analysis are presented regarding the thermal characteristics and exergy distribution of the whole system.

Finally, Chapter 5 summarizes the conclusions of this thesis and the recommendations for the future research

Figure 1.7 summarizes the main contents of each chapter, and the relations between each chapter.

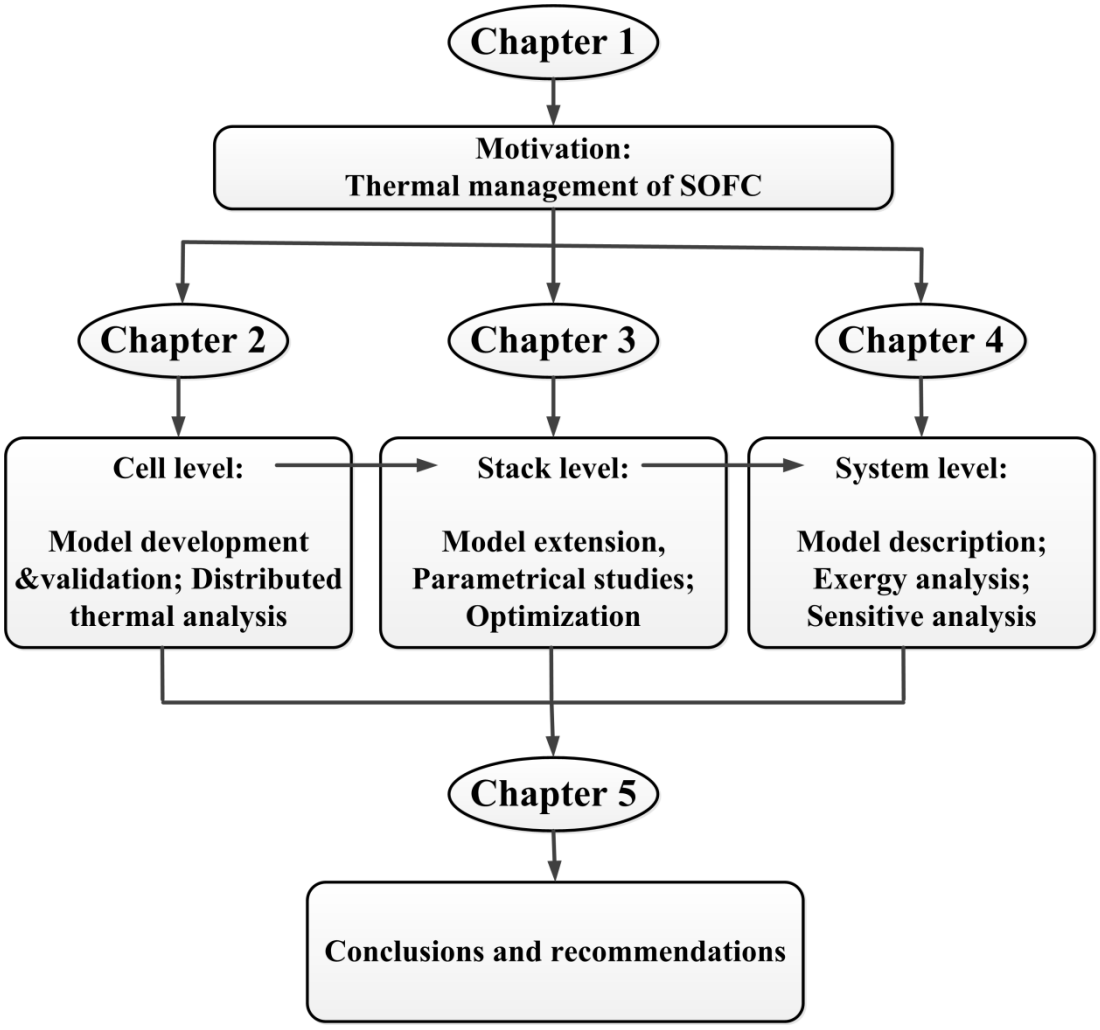

Figure 1. 7: Schematic of the thesis structure and organization.

References:

[1] EIA, International Energy Outlook 2011, U.S. Energy Information Administration, Washington, DC, 2016

[2] Y. Demirel, Energy : production, conversion, storage, conservation, and coupling, Springer, London, 2012.

[3] R.P. O'Hayre, S.-W. Cha, W. Colella, F.B. Prinz, Fuel cell fundamentals, John Wiley & Sons New York2006.

[4] J. Larminie, A. Dicks, J. Larminie, A. Dicks, Introduction, Fuel Cell Systems Explained, John Wiley & Sons, Ltd,.2013, pp. 1-24.

[5] K. Huang, J.B. Goodenough, Solid oxide fuel cell technology: principles, performance and operations, Elsevier2009.

[6] A.B. Stambouli, E. Traversa, Solid oxide fuel cells (SOFCs): a review of an environmentally clean and efficient source of energy, Renewable and Sustainable Energy Reviews 6 (2002) 433-455.

[7] K. Huang, J.B. Goodenough, Solid oxide fuel cell technology: principles, performance and operations, Elsevier2009.

[8] G. Campitelli, S. Cordiner, M. Gautam, A. Mariani, V. Mulone, Biomass fueling of a SOFC by integrated gasifier: Study of the effect of operating conditions on system performance, International Journal of Hydrogen Energy

38 (2013) 320-327

[9] J. Palsson, A. Selimovic, L. Sjunnesson, Combined solid oxide fuel cell and gas turbine systems for efficient power and heat generation, Journal of Power Sources 86 (2000) 442-448.

[10] J. Larminie, A. Dicks, M.S. McDonald, Fuel cell systems explained, Wiley New York2003.

[11] S. Badwal, S. Giddey, F. Ciacchi, R. Clarke, P. Kao, Research and developments in hydrogen technologies, Advances in Applied Ceramics 106 (2007) 40-44.

[12] P. Robert Zogg, K. Roth, Using Solid-Oxide Fuel Cells For Distributed Generation, (2006).

[13] S.A. Hajimolana, M.A. Hussain, W.M.A.W. Daud, M. Soroush, A. Shamiri, Mathematical modeling of solid oxide fuel cells: A review, Renewable and Sustainable Energy Reviews 15 (2011) 1893-1917.

[14] F. Zink, Y. Lu, L. Schaefer, A solid oxide fuel cell system for buildings, Energy Conversion and Management 48 (2007) 809-818.

[15] S.S. Penner, A.J. Appleby, B.S. Baker, J.L. Bates, L.B. Buss, W.J. Dollard, P.J. Farris, E.A. Gillis, J.A. Gunsher, A. Khandkar, M. Krumpelt, J.B. O'Sullivan, G. Runte, R.F. Savinell, J.R. Selman, D.A. Shores, P. Tarman, Commercialization of fuel cells, Progress in Energy and Combustion Science 21 (1995) 145-151.

[16] Wojciech M. Budzianowski and Jarosław Milewski. "Recent key technical barriers in solid-oxide fuel cell technology" Archives of Thermodynamics Vol. 35 Iss. 1 (2014)

[17] U. Krewer, M. Pfafferodt, A. Kamat, D.F. Menendez, K. Sundmacher, Hydrodynamic characterisation and modelling of anode flow fields of Direct Methanol Fuel Cells, Chemical

[18] H. Yakabe, Y. Baba, T. Sakurai, M. Satoh, I. Hirosawa, Y. Yoda, Evaluation of residual stresses in a SOFC stack, Journal of Power Sources 131 (2004) 278-284.

[19] T.-F. Cao, Y.-T. Mu, J. Ding, H. Lin, Y.-L. He, W.-Q. Tao, Modeling the temperature distribution and performance of a PEM fuel cell with thermal contact resistance, International Journal of Heat and Mass Transfer 87 (2015) 544-556

[20] Data from The International Fuel Cells, a United Technology Company. Fuel Cells Review. 2000.

[21] K. Wang, D. Hissel, M.C. Péra, N. Steiner, D. Marra, M. Sorrentino, C. Pianese, M. Monteverde, P. Cardone, J. Saarinen, A Review on solid oxide fuel cell models, International Journal of Hydrogen Energy 36 (2011) 7212-7228.

[22] Braun, R. (2002). Optimal Design and Operation of Solid Oxide Fuel Cell Systems for Small-scale Stationary Applications . Doctoral Dissertation,

[23] J.R. Ferguson, J.M. Fiard, R. Herbin, Three-dimensional numerical simulation for various geometries of solid oxide fuel cells, Journal of Power Sources 58 (1996) 109-122.

[24] H. Yakabe, M. Hishinuma, M. Uratani, Y. Matsuzaki, I. Yasuda, Evaluation and modeling of performance of anode-supported solid oxide fuel cell, Journal of Power Sources 86 (2000) 423-431.

[25] H. Yakabe, T. Ogiwara, M. Hishinuma, I. Yasuda, 3-D model calculation for planar SOFC, Journal of Power Sources 102 (2001) 144-154.

[26] K.P. Recknagle, R.E. Williford, L.A. Chick, D.R. Rector, M.A. Khaleel, Three-dimensional thermo-fluid electrochemical modeling of planar SOFC stacks, Journal of Power Sources 113 (2003) 109-114.

[27] P. Aguiar, C.S. Adjiman, N.P. Brandon, Anode-supported intermediate temperature direct internal reforming solid oxide fuel cell. I: model-based steady-state performance, Journal of Power Sources 138 (2004) 120-136.

[28] P. Aguiar, C.S. Adjiman, N.P. Brandon, Anode-supported intermediate-temperature direct internal reforming solid oxide fuel cell: II. Model-based dynamic performance and control, Journal of Power Sources 147 (2005) 136-147.

[29] R. Bove, S. Ubertini, Modeling solid oxide fuel cell operation: Approaches, techniques and results, Journal of Power Sources 159 (2006) 543-559.

[30] F. Zabihian, A. Fung, A review on modeling of hybrid solid oxide fuel cell systems, International Journal of Engineering 3 (2009) 85-119.

[31] C.M. Huang, S.S. Shy, C.H. Lee, On flow uniformity in various interconnects and its influence to cell performance of planar SOFC, Journal of Power Sources 183 (2008) 205-213.

[32] D. Grondin, J. Deseure, M. Zahid, M.J. Garcia, Y. Bultel, Optimization of SOFC interconnect design using Multiphysic computation, in: B. Bertrand, J. Xavier (Eds.) Computer Aided Chemical Engineering, Elsevier2008, pp. 841-846.

[33] Y. Jiang, S. Pollard., D. Julien, C. Tanner, WO Patent 2 007 126 588A22007.

[34] F. Lange, A. Virkar, WO Patent 2 007 005 767A1, 2007.

[35] M. Dillig, T. Meyer, J. Karl, Integration of Planar Heat Pipes to Solid Oxide Cell Short Stacks, Fuel Cells 15 (2015) 742-748.

[36] M. Yano, A. Tomita, M. Sano, T. Hibino, Recent advances in single-chamber solid oxide fuel cells: A review, Solid State Ionics 177 (2007) 3351-3359.

[37] P. Lisbona, A. Corradetti, R. Bove, P. Lunghi, Analysis of a solid oxide fuel cell system for combined heat and power applications under non-nominal conditions, Electrochimica Acta 53 (2007) 1920-1930.

[38] M. Granovskii, I. Dincer, M.A. Rosen, Performance comparison of two

combined SOFC–gas turbine systems, Journal of Power Sources 165 (2007) 307-314.

[39] R. Toonssen, S. Sollai, P.V. Aravind, N. Woudstra, A.H.M. Verkooijen, Alternative system designs of biomass gasification SOFC/GT hybrid systems, International Journal of Hydrogen Energy 36 (2011) 10414-10425.

[40] A. Faghri, Z. Guo, Challenges and opportunities of thermal management issues related to fuel cell technology and modeling, International Journal of Heat and Mass Transfer 48 (2005) 3891-3920.

Chapter 2

Development and Validation of a Computationally Efficient Pseudo 3D Model for Planar SOFC Integrated with a Heating Furnace †

†Adapted with permission from (S. Tang, A. Amiri, P. Vijay, M.O. Tadé, Development and validation of a computationally epicient pseudo 3D model for planar SOFC integrated with a heating furnace, Chemical Engineering Journal 290 (2016) 252-262) . Copyright (2016) Elsevier

Statement of Contribution to Co-authored Published Paper

This Chapter includes the co-authored paper 'Development and Validation of a Computationally Efficient Pseudo 3D Model for Planar SOFC Integrated with a Heating Furnace ', published in Chemical Engineering Journal. The bibliographic details of the co-authored paper, including all authors are:

Shi Tang, Amirpiran Amiri, Periasamy Vijay, Moses 0. Tade

Centre for Process Systems Computations, Department of Chemical Engineering, Curtin University, GPO Box Ul987, Perth, WA 6845, Australia.

I, Shi Tang, contributed to the paper by conducting all the simulation and analysis work, being the primary writer, including creating figures and tables, and writing the manuscript.

I, as a Co-Author, endorsed that this level of contribution by the candidate indicated above is appropriate.

Amirpiran Amiri

Periasamy Vijay

Moses Tade

2.1 Introduction

As a clean and efficient energy conversion device, the solid oxide fuel cell (SOFC) is currently considered as one of the most promising technologies to replace combustion-based processes for power generation and thereby resolve the problems associated with environmental pollution and shortage of global energy resources. The widespread application of fuel cells, however, still faces several interconnected technical and economic challenges pertaining to efficiency, reliability, and durability. The non-homogeneity of internal profiles such as the temperature distribution [1] can be counted as one of the causes for the mentioned challenges. Therefore, a wide spectrum of experimental and modelling investigations have been executed in the last three decades to overcome these barriers which exist in the commercialization route. Process modelling efforts, compared to experimental studies, are always more economical, safer, and flexible for any analysis of interest while being less time consuming. Furthermore, modelling has been proven as an effective tool in understanding and explaining the multi-physics mechanisms that might be encountered in the fuel cell [2], [3] and [4]. Accordingly, a high-fidelity model offers a reliable and efficient guideline for the design, analysis, optimization, and control of fuel cell processes at various levels. Moreover, design-of-experiments can be significantly enhanced via application of even a simple predictive-model.

Many modelling works have been reported by researchers that study the various aspects of the SOFC. SOFCs have been modelled with different levels of complexity including 0D, 1D, 2D, 3D geometries by using commercial numerical software or programming codes depending on targeted research objectives [2], [3], [4], [5], [6], [7], [8], [9] and [10]. Basically, 2D and 3D models place emphasis on cell or stack design such as its geometry design [7] and [8], where the CFD concepts and tools are commonly utilized. These models allow the user to predict the details of transport

phenomena and reactions that take place inside the operating SOFC. For instance, Yakabe et al. [10] proposed a 3D model for planar SOFC by using CFD tool in which current density, voltage, temperature distribution, and mass transfer rate can be calculated. Further, they also computed the principal thermal stresses by using finite element analysis software ABAQUS. However, computational time is a challenge for the multi-dimensional models due to high complexity. Moreover, they would lose flexibility of application in system design [1] and [11]. Therefore, 0D and 1D models are usually preferred for the dynamic simulations and control purposes [1], [5] and [6]. These reduced models are always based on several simplifications and assumptions; where the computational time is considerably reduced compared to the 2D, and 3D models. Basically, compromise between results' preciseness, tolerance, and computational time needs to be wisely made in the application of these models [11].

Among the wide spectrum of available modelling approaches, reactor approximation through the tank-in-series reactor (TSR) methodology, offers salient features such as simplicity and flexibility, in addition to reliability [12], [13], [14] and [15]. Krewer et al. [13] utilized reduced model of TSR to explore the influence of flow field on the Direct Methanol Fuel Cell behaviour in both steady state and dynamic conditions. Moreover, Danilov et al. [14] developed a TSR model for tubular SOFC having the capability to predict temperature, concentration, and current density distribution in two dimensions. Furthermore, this modelling methodology has been adapted for planar-type SOFC [15]. This work allows capturing the current, temperature, and species concentration distributions and offers flexibility in simulating three flow patterns (co-, counter-, and cross-current for fuel and air flows' pattern). Moreover, their model calculates the dynamic response of cell to a step perturbation in operational voltage. Bozbiyik et al. [12] suggested an improved TSR model for the Proton Exchange Membrane Fuel Cell case study.

The objective of this study is to develop and validate an efficient numerical model for a realistic experimental rig's configuration that could be utilized for further analysis of experimental results and also for the rapid approximations for the future experiments. The main focus is devoted to the thermal phenomena to approximate the cell thermal and electrochemical behaviour as a basic estimation for the detailed design. The latter, however, must be executed by utilising the more detailed models. The previous TSR model proposed by Hosseini et al. [15] only accounts for the reactive areas, including the air/fuel gas channels and PEN structure, while heat transfer phenomena is not limited to the reactive parts only. From thermal assessment viewpoint, heat transfer through non-reactive parts play a leading role in formation of temperature gradients and consequently the cells' overall performance. The model presented in this article, in contrast, considers all geometrical layers in a so-called "Four-Layer TSR" Model" that form an electrochemical cell while still taking advantage of the model's simplicity. Additionally, Hosseini et al. [15] assumed a well-insulated cell that is not the case for a cell embedded inside a furnace. In such a case, heat transfer to the environment and furnace's walls will be a striking feature of a comprehensive model. To address this, an additional compartment is added in current work, i.e., the surrounding furnace equipment. The radiation heat transfer to the cell walls is also added to the model as an extra boundary condition in order to assess its performance under an external heating condition. This is especially important as the experimental cells are usually placed inside a heating chamber for initial warm-up and to keep the reactive cell at designated operating temperature or to minimise the deviation from its set point. We purposefully sought the consistency between the geometries of the improved model and our experimental set-up allowing us to use our experimental results for parameter tuning and model verification.

The study in this chapter is outlined as follows. Firstly, the schematic of the

experimental set up is described and the operating conditions and procedure are briefly presented. Secondly, model structure, assumptions, governing and constitutive equations, and parameters are presented. Thirdly, a parameter tuning is conducted to estimate the uncertain parameters based on experimental data. Subsequently, the model validation against experimental data is carried out to examine both model and adjusted parameters. Finally, the model improvement is illustrated followed by several model-based cell performance analyses.

2.2 Experimental set up and procedure

A series of experiments were carried out to record V-I data of a single electrochemical cell performing under various cell temperatures, which in turn were controlled by furnace temperature controllers. A schematic of the test rig is shown in Figure 2.1.

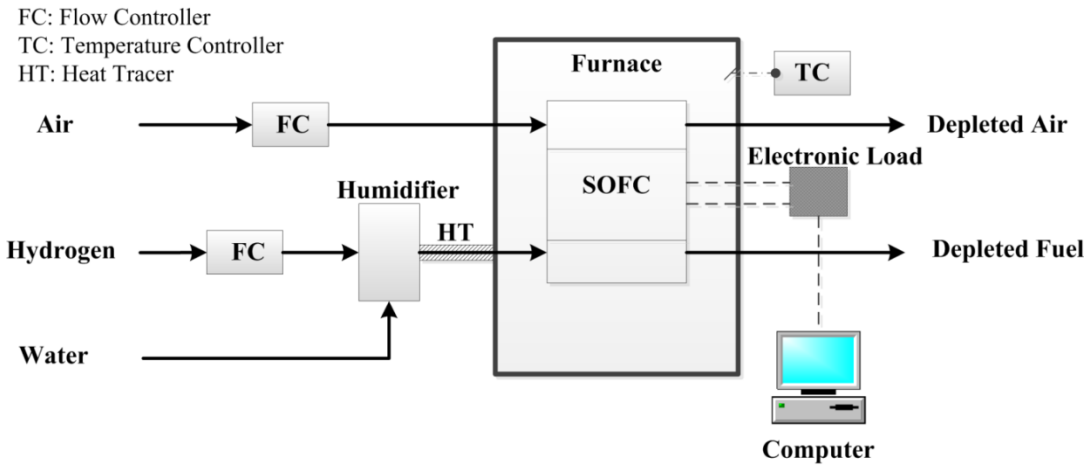

Figure 2. 1: Schematic of the experimental set up.

The set up mainly consists of a furnace chamber, SOFC, humidifier (evaporator),

piping network, and instrumentation. Ceramic Fuel Cells Ltd. (CFCL) supplied the planar SOFC that is used in the experiments. The cell is anode supported, with the anode at the bottom side and cathode at the topside. The cell sizes such as section area, catalyst width, channel height, electrolyte thickness, etc., are listed in Table 2.1.

Table 2. 1: Model parameters mostly compatible with the experimental settings

Parameter	**Anode**	**Cathode**	**Source of data /Comment**
Catalyst width, m	0.25×10^{-3}	0.03×10^{-3}	Experimental set up
Channel height, m	0.45×10^{-3}		Experimental set up
Section area, m^2	3.48×10^{-3}		Experimental set up
Electrolyte width, m	0.03×10^{-3}		Experimental set up
Furnace inner surface area, m^2	0.64		Experimental set up
Pre-exponential kinetic factor, A/m^{-2}	6×10^{8}	9.5×10^{8}	Tuned with experiment
Activation energy, J/mol	1.2×10^{4}	1.2×10^{4}	[21]
Porosity	0.4		Tuned with experiment
PEN conduction coefficient, W/(m K)	2		[26], [27] and [28]
Interconnect conduction coefficient, W/(m K)	24		[29]
Furnace emissivity	0.9		[30]
Cell emissivity	0.1		[30] and [31]

The instrumentation involves elaborately calibrated measurement and control devices such as temperature and mass flow controllers. Moreover, a weight load was placed on the top of the cell to ensure the sealing of the assembly and for establishing contact of the cell with the current collecting layers. Platinum and silver meshes were used for cathode and anode, respectively, to collect the current. In each test run, three stages – heating up, reduction, V-I data recording – were followed.

Firstly in the heating up stage, the furnace and humidifier were set at the required temperature. In this stage, nitrogen and air were introduced for anode and cathode with flow rates around 20 ml/min. Reduction was carried out at 1033 K with a flow of 100 ml/min of hydrogen with humidity of 36%. OCV was monitored until it reached its final value and was compared with theoretical value to ensure that the cell assembly was leak-free. Then, V-I data was collected and recorded for a range of values of I. The electrical load was adjusted through a computer interface with the current sink and the current was set to the maximum value of 12 A. It was then ramped down to 0 A at the rate of 5 A/min to generate the V-I curve. The operating conditions for the experiment are listed in Table 2.2. The operational and physical parameters used for the experiment and model are identical as given in Tables 2.1 and 2.2, respectively.

Table 2. 2: Operating conditions

Variable	**Value**	**Comments**
Fuel (Hydrogen) flow rate, ml/min	100	
Oxidant(Air) flow rate, ml/min	500	
Hydrogen molar fraction in Fuel	0.64	Mixed with steam
Oxygen molar fraction in Air	0.21	Mixed with nitrogen
Furnace Temperature , K	1033, 1053, 1083	3 independent runs
Pressure, Pa	1×10^5	

2.3 Layered-TSR modelling framework

2.3.1 Model structure

The Four-Layer model that is proposed and developed in this work consists of the main structural solid components of planar SOFC including PEN, top and bottom interconnects, and the test stand. The PEN is the media for the electrochemical reaction and possibly the fuel reformation reactions (in internal reforming cases).

The gas channels transport heat, reactants, products, and inert species into and from cell. Additionally, the internal mass and heat transfer between layers and inside structures must be considered in a distributed model. The generated current through the reaction is collected via the interconnect compartment. The test stand is a foundation for fixing and supporting the cell inside the furnace chamber.

Figure 2.2 displays a schematic presentation of the model structure in which multiple layers and air and fuel flow paths inside the cell are shown. The cell structure is divided into four layers. In each layer the solid and gas parts are divided into several lumped elements. A network of these elements/modules, subsequently approximate the flow fields and distributed thermal and electric fields in two dimensions (x, y) for each layer. From reaction engineering viewpoint, the reactive module (element) performs as a 0D reactor in which spatial variations are ignored to reasonably simplify the complexities. The governing and constitutive equations for each lump element of the model mainly consist of mass, energy, and charge balances and those correlations used for species properties such as ideal gas equation of state. These equations describe the different phenomenon such as heat exchange, gas transport, etc., that occur in each module. The interaction between layers such as energy exchanges illustrated in Figure 2.2 or between modules within a layer can be applied through the integration of the adjacent modules. Table 2.3 presents the equations that should be solved simultaneously by using numerical methods. Each layer is simulated through 10×10 elements/tanks. The equations are defined in time. Nevertheless, the results for steady state are reported in this study by solving the equations for time of a 1000s, at which the steady state condition can be achieved. Modular networking subsequently enables us to capture the local values of distributed variables. Detailed description about modular networking including consideration of the flow patterns is presented in our previous studies [15], [16] and [17]. Besides, the estimation of the number of reactor-in-series is presented by some

of the co-authors in [16]. In the experimental set-up, the SOFC is placed in a heating furnace, where radiation heat exchange occurs between the outer surface of the cell and the inner wall of the furnace. This heat transfer interaction affects the external and internal temperature distribution of the cell and therefore its internal performance [18]. The inner surface of the electric furnace chamber is normally kept at a constant temperature through a temperature controller. By incorporating these phenomena the enhanced model becomes general enough to simulate a perfectly insulated cell and also a cell with radiation at outer surfaces. In this study, these two cases are referred to as "simple model" and "comprehensive model", respectively. Meanwhile, a case in which heat conduction occurs from PEN to interconnect, in addition to convective heat transfer from PEN to fluids, can also be simulated while the cell is well insulated. We call this case as the "improved model" in this study.

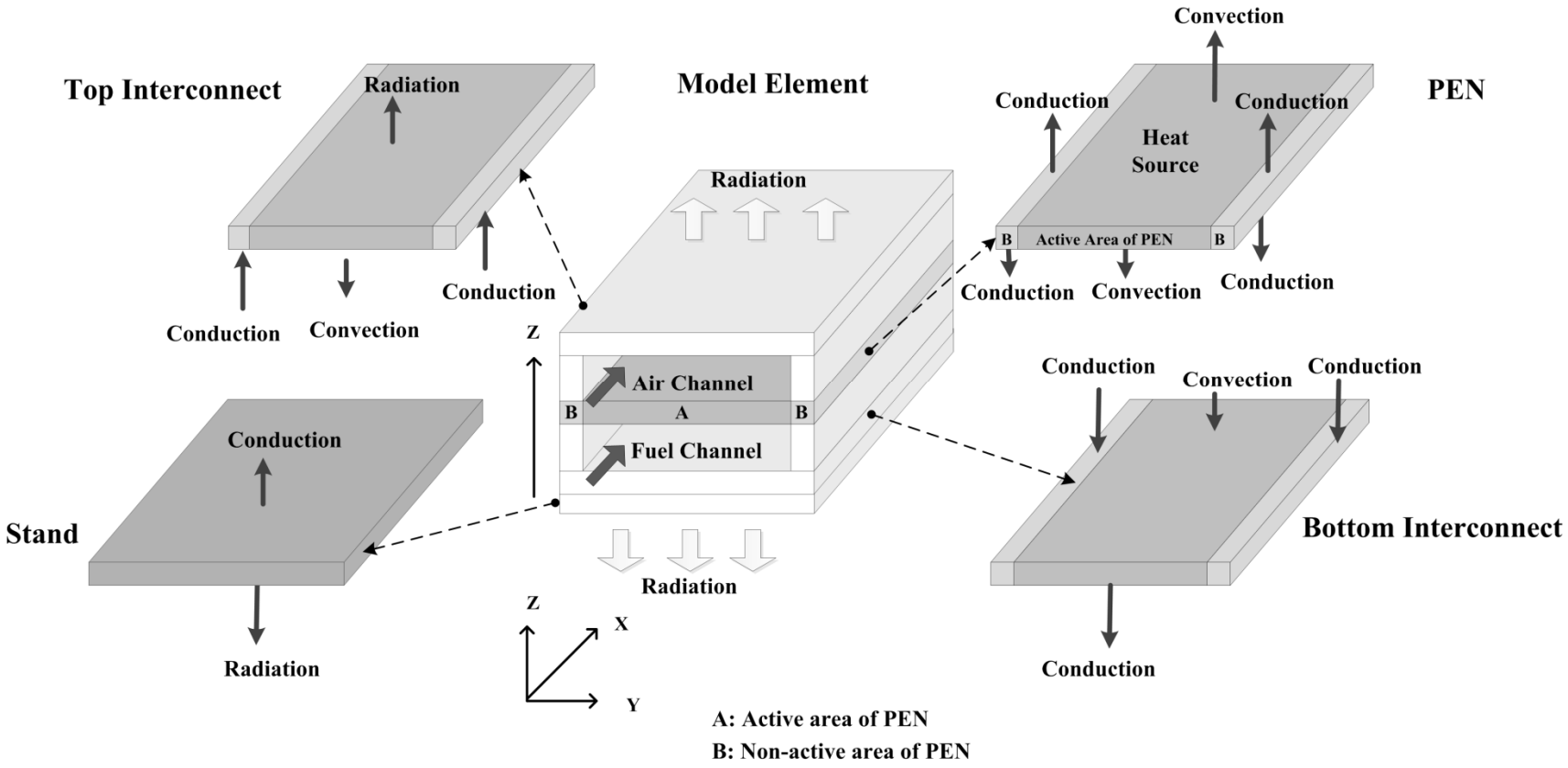

Figure 2. 2: Schematic of the model's layers

Table 2. 3: Governing and constitutive equations for layers [15], [20] and [21]

Energy Balances	**Equations set**
Stand	$V^{St}\rho^{St}C_p^{St}\frac{dT^{St}}{dt}=Q_{cond}^{St-Ib}+Q_{radi}$
Bottom interconnect	$V^{f}\rho^{f}C_p^{f}\frac{dT^{f}}{dt}=(F_{in}^{f}\Delta h_{in}^{f}-F_{out}^{f}\Delta h_{out}^{f})+Q_{conv}^{Ib-f}$
	$V^{a}\rho^{a}C_p^{a}\frac{dT^{a}}{dt}=(F_{in}^{a}\Delta h_{in}^{a}-F_{out}^{a}\Delta h_{out}^{a})+Q_{conv}^{Ib-a}$
	$V^{Ib}\rho^{Ib}C_p^{Ib}\frac{dT^{Ib}}{dt}=Q_{cond}^{Ib-St}+Q_{cond}^{Ib-PEN}+Q_{conv}^{Ib-a}+Q_{conv}^{Ib-f}$
PEN	$V^{a}\rho^{a}C_p^{a}\frac{dT^{a}}{dt}=(F_{in}^{a}\Delta h_{in}^{a}-F_{out}^{a}\Delta h_{out}^{a})+Q_{conv}^{PEN-a}$
	$V^{f}\rho^{f}C_p^{f}\frac{dT^{f}}{dt}=(F_{in}^{f}\Delta h_{in}^{f}-F_{out}^{f}\Delta h_{out}^{f})+Q_{conv}^{PEN-f}$
	$V^{PEN}\rho^{PEN}C_p^{PEN}\frac{dT^{PEN}}{dt}=Q_{cond}^{PEN-Ib}+Q_{cond}^{PEN-It}+Q_{conv}^{PEN-a}+Q_{conv}^{PEN-f}+Q_{gen}$
Top interconnect	$V^{a}\rho^{a}C_p^{a}\frac{dT^{a}}{dt}=(F_{in}^{a}\Delta h_{in}^{a}-F_{out}^{a}\Delta h_{out}^{a})+Q_{conv}^{It-a}$
	$V^{It}\rho^{It}C_p^{It}\frac{dT^{Ib-It}}{dt}=Q_{cond}^{It-PEN}+Q_{conv}^{It-f}+Q_{radi}$
Constitutive equations	$Q_{gen}=((-\frac{\Delta H_R}{2F_N}-U_{cell})+(\frac{C_p^{H_2}-C_p^{H_2O}}{2F_N})(T^{f}-T^{PEN})+(\frac{C_p^{O_2}}{4F_N})(T^{a}-T^{PEN}))I$
	$Q_{conv}^{S-G}=\alpha\, S_c(T^{S}-T^{G})$
	$Q_{cond}^{S_1-S_2}=\frac{K}{d}S_c(T^{S_1}-T^{S_2})$
	$Q_{radi}=\frac{5.67S_{e\,fur}[(\frac{T_{fur}}{100})^4-(\frac{T_{cell}}{100})^4]}{\frac{1}{\varepsilon_{fur}}+\frac{S_{e\,fur}}{S_{e\,cell}}(\frac{1}{\varepsilon_{cell}}-1)}$
Mass Balances	
Gas Channels	$V^{f}\rho^{f}\frac{dy^{H_2}}{dt}=F_{in}^{f}y_{in}^{H_2}-F_{out}^{f}y_{out}^{H_2}-\rho^{f}K_e^{H_2}S_e(y^{H_2}-y_{cat}^{H_2})$
	$V^{f}\rho^{f}\frac{dy^{H_2O}}{dt}=F_{in}^{f}y_{in}^{H_2O}-F_{out}^{f}y_{out}^{H_2O}-\rho^{f}K_e^{H_2O}S_e(y^{H_2O}-y_{cat}^{H_2O})$
	$V^{a}\rho^{a}\frac{dy^{O_2}}{dt}=F_{in}^{a}y_{in}^{O_2}-F_{out}^{a}y_{out}^{O_2}-\rho^{a}K_e^{O_2}S_e(y^{O_2}-y_{cat}^{O_2})$

Diffusion Layers	$V_{cat}^{f}\ \rho^{f}\ \frac{dy_{cat}^{H_2}}{dt} = \rho^{f} K_e^{H_2} S_e (y^{H_2} - y_{cat}^{H_2}) - r^{H_2}$
	$V_{cat}^{f} \rho^{f}\ \frac{dy_{cat}^{H_2O}}{dt} = \rho^{f} K_e^{H_2O} S_e (y^{H_2O} - y_{cat}^{H_2O}) + r^{H_2O}$
	$V_{cat}^{a} \rho^{a}\ \frac{dy_{cat}^{O_2}}{dt} = \rho^{a} K_e^{O_2} S_e (y^{O_2} - y_{cat}^{O_2}) - r^{O_2}$
Constitutive equations	$r^{H_2} = S_e \frac{\upsilon^{H_2} i^{A}}{n_e^{A} F_N}$
	$r^{H_2O} = S_e \frac{\upsilon^{H_2O} i^{A}}{n_e^{A} F_N}$
	$r^{O_2} = S_e \frac{\upsilon^{O_2} i^{C}}{n_e^{C} F_N}$
	$K_e(T) = \frac{D_{298}}{L} (\frac{T}{298})^{1.5} \delta^{\tau}$
Charge Balance	
Anode-electrolyte Interface	$C_{dl}^{A} \frac{d\eta_A}{dt} = (i_{cell} - i^{A})$
Cathode-electrolyte Interface	$C_{dl}^{C} \frac{d\eta_C}{dt} = (-i_{cell} - i^{C})$

2.3.2 Model development

The following assumptions are used in formulating and solving the model:

- Each gas module is considered as a CSTR;
- Electrochemical reactions take place at the interface of the anode/cathode and the electrolyte;
- The operatingng pressure and voltage are assumed to be constant;
- Ohmic drops in the current collectors and electrical connections are negligible;
- All gases are treated as ideal gas;
- Radiation heat transfer within the cell is not considered.

- Although the model is essentially capable for 2D cell simulation (x, y in Figure 2.2), a co-flow pattern for fuel and air is emphasized in this study in which distributions are just significant in the flow direction (x). Nevertheless, for temperature distribution analysis a multi-layer geometry is considered. Therefore, the third dimension (z) in this study refers to the layering direction as shown in Figure 2.2.

The physicochemical phenomenon involved in this model comprises of electrochemical reaction, heat transfer (conduction, convection, and radiation), and diffusion in the pores, mass transfer, and charge transfer.

2.3.3 Parameter adjustment and model validation

The model was programmed and numerically solved in Matlab®R2010b by using its numerical facilities for simultaneously solving the differential and algebraic equations, and it took approximately150 seconds for the computation of each case. The computation time is largely reduced compared to the common 3D CFD models, which would take several hours to converge. The operational and physical parameters used in the solution are similar to those applied in the experiments as mentioned before and are presented in Tables 2.1 and 2.2, respectively. The constant value for the parameters are used and selected according to the literature, where similar operation is processed. Nevertheless, model verification and validation are conducted with the experimental data in different conditions in order to eliminate the inaccuracy caused by the variation of parameters under different conditions.

Significant uncertainty in kinetics and physical parameters is reported in literature. For instance, a large variation for K_0^A , K_0^C (2.9×10^8 ~2.35×10^{11} A/m^{-2}, 7×10^8

~6.54×10^{11} A/m^{-2} for K_0^A, K_0^C, respectively) can be seen in references. [8], [19], [20] and [21]. Different porosity values (0.2 ~0.5) are also used in various studies [22], [23], [24] and [25]. In this study, therefore, we conducted parameter adjustment calculations prior to the final step of model verification. Initially, the values of the uncertain parameters including pre-exponential factor (K_0 in Equation 2.1 and 2.2 from references [20] and [21]) and porosity coefficient (δ in Equation 2.3) were estimated by minimising an error function that is defined by Equation 2.4, wherein the minimization of the deviation between experimental data and simulation results is targeted. For each set of data, 10 points are selected accordingly for this parameter fitting calculation. The initial values of K_0^A, K_0^C and δ were selected as 2.9×10^8 A/m^{-2} , 7×10^8 A/m^{-2} [21] and 0.3 [22]. The optimum values found for these parameters are within the range reported in literature as are shown in Table 2.1.

$$i_0^A = K_0^A (y^{H_2})^{\gamma_{H_2}} (y^{H_2O})^{\gamma_{H2O}} \exp(-\frac{E_{act}^A}{RT}) \quad (2.1)$$

$$i_0^C = K_0^C (y^{O_2})^{\gamma_{O_2}} \exp(-\frac{E_{act}^C}{RT}) \quad (2.2)$$

$$K_e(T) = \frac{D_{298}}{L} (\frac{T}{298})^{1.5} \delta^{\tau} \quad (2.3)$$

$$E(K_0^A, K_0^C, \delta) = \sum_{i=1}^{k} (i_{\exp,i} - i_{sim,i})^2 \quad (2.4)$$

where i_{exp} and i_{sim} are current density, at a given voltage, measured by experiments and calculated by the model, respectively. Reaction orders/exponents (γ) in Equations 2.1 and 2.2 are 1, –0.5, 0.25 for hydrogen, water, and oxygen, respectively [21]. L stands for the diffusion layer thickness which is considered to be equal to the channel height. Minimization of the objective function by manipulating uncertain values, results in the best possible fitting between model predictions and experimental data at a given temperature (1053 K), as presented in

Figure 2.3.

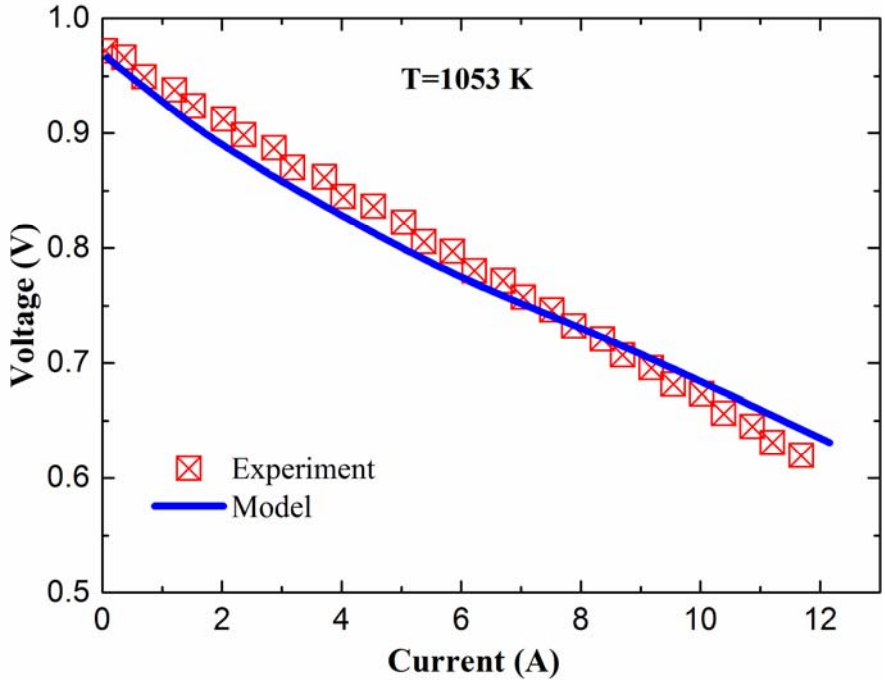

Figure 2. 3: The results of parameter adjustment at 1053 K

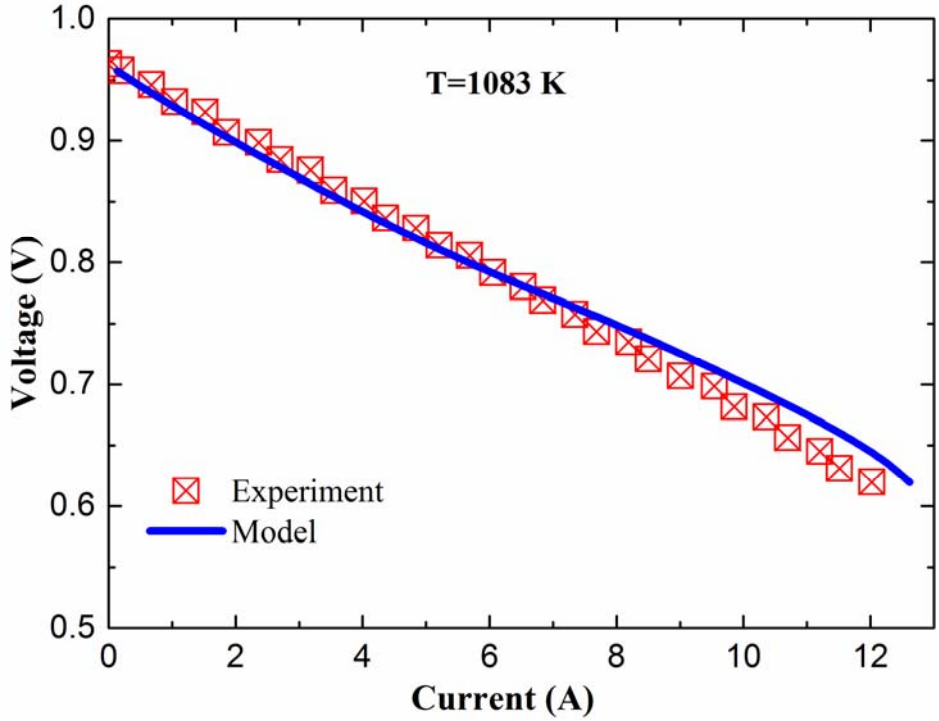

Figure 2. 4: Model validation at 1083 K

The optimized parameters, therefore, were estimated based on a set of V-I data as presented in Table 2.1. Subsequently, optimized parameters estimated in the previous step and an independent set of practical V-I data–achieved at a different temperature (1083 K) were utilized to examine the model performance under a varied operational condition. The model validation is shown in Figure 2.4. As can be seen in this figure, the model's prediction properly matches the experimental data. Moreover, the errors (listed in Table 2.4) measure the deviation of the calculated data from their corresponding experimental data. For both cases, small error values are obtained, which indicates that the model's prediction is in good agreement with the practical data at different conditions without the necessity of any further parameter adaptation /variation.

Table 2. 4: Error function values for two models at different temperatures

Furnace Temperature, K	**1083**	**1033**
Adiabatic	1.71	1.96
Non-adiabatic	0.33	0.50

2.4 Results and discussion

A characteristic V-I curve enables the interpretation of the overall performance of the electrochemical reactor. Further detailed-insights, however, must be attained by analysing the internal distributed variables' profiles, such as the spatial distribution of temperature, current, voltage, species, and over-potentials to appropriately assess the cell's efficiency, reliability, and durability under various operational conditions. In this part, comparison between adiabatic and non-adiabatic processes is conducted initially through V-I curve analysis (Figure 2.5) followed by the

evaluation of the distributed variables (Figure 2.6–2.9). The main objective of this model-based analysis is to quantify and explain the role of external heat losses on the cell's behaviour.

2.4.1 Demonstration of the model improvement

The simulated V-I for two operating modes are compared to the experimental data obtained with two furnace temperatures (1033 K and 1083 K) as depicted in Figure 2.5(a) and (b), respectively. In order to quantify the deviations of the model predictions from the test data, the error values are also estimated based on Equation 2.4 and presented in Table 2.4. As can be observed in these characteristics graphs, over the low current range, adiabatic and non-adiabatic models perform almost close to the experimental data. However, discrepancy between adiabatic and non-adiabatic models results becomes more significant with increasing current. The latter case reasonably represents the practical data. This observation can be attributed to the temperature increase with the drawn current. Higher current withdrawal drives the exothermic reaction and hence the heat generation. The predicted temperature under adiabatic condition, therefore, is more likely to be overestimated due to heat accumulation caused by ignoring the heat loss across the cell's boundaries. As the electrochemical reaction inside the fuel cell has an autothermal nature, the reaction progress and hence the generated current might be overestimated too. These are reciprocal impacts indeed. For the non-adiabatic model, the formulated heat loss from boundaries leads to a more realistic temperature prediction as the V-I outcome is consistent with the experiments.

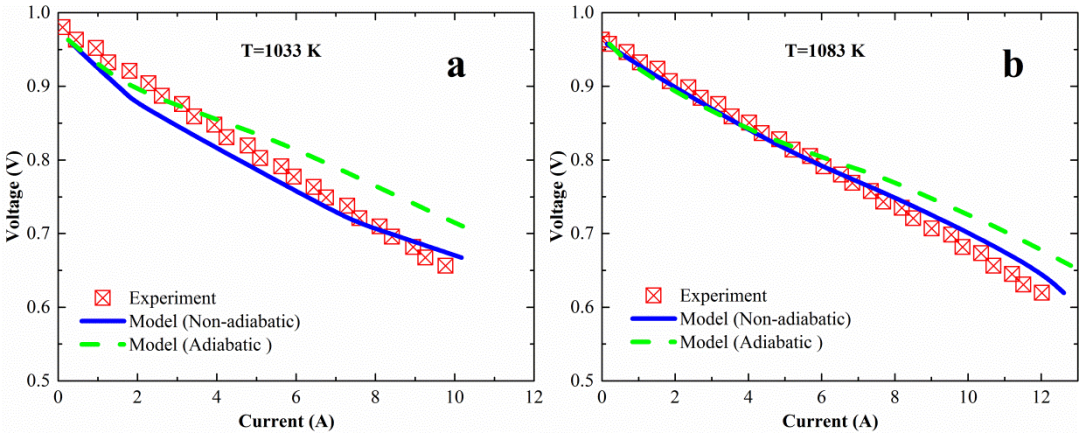

Figure 2. 5: Model improvement demonstration at: (a) 1033 K, (b) and 1083 K

Moreover, the predicted operating voltage for the adiabatic condition is higher than the experimental value for a given amount of produced current due to the lower total voltage losses estimated under an unrealistic temperature. The detailed breakdown of the overpotentials evaluated at low (1.3 A) and high (7.8 A) currents is tabulated in Table 2.5.

Table 2. 5: Voltage losses under different operating conditions

Variable	Current = 1.3 A		Current = 7.8 A	
	Non-adiabatic	Adiabatic	Non-adiabatic	Adiabatic
Temperature, K	1042	1055	1115	1227
OCV, V	0.965	0.961	0.889	0.867
Activation overpotential, V	0.048	0.041	0.159	0.085
Ohmic overpotential, V	0.006	0.006	0.021	0.011
U_{cell}, V	0.910	0.914	0.710	0.771

For two parallel surfaces at temperatures T_1 and T_2, the amount of heat transferred through radiation is proportional to $T^3\Delta T$ where T is average of T_1 and T_2, i.e., $(T_1+T_2)/2$, and ΔT is the temperature difference i.e., $(T_1 - T_2)$ between the surfaces. Since the furnace temperature is constant, external heat transfer through radiation becomes more significant at higher reactive-cell temperature. Therefore, the observed discords between adiabatic and non-adiabatic models' results become more significant at elevated temperatures that correspond to higher current values.

2.4.2 Thermal comparison of adiabatic and non-adiabatic operations

Figure 2.6 displays the electrochemical reaction heat and also the contribution of different mechanisms in cooling of the PEN structure along the fluids' path for both adiabatic and non-adiabatic operations. In Figure 2.7, the temperature profiles in various parts of the cell structure are presented.

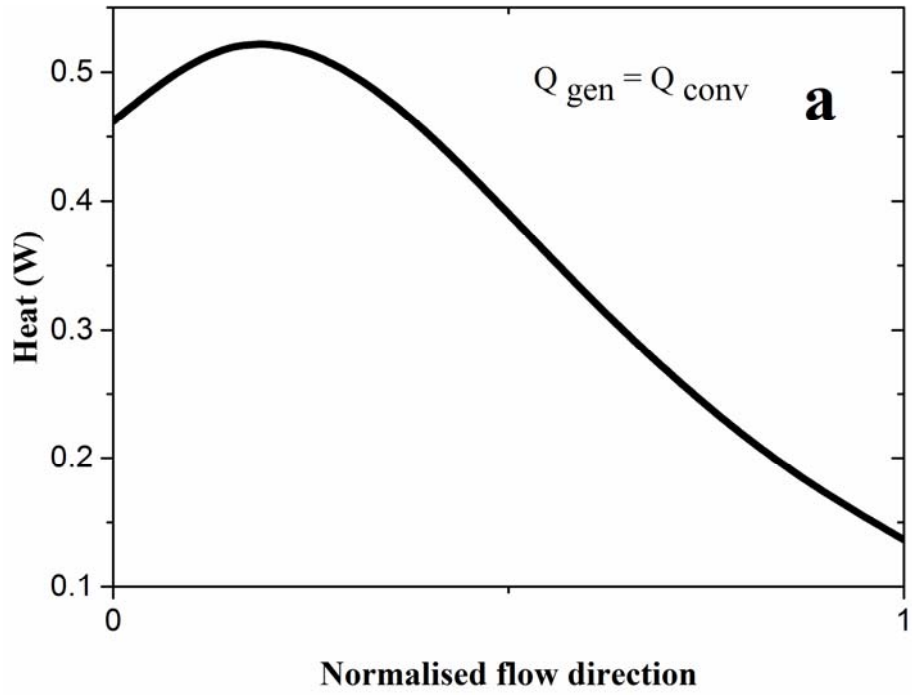
Q gen = Q conv
a
Heat (W)
0.5
0.4
0.3
0.2
0.1
0
1
Normalised flow direction

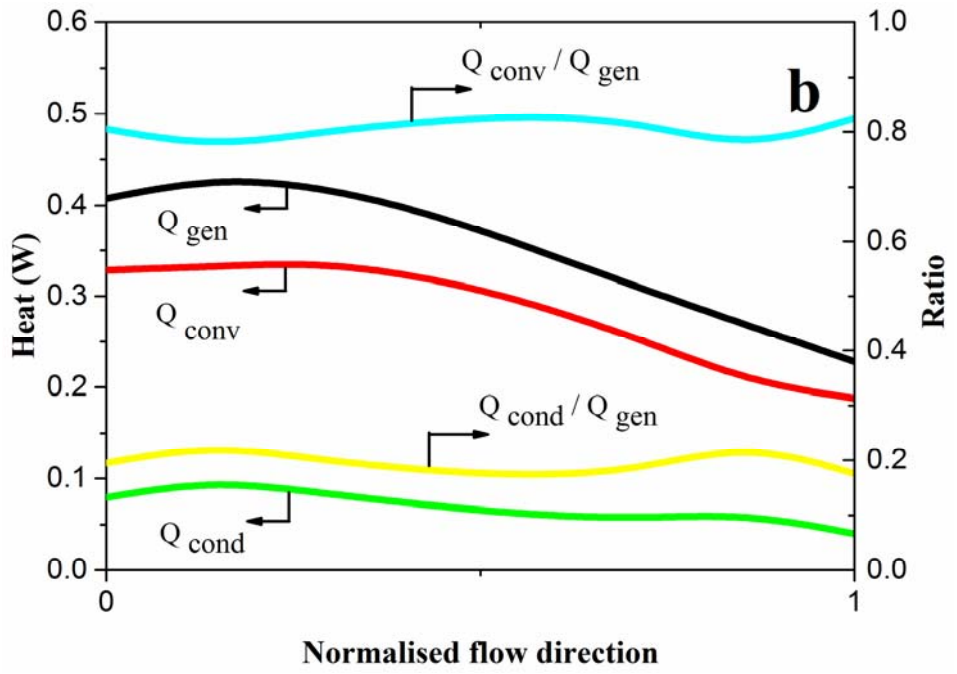
Q conv / Q gen
b
Q gen
Q conv
Q cond / Q gen
Q cond
Heat (W)
Ratio
0.6
0.5
0.4
0.3
0.2
0.1
0.0
1.0
0.8
0.6
0.4
0.2
0.0
0
1
Normalised flow direction

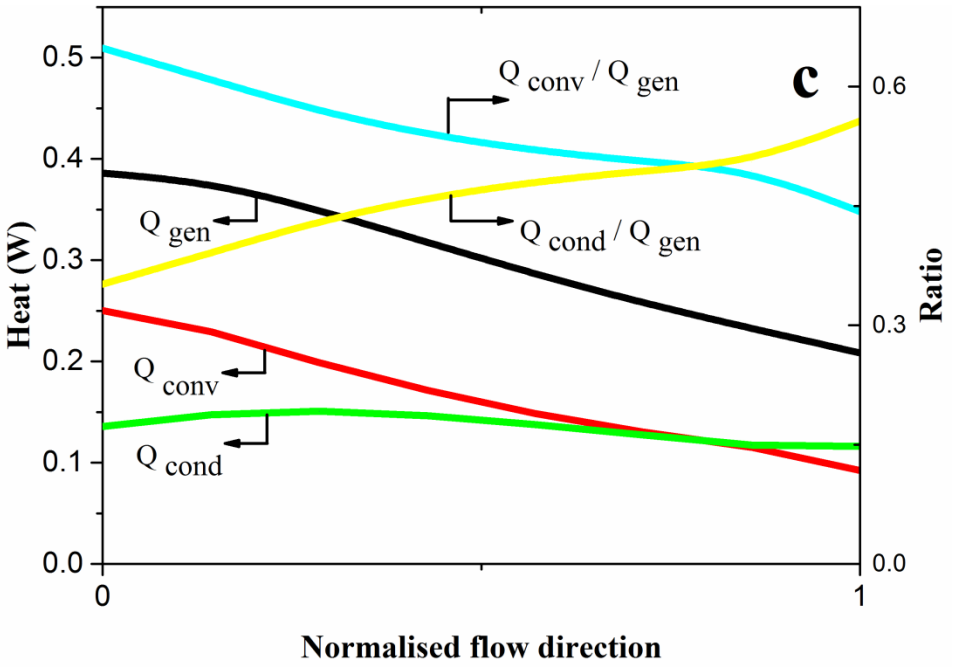

Figure 2. 6: Heat transfer distributions: (a) adiabatic condition ("simple model"), (b) adiabatic condition ("improved model"), (c) non-adiabatic condition ("comprehensive model").

For a well-insulated system predicted by the "simple model", the electrochemical reaction reaches a peak rate as indicated through the maximum point observed in the generated-heat profile shown in Figure 2.6(a). While the formation of such a peak can be explained based on mutual impact of elevated temperature and the authothermal reaction's progress, the declining region seen after this peak is mainly because of the depletion in hydrogen/fuel concentration. Note that according to this level of modelling, the heat removal from PEN proceeds just through convection to air and fuel sides cause temperature growth in them as can be seen in Figure 2.7(a). This figure also shows that fluids temperature can be a reasonable approximation, but not perfect, indication for PEN temperature at cell's outlet point.

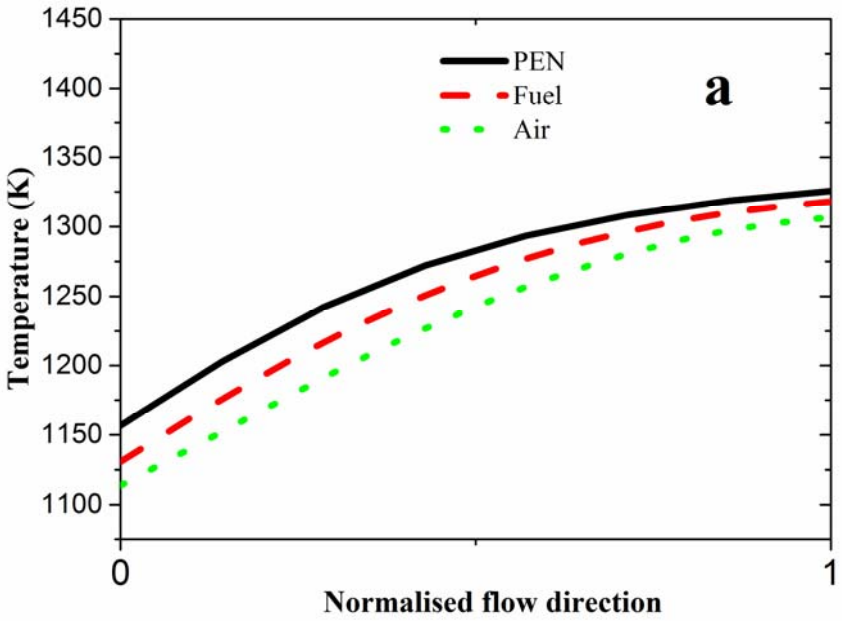
1450
1400
1350
1300
1250
1200
1150
1100
Temperature (K)
PEN
Fuel
Air
a
0
1
Normalised flow direction

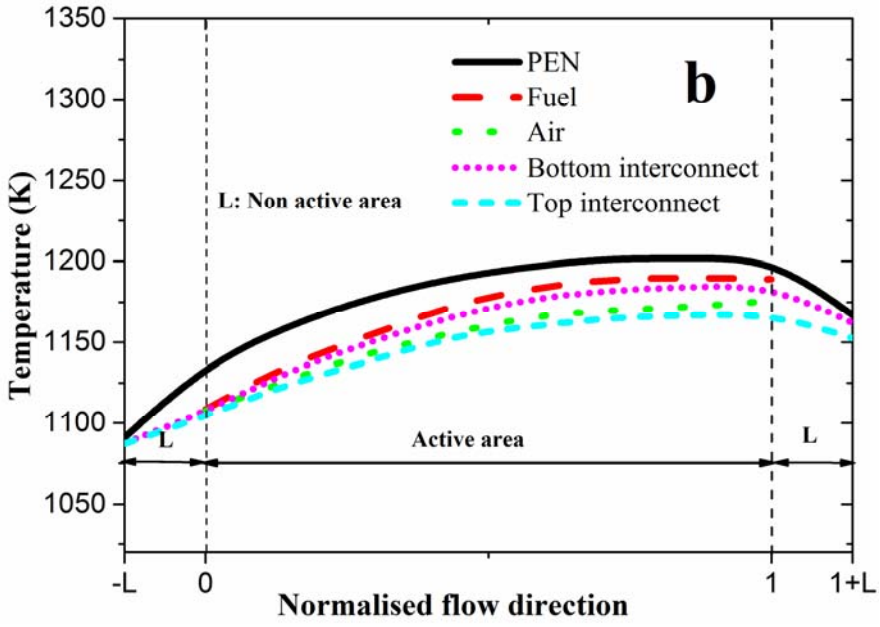
1350
1300
1250
1200
1150
1100
1050
Temperature (K)
PEN
Fuel
Air
Bottom interconnect
Top interconnect
b
L: Non active area
L
Active area
L
-L
0
1
1+L
Normalised flow direction

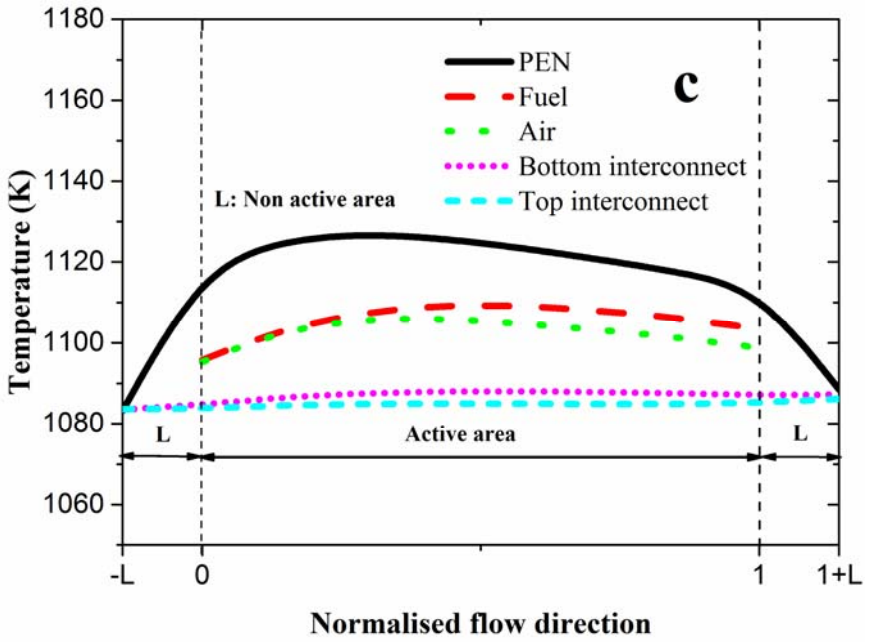

Figure 2. 7: Temperature distributions: (a) adiabatic condition ("simple model"), (b) adiabatic condition ("improved model"), (c) non-adiabatic condition ("comprehensive model")

In the "improved model" heat conduction to other layers (interconnects in particular) are also taken into account, in addition to the heat convection to fluids, Figure 2.6(b), while still assuming no heat loss to the surrounding environment. The trends of the released enthalpies, associated with the electrochemical reaction, are generally similar to those achieved by the "simple model". In spite of this, there are significant differences among the role of the heat transfer mechanisms, temperature profiles, and gradient. In the "improved model", the average generated enthalpy, known as the reaction progress characteristic, is essentially lower and spatially smoother than that observed for the "simple model". This is fundamentally rooted in the role of the conduction mechanism in increasing the total heat transport from PEN and hence creates a cooler media for running the reaction and in return resulting in less reaction enthalpy. Moreover, heat conduction improves the spatially distributed heat removal that results in a smoother PEN temperature

profile as shown in Figure 2.7(b). Nevertheless, the share of the convection mechanism in the cooling process is significantly higher than the conduction, which might be justified based on the values of heat exchange coefficients as well as the effective areas allocated to each mechanism. Moreover, their contributions in cooling (Q_{conv}/Q_{gen} and Q_{cond}/Q_{gen} in Figure 2.6(b)) do not change considerably along the cell's length because the driving forces for heat transfer, i.e., fluids-PEN and interconnects-PEN temperature differences, decline in a similar way for both heat transport mechanisms. In this model, estimation of the temperature profiles for bottom and top interconnects are also feasible, as presented in Figure 2.7(b). These are supposed to be close to the values measured at the outer surface of a cell. Generally, having no thermal exchange to the surrounding environment results in the warming up of the cell's structure along the cell's length due to the heat accumulation inside its boundaries.

For the most comprehensive scenario in which cell insulation is absent, the radiation from the boundaries to the furnace is accounted for in a so-called "comprehensive model". The model results for heat transfer rates and temperature profiles are presented in Figures 2.6(c) and 2.7(c), respectively. Note that heat radiation from PEN is neglected in this article, as has already been indicated in section 2.3.2.

For a comprehensive case study, the trend of the reaction progress (Figure 2.7(c)) and its maximum is observed to be essentially similar to those seen in Figures 2.6(a) and (b). However, the peak of the profile is suppressed and shifted to the cell's inlet, where the reaction rate reduces with the with cell length after passing its maximum. The reaction suppression can be attributed to the depletion of both reactants and temperature reduction. The latter can be seen in Figure 2.7(c).

From a thermal management viewpoint, the comprehensive case behaves

significantly different to the two simpler cases mentioned before emphasising the importance and added-value of modelling improvement proposed in this study. The reduced temperature gradient verifies the role of the auxiliary furnace in achieving a more homogeneous operation. Moreover, the reason behind the reaction behaviour mentioned for previous two cases can also be sought for the observed thermal homogeneity. In other words, the mutual interaction between reaction progress and temperature distribution describes the lower gradients observed in such a case. It should be noted that neither equal nor constant contributions were recorded for the heat transport mechanisms in PEN cooling process along the length of cell. As Figure 2.6(c) shows, convection phenomena has crucial role at cell's inlet zone while considerably declining along the fluid route. The conduction rate experiences slight changes in its total amount but its contribution to the PEN cooling process rises by the cell's length outweighing the convection's role at the cell's outlet. Discrete temperature profiles in various parts of the cell allow us to appropriately interpret these observations. As is shown in Figure 2.7(c), decreasing PEN–fluids temperatures' difference across the fluids' path is captured. This consequently suppresses the heat convection for given heat transfer coefficient and surface. The most important outcome of this analysis is to figure out the error that may occur in the cell's design, thermal management, and operation simulation by ignoring the heat transport through radiation/conduction when the system is not perfectly insulated. The temperature profile is a key factor for the cell performance. Moreover, the temperature gradient along the cell is the most important cause for the thermal stresses inside the cell, which would result in the cracking and/or the degradation. The distributed temperature estimation in all involved layers, therefore, plays a pivotal role in managing the cell's reliability and life-durability. This article emphasises these insights. This study also demonstrates that thermal analysis outcome of a single cell under the external heating condition cannot be directly generalised for the insulated commercial stack.

Besides, in some studies the temperature gradient along the fluid's path is neglected. Furthermore, the cell temperature is assumed to be identical to the gases' temperature. These simplifications are declared to be more applicable for the low flow rates of gases [32]. Our analysis shows that there could be some notable concerns about these simplifying assumptions. As can be seen in Figures 2.7(a) and (b) there might be a considerable temperature gradient in all directions of an externally insulated cell. For a cell without insulation, conversely, the homogenous temperature profile along the cell length seems reasonable, whilst equality of fluid temperatures to the PEN and the interconnects temperatures along the flow course could be a restrictive assumption (Figure 2.7(c)) though it is relevant at the outlet point. Therefore, the justification of the mentioned assumptions for a reactive cell is strongly dependent on whether it is operating adiabatically or non-adiabatically and also the operatingng conditions such as gas flows.

Note that in spite of the small changes observed in interconnects' temperature in Figure 2.7(c), it is gentle enough to reasonably justify the middle point of interconnect as the suitable location to install a measuring thermocouple in an experiment with air/fuel co-current flow pattern.

In order to further analyse the cell's behaviour, the process performance in terms of the voltage values is assessed. A constant operational voltage is considered in this study (U_{cell} = 0.81 V). However, open circuit voltage (OCV) and voltage losses (overpotentials or polarizations are alternative terminologies) may vary according to local temperature and species compositions. The difference between OCV and operational voltage indicates the total voltage losses including electrochemical activation obstacles at anode and cathode and the ohmic resistance. Note that concentration overpotential is neglected in this study as it is only significant at very low reactants concentrations (very high fuel utilization) that cause insufficient diffusion of reactants and products in electrodes. Figure 2.8 shows variation of

OCV and potential losses captured through different modelling approaches. The adiabatic and non-adiabatic processes are modelled by "improved" and "comprehensive" models, respectively. As can be seen in Figure 2.8, OCV values are higher in a non-adiabatic process compared to that of an adiabatic process, which is attributed to the differences in temperature and hydrogen partial pressure. In other words, summation of voltage losses is higher in a cell with thermal interaction with environment because of lower average temperature. This results in decreasing current generation. Accordingly, lower temperature gradients and reduced current are two sides of a coin that must be compromised in a controlled operation. Lower gradient in OCV profile associated with non-adiabatic system can be linked to its temperature and reaction characteristics profiles as shown in Figures 2.7(c) and 2.6(c), respectively.

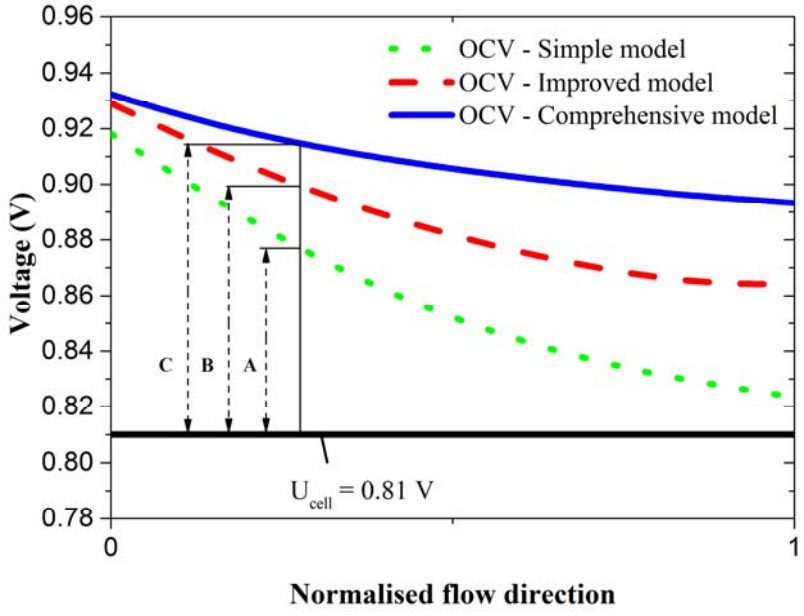

Figure 2. 8: OCV and Voltage losses captured through different modelling approaches. Voltage losses are summation of ohmic and activation losses shown by A for "simple model", B for "improved model", and C for "comprehensive model" all under same operating conditions**.**

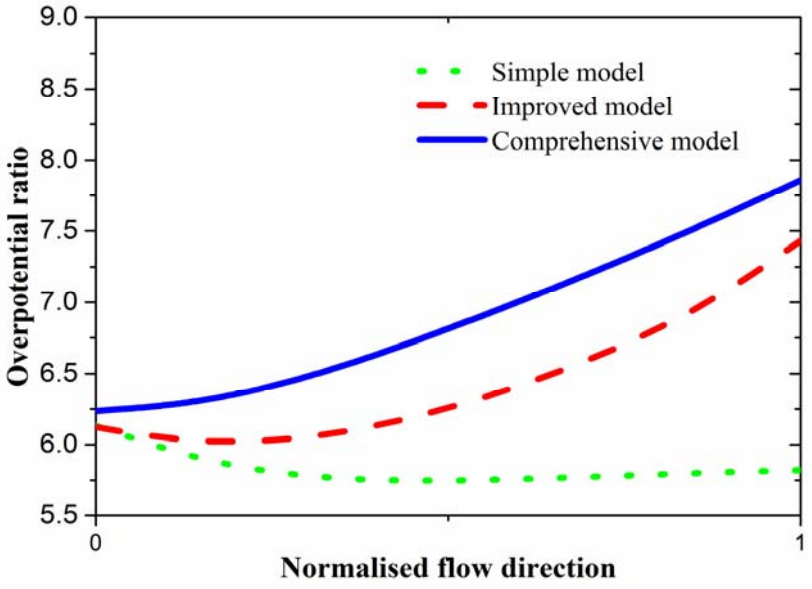

Figure 2. 9: Overpotentials' ratio (activation-to-ohmic) for adiabatic and non-adiabatic operations.

The contributions of voltage losses in the reduction of operation voltage, from ideal to practical values, allow more precise understanding of the controlling polarization mechanism along the cell. Figure 2.9 shows the ratio of activation-to-ohmic polarization for adiabatic and non-adiabatic processes along the flow direction. The profile indicates that activation polarization outweighs the ohmic polarization in both operational modes and at all points of cell. Nevertheless, the ratio trends are considerably different for the different modelling approaches that emphasises the importance of appropriate thermal modelling.

2.4.3 Model-based design of experiments

Among the striking features of a reliable mathematical model is to provide us with a tool for shortlisting the experiments in order to avoid unnecessary runs and subsequently reduce the research and development costs, safety risks, and time. A

decision-making procedure is exemplified here to illustrate the proposed model capabilities assisting the design-of-experiments. The term ‘design-of-experiment’ here refers to parameter adjustment for experiment, but not from a system perspective.

Even though, internal endothermic fuel reforming reactions may reduce the cell’s temperature in the case of hydrocarbon fed SOFC; this is not the case for external reforming and pure hydrogen fuelled cells. For an adiabatic cell fed with pure hydrogen, air acts as the main coolant dominating the cell temperature, even though fuel stream can be slightly effective too [16]. For a non-adiabatic system, however, ambient/furnace temperature and gas streams might have influence on the heat-removal rates. Therefore, these variables are central to adjusting the operational temperature of a reactive cell. Due to the high non-linearity of the system, the interactions between these variables are very complicated and make the utilization of numerical model inevitable.

The PEN temperature is the most appropriate indicator of thermal status of a reactive cell as it would be used for calculation of diffusion and reactions rates, heat and ion conductions, voltage losses, etc. Unfortunately, it is technically complicated and costly to measure the PEN temperature and its distribution, in particular, via thermocouple due to difficulties associated with sealing. Moreover, in order to safely and efficiently run a SOFC in practice, PEN temperature is always among the operating variables that ideally are supposed to be constant or experience very minor spatio-temporal changes. Figure 2.10 depicts a model-based operational map to adjust furnace temperature under various fuel flows rates in order to achieve desired PEN temperature value as a model-based approximated value. It should be noted that the reasonable excess air range is considered from references [33] and [34]. The operational map is strongly dependent on the set-up properties and operating conditions. Therefore, generalization of the mentioned graph to other

setups and conditions is not the goal here. In contrast, the methodology presented in the current work may be applied to any case of interest subject to the appropriate parameter adjustments and model modifications

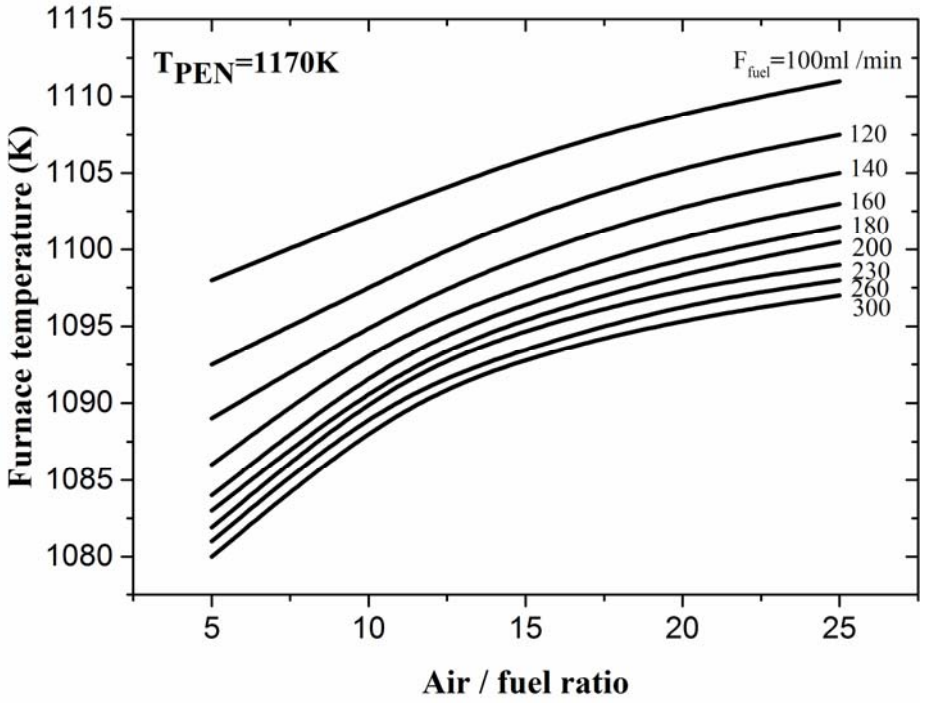

Figure 2. 10: Furnace temperature required to active a particular average cell temperature (1170 K) under different fuel and air flow rates.

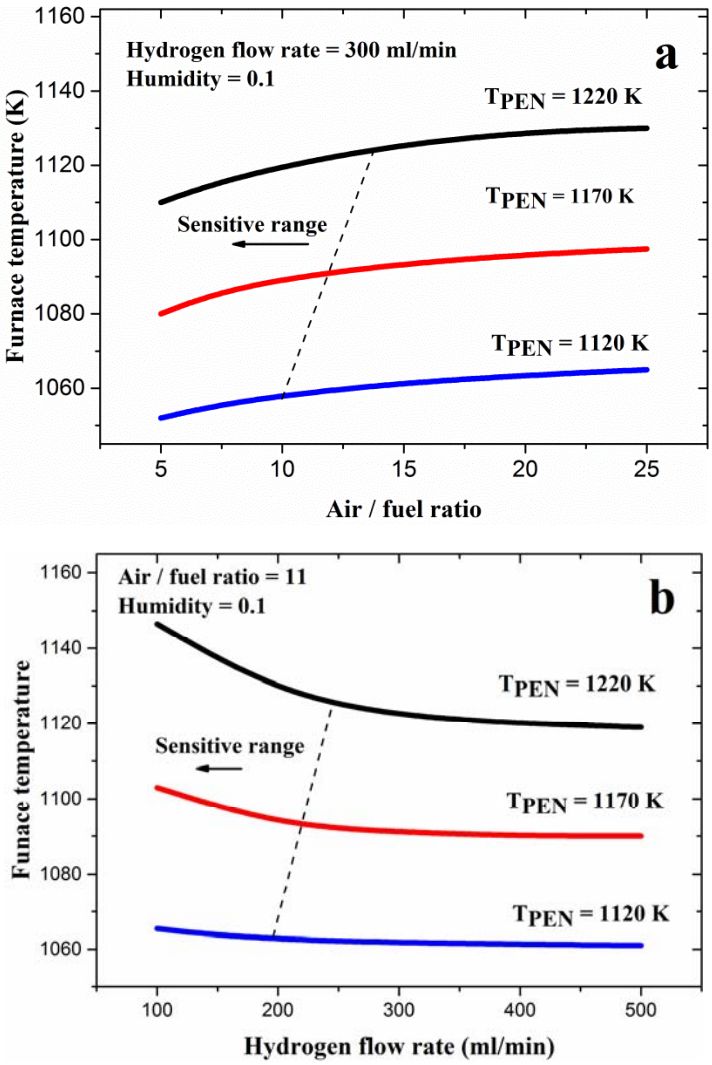

Figure 2. 11: Estimation of PEN temperature based of furnace temperature and fuel and air flows: (a) different air flow rates, (b) different fuel and air flow rates (constant flows' ratio)

From another viewpoint, model based approximation could also be appropriately employed to predict the PEN temperature based on other operational variables. For instance, an operation map might be proposed to enable estimation of the average internal PEN temperature based on air and/or fuel flow rates and furnace temperature that are much easier for measurement purposes. Figure 2.10 displays typical operational maps that can be used at a fixed, (Figure 2.11(a)), and varying, (Figure 2.11(b)), fuel flows.

2.5 Conclusions

In this article an effective model for the laboratory scale SOFC rig was proposed and validated against experimental data. Parameter adjustment was also carried out by using an independent set of practical data. The V-I data used for model training and validation was attained in an experimental study that was carried out in parallel. For the distributed profiles, however, validation will be open for further work due to the lack of internally distributed measurements from the test rig. The model was found to be flexible enough to simulate a simple cell structure and the multi-layer cell consisting of various heat transfer zones. Distributed heat generation rates– as an indicator of reaction progress– along with the role of different heat removal mechanisms were subsequently assessed that gives better insight for thermal management. Moreover, spatially distributed temperatures within different layers of the cell structure also became predictable through the model. Process analysis was executed through a comprehensive comparison of cell's behaviour under adiabatic and non-adiabatic conditions. Furthermore, parameter adjustment for the test rig as well as PEN temperature approximation for a reactive cell was exemplified via typical operational maps.

Nomenclature

C_{dl}	Double layer capacitance (A s V^{-1} m^{-2})
C_p	Specific heat (J $mol^{-1}K^{-1}$)
d	Thermal conduction distance (m)
D_{298}	Mass diffusivity coefficient at 298K (m^2 s^{-1})
E	Least-squares error function
E_{act}	Activation energy
F	Molar flow rate (mol s^{-1})
F_N	Faraday's constant (96,485 C mol^{-1})
Δh	Enthalpy change (J mol^{-1})
ΔH_R	Reaction enthalpy (J mol^{-1})
I	Current (A)
i	Current density (A m^{-2})
i_0	Exchange current density (A m^{-2})
K	Coefficient of heat conduction (W m^{-1} k^{-1})
K_e	Effective diffusivity (m s^{-1})
K_0	Pre-exponential factor (A m^{-2})
k	Number of experimental data
L	Diffusion layer thickness (m)
N	Calculated numbers of tanks in model
n_e	Number of electrons
OCV	Open circuit voltage (V)
Q	Heat transfer rate (J s^{-1})
Q_{gen}	Reaction heat (J s^{-1})
R	Ideal gas constant (J mol^{-1} k^{-1})
r	Mass source term (mol s^{-1})
S_e	Effective area (m^2)

S_c	Contact area (m^2)
T	Temperature (K)
U	Cell voltage (V)
V	Volume (m^3)
y	Species mole fraction

Greek Letters

α	Coefficient of convection heat transfer ($W\ m^{-2}\ K^{-1}$)
ρ	Density ($mol\ m^{-3}$)
ε	Emissivity
$\boldsymbol{\eta}$	Overpotential (V)
δ	Porosity
ɤ	Reaction orders
υ	Stoichiometric coefficient
τ	Tortuosity (= 3)

Sub-/Superscripts

A	Anode
a	Air
C	Cathode
cat	Catalyst layer
cond	Thermal conduction
conv	Thermal convection
cell	SOFC cell
exp	Experimental
f	Fuel

fur	Furnace
G	Gas (fuel/ air)
Ib	Bottom interconnect
It	Top interconnect
in	Inlet
out	Outlet
PEN	Positive electrode–Electrolyte–Negative electrode
radi	Thermal radiation
S	Solid
St	Stand
sim	Simulation
1, 2	Number for adjacent solids

Acronyms:

CSTR:	Continuous Stirred Tank Reactor
PEN:	Positive electrode–Electrolyte–Negative electrode
OCV:	Open Circuit Voltage
SOFC:	Solid Oxide Fuel Cell
TSR:	Tank-In-Series Reactor

References:

[1] R. Bove, S. Ubertini, Modeling solid oxide fuel cell operation: Approaches, techniques and results, J. Power Sources 159 (2006) 543-559.

[2] E. Achenbach, Three-dimensional and time-dependent simulation of a planar solid oxide fuel cell stack, J. Power Sources 49 (1994) 333-348.

[3] N.F. Bessette Ii, W.J. Wepfer, J. Winnick, Mathematical model of a solid oxide fuel cell, J. Electrochem. Soc. 142 (1995) 3792-3800.

[4] L. Petruzzi, S. Cocchi, F. Fineschi, A global thermo-electrochemical model for SOFC systems design and engineering, J. Power Sources 118 (2003) 96-107.

[5] R. Bove, S. Ubertini, Modeling Solid Oxide Fuel Cells: Methods, Procedures and Techniques, Springer 2008.

[6] P. Costamagna, L. Magistri, A.F. Massardo, Design and part-load performance of a hybrid system based on a solid oxide fuel cell reactor and a micro gas turbine, J. Power Sources 96 (2001) 352-368.

[7] K.P. Recknagle, R.E. Williford, L.A. Chick, D.R. Rector, M.A. Khaleel, Three-dimensional thermo-fluid electrochemical modeling of planar SOFC stacks, J. Power Sources 113 (2003) 109-114.

[8] X. Xue, J. Tang, N. Sammes, Y. Du, Dynamic modeling of single tubular SOFC combining heat/mass transfer and electrochemical reaction effects, J. Power Sources 142 (2005) 211-222.

[9] V.A. Danilov, M.O. Tade, A CFD-based model of a planar SOFC for anode flow field design, Int. J. Hydrogen Energy 34 (2009) 8998-9006.

[10] H. Yakabe, T. Ogiwara, M. Hishinuma, I. Yasuda, 3-D model calculation for planar SOFC, J. Power Sources 102 (2001) 144-154.

[11] K. Wang, D. Hissel, M.C. Péra, N. Steiner, D. Marra, M. Sorrentino, C. Pianese, M. Monteverde, P. Cardone, J. Saarinen, A Review on solid oxide fuel cell models, Int. J. Hydrogen Energy 36 (2011) 7212-7228.

[12] B. Bozbiyik, V.A. Danilov, J. Denayer, An improved tank in series model for PEMFC, Int. J. Hydrogen Energy 36 (2011) 14552-14561.

[13] U. Krewer, M. Pfafferodt, A. Kamat, D.F. Menendez, K. Sundmacher, Hydrodynamic characterisation and modelling of anode flow fields of Direct Methanol Fuel Cells, Chem. Eng. J. 126 (2007) 87-102.

[14] V.A. Danilov, P. Vijay, M.O. Tade, Improved Tank in Series Reactor Model for Tubular Solid Oxide Fuel Cell Stacks, Chem. Eng. Technol. 34 (2011) 737-745.

[15] S. Hosseini, V.A. Danilov, P. Vijay, M.O. Tadé, Improved Tank in Series Model for the Planar Solid Oxide Fuel Cell, Ind. Eng. Chem. Res. 50 (2010) 1056-1069.

[16] A. Amiri, P. Vijay, M.O. Tadé, K. Ahmed, G.D. Ingram, V. Pareek, R. Utikar, Solid oxide fuel cell reactor analysis and optimisation through a novel multi-scale modelling strategy, Comput. Chem. Eng. 78 (2015) 10-23.

[17] A. Amiri, P. Vijay, M.O. Tadé, K. Ahmed, G.D. Ingram, V. Pareek, R. Utikar, Planar SOFC system modelling and simulation including a 3D stack module, Int. J. Hydrogen Energy (Accepted).

[18] D.L. Damm, A.G. Fedorov, Radiation heat transfer in SOFC materials and components, J. Power Sources 143 (2005) 158-165.

[19] P. Aguiar, C.S. Adjiman, N.P. Brandon, Anode-supported intermediate temperature direct internal reforming solid oxide fuel cell. I: model-based steady-state performance, J. Power Sources 138 (2004) 120-136.

[20] M. Mangold, M. Krasnyk, K. Sundmacher, Theoretical investigation of steady state multiplicities in solid oxide fuel cells, J. Appl. Electrochem 36 (2006) 265-275.

[21] P. Costamagna , G. wang, J. Saarinen, I. Wærnhus, I. Wærnhus, Modeling of Solid Oxide Heat Exchanger Integrated Stacks and Simulation at High Fuel Utilization, J. Electrochem. Soc. 145 (1998) 3995-4007.

[22] L.-K. Chiang, H.-C. Liu, Y.-H. Shiu, C.-H. Lee, R.-Y. Lee, Thermo-electrochemical and thermal stress analysis for an anode-supported SOFC cell, Renew. Energy 33 (2008) 2580-2588.

[23] L. Liu, G.-Y. Kim, A. Chandra, Modeling of thermal stresses and lifetime prediction of planar solid oxide fuel cell under thermal cycling conditions, J. Power Sources 195 (2010) 2310-2318.

[24] A. Mauro, F. Arpino, N. Massarotti, Three-dimensional simulation of heat and mass transport phenomena in planar SOFCs, Int. J. Hydrogen Energy 36 (2011) 10288-10301.

[25] Y. Wang, F. Yoshiba, T. Watanabe, S. Weng, Numerical analysis of electrochemical characteristics and heat/species transport for planar porous-electrode-supported SOFC, J. Power Sources 170 (2007) 101-110

[26] H. Cao, X. Li, Z. Deng, J. Jiang, J. Yang, J. Li, Y. Qin, Dynamic modeling and experimental validation for the electrical coupling in a 5-cell solid oxide fuel cell stack in the perspective of thermal coupling, Int. J. Hydrogen Energy 36 (2011) 4409-4418.

[27] L. Zhang, X. Li, J. Jiang, S. Li, J. Yang, J. Li, Dynamic modeling and analysis of a 5-kW solid oxide fuel cell system from the perspectives of cooperative control of thermal safety and high efficiency, Int. J. Hydrogen Energy 40 (2015) 456-476.

[28] K. Sudaprasert, R.P. Travis, R.F. Martinez-Botas, A Study of Temperature Distribution Across a Solid Oxide Fuel Cell Stack, J. Fuel Cell Sci. Technol. 7 (2009) 011002-011002.

[29] ThyssenKrupp DVM, Crofer 22 APU Material Data Sheet No. 4046, (2010).

[30] D. R.Lide, D.L. Damm, dw, J. Saarinen, E. Achenbach, CRC handbook of chemistry and physics, Handbook of chemistry and physics, CRC Press, Cleveland, Ohio, 2003.

[31] Y. Shi, H. Wang, N. Cai, Simulation of Two-Dimensional Electrochemical Impedance Spectra of Solid Oxide Fuel Cells Using Transient Physical Models, ECS Trans. 35 (2011) 871-881.

[32] V. Liso, A.C. Olesen, M.P. Nielsen, S.K. Kær, Performance comparison between partial oxidation and methane steam reforming processes for solid oxide fuel cell (SOFC) micro combined heat and power (CHP) system, Energy 36 (2011) 4216-4226.

[33] C.O. Colpan, F. Hamdullahpur, I. Dincer, Transient heat transfer modeling of a solid oxide fuel cell operating with humidified hydrogen, Int. J. Hydrogen Energy 36 (2011) 11488-11499.

[34] H. Apfel, M. Rzepka, H. Tu, U. Stimming, Thermal start-up behaviour and thermal management of SOFC's, J. Power Sources 154 (2006) 370-378.

Chapter 3

Planar Solid Oxide Fuel Cell Modelling and Optimization Targeting the Stack's Temperature Gradient Minimization[†]

A. Amiri*, S. Tang*: **Co-first Author**

Statement of Contribution to Co-authored Published Paper

This Chapter includes the co-authored paper 'Planar Solid Oxide Fuel Cell Modeling and Optimization Targeting the Stack's Temperature Gradient Minimization', published in Industrial & Engineering Chemistry Research. The bibliographic details of the co-authored paper, including all authors are:

Amirpiran Amiri†; Shi Tang†; Periasamy Vijay, and Moses O. Tade*

Centre for Process Systems Computations, Department of Chemical Engineering, Curtin
University, GPO Box U1987, Perth, WA 6845, Australia

I, Shi Tang, contributed to the paper by conducting all the simulation and analysis work, being the primary writer, including creating figures and tables, and writing the manuscript.

I, as a Co-Author, endorsed that the level of contribution by the candidate indicated above is appropriate.

Amirpiran Amiri

Periasamy Vijay

Moses Tade

3.1 Introduction

SOFC requires high temperature operation that offers higher efficiency and broader fuel diversity [1], [2], [3] and [4]. Essentially, operation in such a condition needs elaborate thermal management throughout the plant, especially for the temperature gradients inside the fuel cell itself. This becomes more involved when a multi-layered stack is of interest rather than a single (isolated) cell.

Many studies on temperature monitoring and control of a SOFC cell unit can be found in the literature. The intention in these works was to figure out the proper methods to achieve the most uniform temperature distribution inside the cell. Different features of the SOFC, such as, the flow configuration, geometries, flow distributors, operating conditions, etc., were numerically and experimentally tested for this purpose [1], [5], [6], [7], [8], [9], [10], [11] and [12]. Although the analysis of the SOFC's performance at cell scale provides the fundamental insights for design, operation, control, and optimization purposes, the thermal management of a marketable SOFC must be extended initially to the stack and ultimately to the system levels. This is mostly because of several reasons. First of all, unalike performances for a cell might be captured depending on being implanted inside a stack or being set individually. This cell-to-cell variation has root in the thermal interactions between cells and also in the probability of fuel and/or air maldistribution between different layers of the stack. This anisotropic structure is also another cause. This affects the local physicochemical properties of the material and hence the (electro-) chemical reactions and heat and mass transport rates. In practice, therefore, variation between the thermochemical performances of cell units (layers) might be observed. As a result, generalization of the single cell's performance as the representative of whole stack's functioning could cause some inaccuracies in numerical predictions. Another important remark is about the

model-based experiments. Nowadays, the experimental research and development efforts on fuel cell technology have been extended to the upper scales, encompassing the stack and system levels. This fact imposes the inevitability of the scale-up of high fidelity models for additional design-of-experiments and rigorous process plant interpretations.

So far, several investigations have been conducted on the thermal management of a SOFC stack. Achenbach et al. [13] studied an adiabatic SOFC stack of 50 cells, and pointed out that the highest temperature was found near the middle of the stack and the heat loss was considerable. In study of Ref. 14, the temperature profiles were obtained and compared for short (5 cells) and long (10 cells) stacks. Burt et al. [15] presented a 2-D SOFC model to study the cell-to-cell temperature variation under an adiabatic assumption for short to relatively long stacks (5, 10, and 20 cells). However, very limited works have been published on the stack level thermal study especially focusing on the methodologies to enhance the interior temperature homogeneity. In addition, to the authors' best knowledge; there is no publication on combination of prospective strategies to achieve such a target.

The sustainable operation of a stack is subject to several requirements that must be met simultaneously. These requisites comprise the cost, efficiency, reliability, and durability [16–17], which are always conflicting objectives. Thus, the system optimization must be accomplished via the multi-objective optimization (MOO) methods. Several studies have conducted the MOO with various focusses, such as system efficiency and cost [18], total cost and CO_2 emissions [19], production cost and integrated performance [20], stack efficiency and membrane electrode assembly size [21]. In spite of this, the optimization of the stack performance still faces challenging issues in the literature as numerous combinations of optimization targets can be proposed. The concurrent optimization of stack's efficiency and its

thermal management, for instance, is another issue that needs further investigations.

Fulfilment of some of the above-mentioned gaps forms the core of this study. In brief, the main contributions are as follows. Firstly, the modelling methodology is significantly extended to capture the thermal concerns imposed by the layering of multiple cells. The thermal features that need to be taken into account are mainly associated with the cell-to-cell interactions. Essentially, the analysis at this scale is important as it is a step closer to the commercial scale. Secondly, individual and combined strategies are investigated to critically analyse their practical advantage/disadvantages in achieving the temperature homogeneity across the stack's dimensions. This extensive analysis is vital to understand the effectiveness of the alternative strategies for thermal management. A simple economic estimation is also presented to support the technical analysis. And last but not the least, a multi-objective optimization study is conducted to find an effective operating condition in which the controversial operating goals can reasonably be compromised. More specifically, optimum thermal management while minimising the stack's efficiency reduction is the target of this part of the current study.

3.2 Modelling

The Stack subcomponents and model framework

The cell scale mathematical model demonstrated in Tang et al. [22] has been verified for a reasonable spectrum of temperatures and gas flowrates. For the stack level modelling we used that model, as the repeating-element, with appropriate modifications. The simulation flexibility was targeted as a key to scale up and strengthen the model's applicability particularly to evaluate the cell-to-cell thermal interactions.

Figure 3.1 displays the schematic of the stack model with three cells developed for this study. The heat transport between different control volumes and the environment are outlined. The governing and constitutive equations of the cell model, which is employed as the building compartment of the stack model, as well as the physical parameters, are extensively demonstrated in Ref. 22. The model takes into account all the phenomena involved in the stack's performance including energy, mass, and charge balances as well as the electrochemical reaction. The energy exchange between the neighbouring cells was also added to simulate the thermal effects caused by the stacking. Furthermore, when surrounding environment was taken into account, the thermal radiation exchange between the stack and the environment was formulated. The stack was simulated under steady state and potentiostatic condition, whilst a constant voltage E_{stack} was applied for the whole stack. Hence, the produced current density throughout the stack, operating under the mentioned conditions, can be worked out by means of Equation 3.1. Note that the activation and ohmic resistances, for each cell, were calculated locally.

$$I_{stack} = \frac{\sum_{i=1}^{3} E_{cell_i}^{OCV} - \sum_{i=1}^{3} (\eta_{act,cell_i}^{A} + \eta_{act,cell_i}^{C}) - E_{stack}}{R_{stack}^{Ohmic}} \tag{3.1}$$

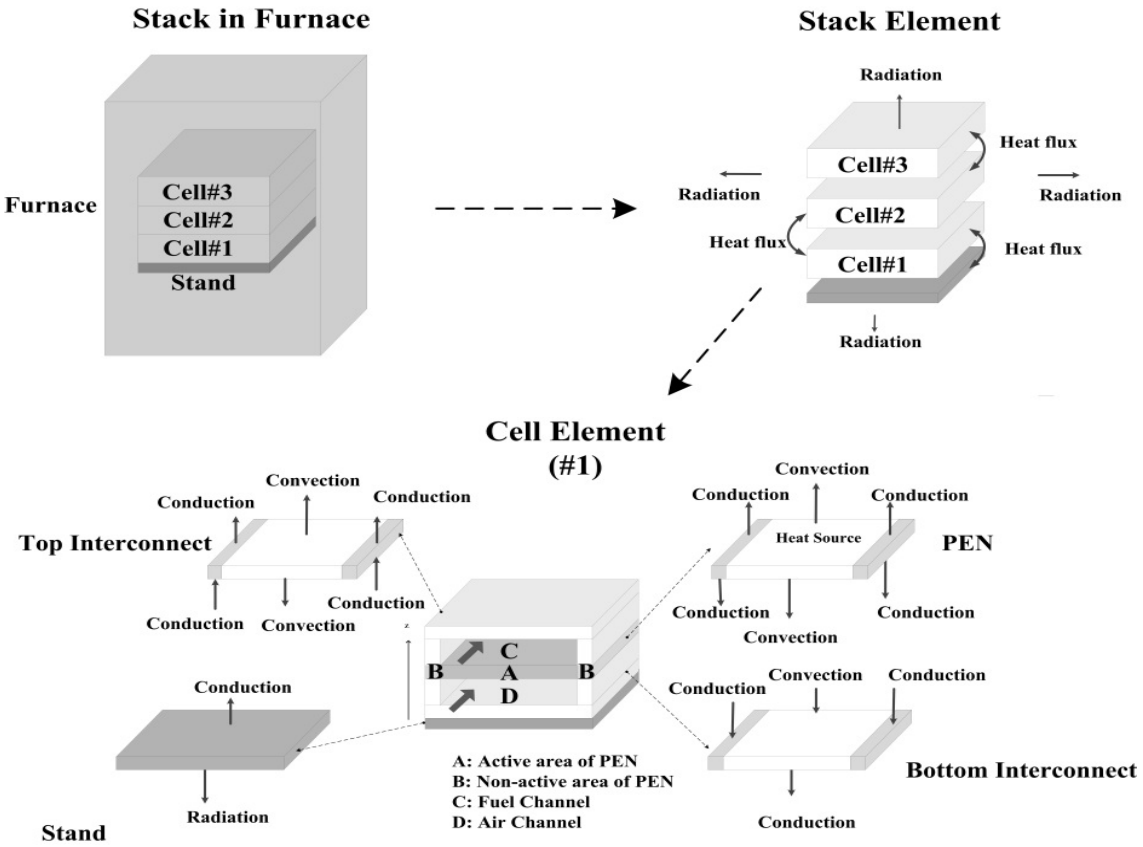

Figure 3. 1: Schematic diagram of SOFC stack model (adapted from Ref. 22).

Considering the entire stack fabrication as the control volume, the temperature distribution is a scalar field within this space. The gradient of a scalar field, T(x, y, z), is the vector derivative of this function with respect to three dimensions. As a case study, a stack with a co-flow pattern for fuel and air streams was assumed. Accordingly, the temperature variation in y direction was ignored (Equation 3.2). The temperature and its variations were approximated according to the Equations 3.2–3.7 as listed in Table 3.1.

Table 3. 1: Equations for temperature evaluation

Equation	Comment	Equation number
$dT = \frac{\partial T}{\partial x}dx + \frac{\partial T}{\partial z}dz$	Stack's total temperature gradient	(3.2)
$\overline{T}^{Stack} = \frac{1}{3}\sum_{i=1}^{3}\overline{T}^{Cell,i}$	Stack's average temperature.	(3.3)
$\overline{T}^{Cell} = \frac{1}{n}\sum_{i=1}^{n}T^{i}$	Cell's average temperature.	(3.4)
$\left(\frac{\partial T}{\partial x}\right)^{cell} \cong \frac{\Delta T^{\max}}{L_x}$	Cell's temperature gradient in x direction.	(3.5)
$\left(\frac{\partial T}{\partial x}\right)^{Stack} = \frac{1}{3}\sum_{i=1}^{3}\left(\frac{\partial T}{\partial x}\right)^{cell,i}$	Stack's average temperature gradient in x direction.	(3.6)
$\left(\frac{\partial T}{\partial z}\right)^{Stack} \cong \frac{\Delta T^{\max}}{L_z}$	Stack's temperature gradient in z direction.	(3.7)

Moreover, the stack electrical efficiency can be calculated according to Equation 3.8 [23] and [24].

$$Eff_{el} = \frac{P_{net}}{F_{H_2,in}LHV_{H_2}} \qquad (3.8)$$

where F_{H_2}, LHV_{H_2}, P_{net} stand for the hydrogen flow rate, hydrogen Lower

Heating Value, and the net electric output, respectively. P_{net} should be estimated based on all power generation and consumption sources in the subsystems including power generated by the electrochemical and combustion reactions and that consumed for conditioning the temperature and pressure of the fluids. Due to the scope of this work, only the power consumed by the air blower was considered. Hence, the electric net output was calculated as Equations 3.9 and 3.10 [23] and [25]:

$$P_{net} = E_{stack} I_{stack} - P_{bl} \tag{3.9}$$

$$P_{bl} = F_a C_p T_0 \left[\frac{(\frac{P_{out}}{P_0})^{\frac{\kappa-1}{\kappa}} - 1}{Eff_{isen}} \right] \tag{3.10}$$

P_{out}, P_0, and T_0 are the blower output pressure, ambient pressure and temperature respectively; Eff_{isen} is isentropic efficiency that is assumed to be 60% [25].

3.3 Results and discussions

3.3.1 Temperature gradients in two dimensions

Simulation of the stack's thermal performance was carried out to estimate the thermal variations in the stacking and flow-path directions. Two operating modes were considered; (i) a well-insulated stack, (ii) and stack surrounded by a heating chamber. They represent adiabatic and non-adiabatic operations, respectively. The operating conditions used for the model solution are presented in Table 3.2. Both of these processing scenarios are of practical importance. While the earlier is always common for the commercial cases, the latter has been widely encountered in experimental test rigs where heat exchange between stack and surrounding furnace occurs. Note that the non-adiabatic scenario also sounds promising for design of the future novel processes in which the thermal coupling of the external fuel reformer and stack could be a tactic to improve the system's thermal efficiency [26] and [27].

Table 3.2 : Operating conditions used for SOFC stack simulation

Variable	Value	Comments
Fuel (Hydrogen) flow rate, ml/min	0.90×10^{3}	
Oxidant (Air) flow rate, ml/min	9.00×10^{3}	
Hydrogen molar fraction in Fuel	0.90	Mixed with steam
Oxygen molar fraction in Air	0.21	Mixed with nitrogen
Temperature , K	1.053×10^{3}	Applied for the inlet gases and furnace in adiabatic and non-adiabatic cases, respectively.
Pressure, kPa	1×10^{5}	

Temperature profiles of individual cells, inside a stack, are shown in Figure 3.2. Moreover, the maximum temperature differences (between the "hottest" and "coldest" cells) along the stacking direction are included in the same graph. Note that cell-to-cell temperature variations are caused by heat exchange between the cells and also from the stack walls to the environment (in non-adiabatic case). An uneven air and/or fuel distribution between the cell units also can worsen such a variation. The gases maldistributions effect is out of the scope of this work. However, this has been already investigated by authors in another work [28]. Cell-to-cell heat transfer and manifold considerations are associated with the multi-cell structure. Therefore, cell may behave differently when embedded in a stack, revealing the necessity of assessing the cell's thermal performance not only individually, but also inside a multi-cell stack.

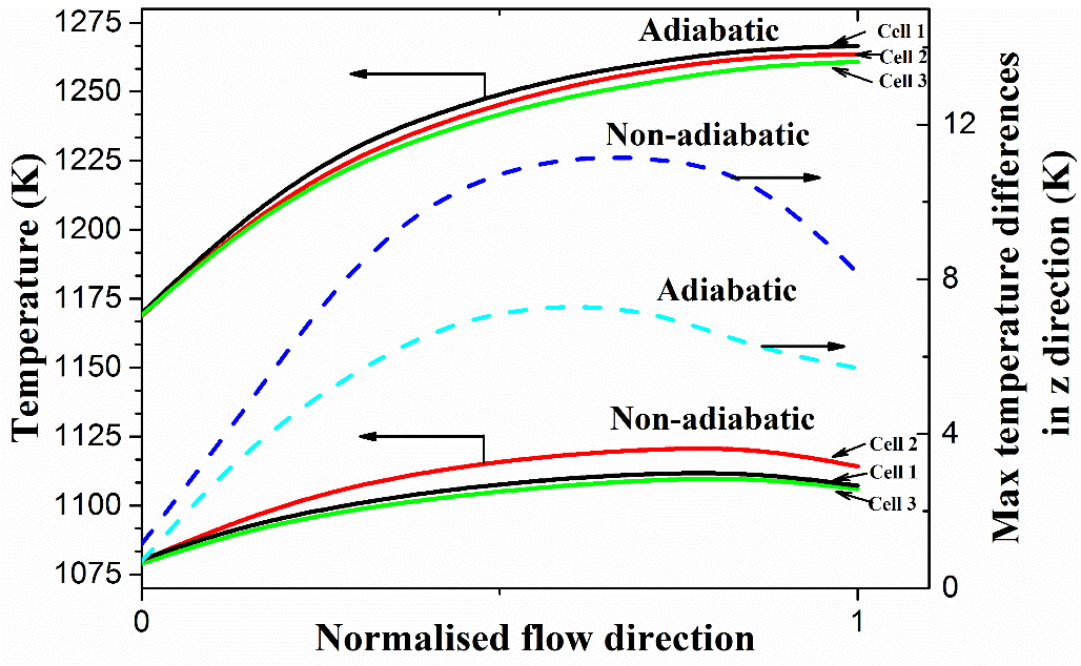

Figure 3. 2: Temperature profiles and maximum temperature differences between the "hottest" and "coldest" cells embedded inside a stack and operating under adiabatic and non-adiabatic conditions with basis operating conditions.

For the adiabatic process, as can be seen in Figure 3.2, all of the triple cells show a significant temperature rise (about 100 K) along the fuel path direction. This has also been reported in previous studies [10] and [14]. This significant temperature growth can be divided into two intervals, an initial steep rise (up to 30% of cell length) followed by a gentle increase. The conspicuous initial heat up in the first interval is essentially because of it being rich in terms of the fresh reactant (hydrogen). The resulting significant reactive heat, in return, runs the autothermal reaction. The second interval of the cell's length receives the depleted fuel from the first interval that downgrades the released heat from the exothermic reaction. Therefore, PEN's temperature does not rise significantly. It is not an easy task to pin a sharp boundary between the mentioned intervals. The span of these regions is strongly dependent on the prominent operational variables such as, but not limited to, gas flowrates and average operating temperature.

In the stacking direction, the cell-to-cell temperature variation can also be observed. As the same fuel and air were provided to each cell unit with isentropic assumption, this temperature difference could be explained based on the cell-to-cell heat transfer.

Basically, heat transport has substantial driving force to occur when anode side of a cell is located in the neighbourhood of cathode side of the adjacent cell inside the stack assembly. The temperature difference between anode and cathode channels has been reported in both numerical and practical studies [14], [15] and [29]. A temperature difference up to 6 K was attained for the stacking direction, as shown in Figure 3.2, which is much less than the value captured for the fuel course direction. It must be noted that the reactor dimension in z direction is also smaller, in contrast to x direction that makes temperature gradients comparable. Furthermore, this disparity, along the z course, can become more crucial when fuel and air uneven distributions, unequal inlet gas temperatures and the larger number of cells-in-parallel are taken into account [14] and [28].

Regarding the non-adiabatic operation, in which there is a thermal interaction between stack and furnace, the temperature trends remarkably deviate from that observed in the adiabatic case. The notable dissimilarities belong to the rates of the temperature increase and also to the slight decrease observed at cell outlet. The earlier can be attributed to the removal of the system's heat through radiation from stack boundaries that results in lower temperature and more homogenous distribution for that. The reason behind the latter, however, must be explored in the reaction progress as a function of reactant depletion, decreased temperature and the mutual interaction between them.

We focused on the adiabatic case in the rest of this article, as it is more likely to have immediate practical application in the current devices available in the market.

3.3.2 Sensitivity analysis

Temperature gradient over a cell surface is a critical challenge that affects the reliability of the stack. Serious technical faults such as cell degradation and cracking are attributed to this concept. In the research of Chiang et al. [5], control of temperature growth throughout the cell surface below 50K is mentioned as a reasonable criterion to minimize undesirable consequences. Temperature variation of

10 K/cm ,and 8 K/cm are mentioned as reasonable values by Aguiar et al. [1] and Zhang et al. [23], respectively. Temperature variation in stacking direction is also notable, that may increase the aforementioned problems [30].

Technically and economically applicable methods must be implemented to manage the thermal behaviour of the stack. In this work, three tactics for the stacks' temperature and efficiency regulation were studied to obtain a quantitative and qualitative assessment.

3.3.2.1 Strategy #1: excess air flow

Utilization of surplus air, further than the stoichiometry, has been broadly acknowledged as the first strategy to restrain the temperature of electrochemical fuel cells [31]. Likewise, the approach is effective in enhancing the interior temperature uniformity within the whole stack. Figure 3.3 (a) displays the stack's temperature and its gradient (in both x and z directions indicated in Figure 3.2) for a span of cathode to anode flow ratio ($\varphi = \frac{F_C}{F_S}$). It should be noted that fuel flow rate is kept constant. Therefore, the φ would be a representative for the quantity of excess air. From the heat exchange viewpoint, the intensification of heat convection mechanism at higher coolant flows is the principal reason for cell's temperature decline. The downswing effect is noteworthy along the flow direction (x), which is properly consistent with the literature [11] and [31]. Smaller influences are observed in the stacking direction (z). Although the applicability of this strategy is rationally supported by the availability of cheap air, it may instantaneously lead of efficiency loss due to the higher potentiostatic loss at the higher fluid flows (Figure 3.3 (b)). Therefore, it is difficult to achieve the efficiency and thermal management goals at the same time via this approach. This must be dealt with through a trade-off decision-making. Figure 3.3 (c) shows how the temperature gradient reduction in stack may sacrifice the total yield.

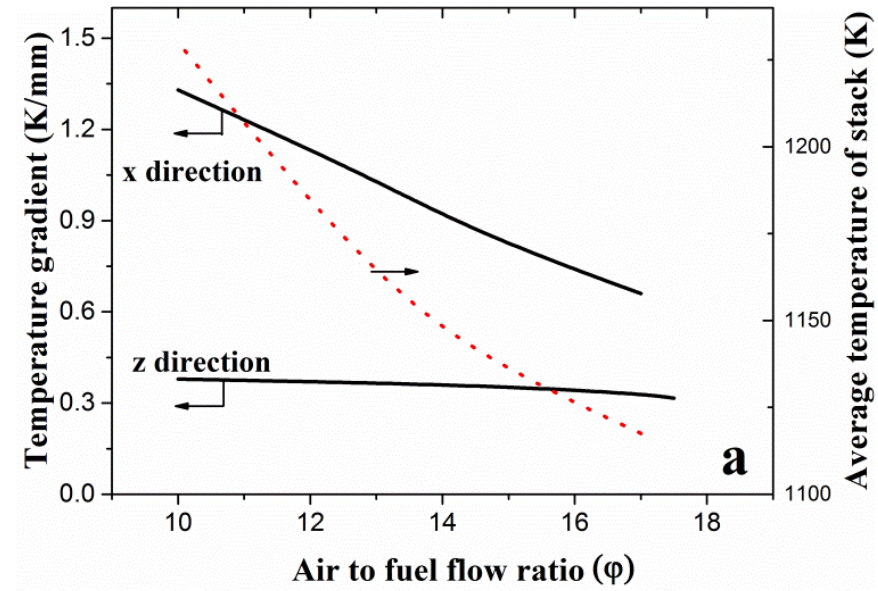
Temperature gradient (K/mm)
Average temperature of stack (K)
x direction
z direction
a
Air to fuel flow ratio (φ)

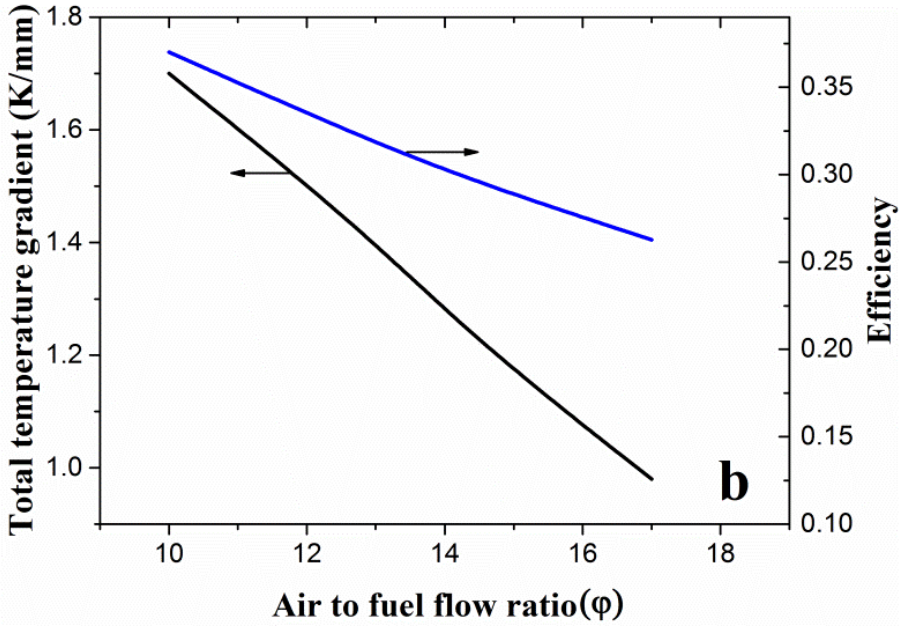
Total temperature gradient (K/mm)
Efficiency
b
Air to fuel flow ratio(φ)

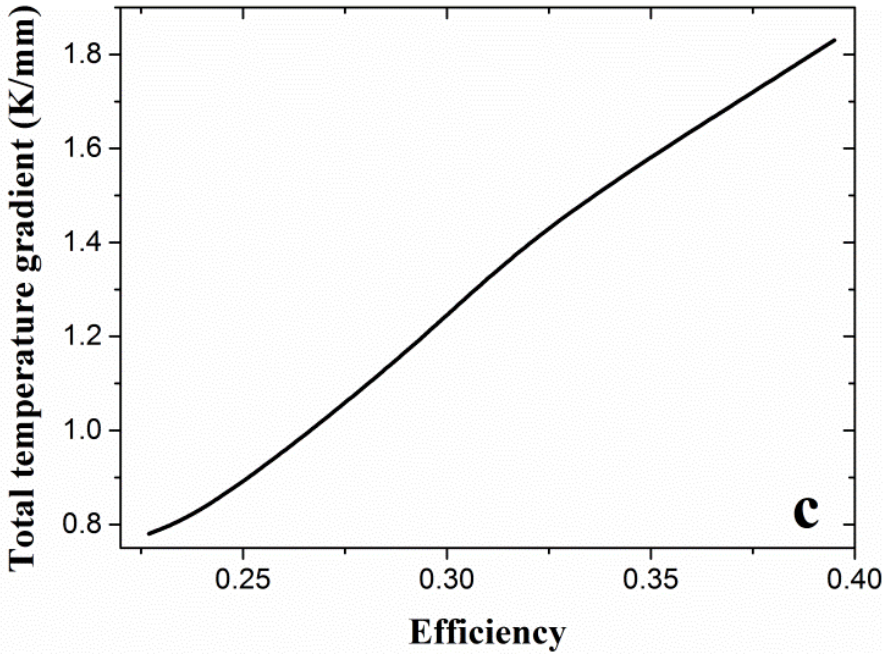

Figure 3. 3: (a) Effect of excess air flow on stack's average temperature and temperature gradient elements; (b) Effect of excess air flow on temperature gradient and efficiency; (c) Stack's efficiency versus stack's temperature gradient regulated by applying excess air ($F_{H_2} = 900 ml / \min$).

From this analysis, it can be understood that the effect of the coolant flow on the temperature gradient is more significant in the gas flow direction. In general, the average temperature of the stack also decreases. However, there are some concerns associated with this approach. Firstly, its impact declines at high air flow rates. For instance, it can be seen in Figure 3.3(a) for φ > 14 that usage of further air becomes less effective compared to the lower ranges. Secondly, the amount of applied excess air/coolant must be reasonably constrained to justify the air compression costs. Furthermore, the electrochemical reaction would be decelerated at lower average temperatures resulting from the excess air. These concerns place a limitation on usage of excess air. As a result, alternative approaches should be undertaken individually or in combination with excess air strategy to meet the thermal management targets without imposing significant efficiency loss. The main objective of the next sections in this article is to technically and economically evaluate the potential options via a so-called "feasibility study".

3.3.2.2 Strategy #2: adjustment of the gases' temperature difference at cell's inlet (ΔT_{in})

Anode and cathode gases may be fed into the cell with either the same or different temperatures [32] and [33]. In this part we show how the ΔT_{in} ($\Delta T_{in} = T_{in}^{A} - T_{in}^{C}$) may influence the temperature gradients inside the stack. In this analysis the stack efficiency was kept constant while operating with different ΔT_{in}. Manipulation of ΔT_{in} has been implemented by the increase in T_{in}^{A} and decrease in T_{in}^{C} in a way that average temperature of the cell does not change significantly. Therefore, the electrochemical reaction rate was reasonably constant, leading to almost constant current generation. Since the air flow rate was also constant, based on Equation 9 the efficiency does not change.

For analysis of strategy 2, ΔT_{in} was varied from 0 to 260 K, as presented in Figure 3.4(a). This is achieved by changing the temperature of the inlet fuel between 1023 K and 1250 K. It must be noted that this change was accompanied by a simultaneous reduction in the air temperature resulting in the maintenance of the average cell temperature at around 1200 K throughout. This is a reasonable operating temperature range for a high temperature SOFC [34] and [35]. Therefore, this approach can be safely implemented without a serious risk to the materials used in cell. The simulation results are presented in Figure 3.4. As the profiles indicate, the operation under various ΔT_{in} may positively affect the temperature smoothness in the x direction, while it has an opposite influence in the z direction. The total temperature gradient, which attained by adding gradients in the x and z directions, is also presented in Figure 3.4(a). The reduction of temperature gradient in the x direction can be explained based on the reaction rate variations at the cell's inlet and outlet regions. The higher fuel temperature at the inlet (T_{in}^{A}) would improve the electrochemical reaction that results in higher heat release and more reactant consumption. At the cell's outlet region, in contrast, the amount of released heat declines due to lower hydrogen concentration. These two subsequent effects lead to a lower temperature gradient along the flow path. On the other hand, the temperature gradient in the z direction increases because of the higher temperature differences between anode and cathode channels, as illustrated in Section 3.3.1.

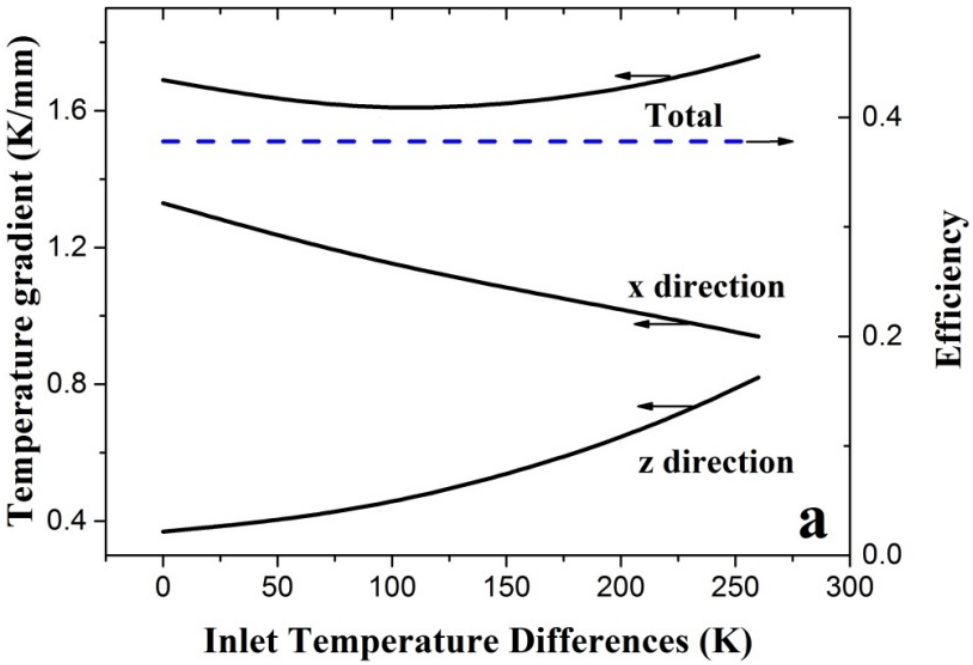
Temperature gradient (K/mm)
1.6
1.2
0.8
0.4
Total
x direction
z direction
a
0.4
0.2
0.0
Efficiency
0
50
100
150
200
250
300
Inlet Temperature Differences (K)

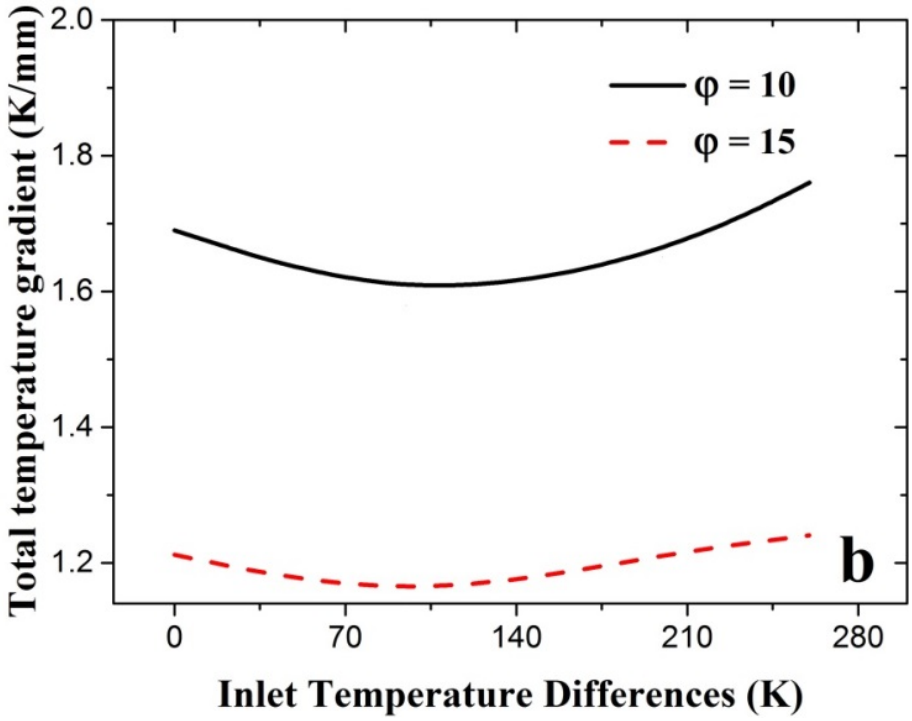
Total temperature gradient (K/mm)
2.0
1.8
1.6
1.4
1.2
φ = 10
φ = 15
b
0
70
140
210
280
Inlet Temperature Differences (K)

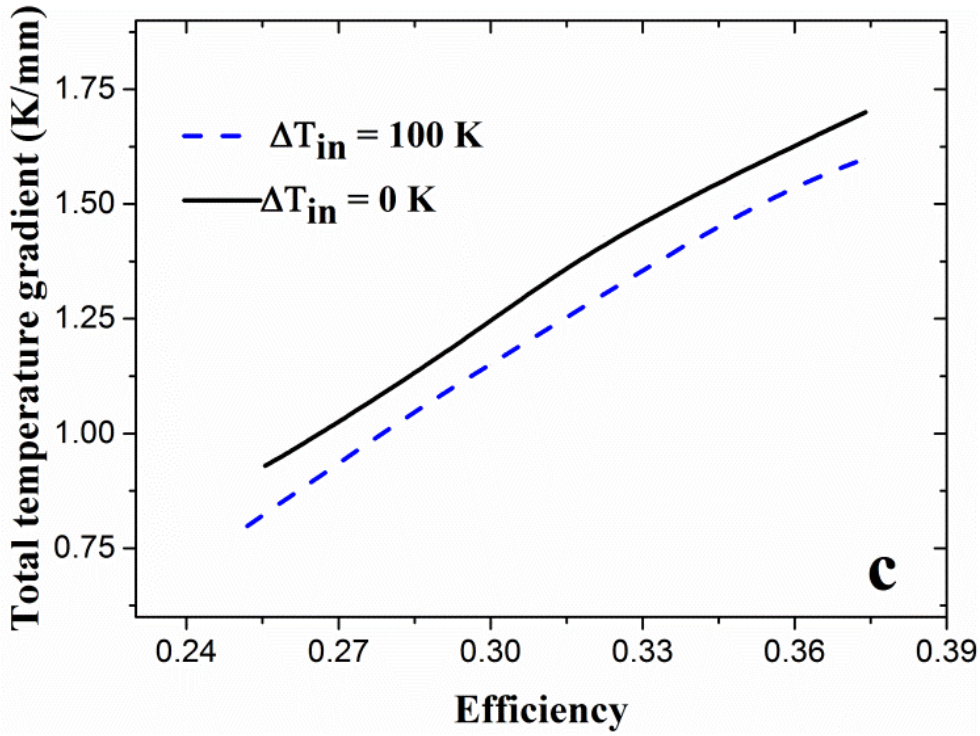

Figure 3. 4: (a) Temperature gradient of stack with different ΔT_{in} ($i = 5245\ A/m^2$); (b) Total temperature gradient of stack with different $\Delta T_{in;}$ (c) Stack efficiency achieved under different temperature gradient in varied operating condition ($F_{H_2} = 900\ ml/\min$).

In this case study, the minimum point of total temperature gradient was found for $\Delta T_{in} \approx 110$ K. Higher value for ΔT_{in} would not be advantageous, as evident from Figure 3.4(a) and (b). Therefore a most favorable range should be searched for appropriate implementation. In Figure 3.4(b), variation in overall temperature gradients with the increase of ΔT_{in} is shown for two different values of φ. At higher φ value the minimum point was slightly shifted towards the smaller ΔT_{in}. This is basically because of the lower temperature gradient obtained in the x direction with larger air flowrates while the change of temperature gradient in z direction is minor as discussed in Section 3.3.2.1. The minimum point was observed with both values of φ. Note that the main manipulating variable in this analysis was ΔT_{in}, while calculations have been repeated for two values of φ (i.e., 10 and 15).

To expand the analysis, a case with ΔT_{in} of 100 K and variable φ is compared to the basis case in which ΔT_{in} is zero, as per Figure 3.4. The advantage of application ΔT_{in}

can be observed in that higher efficiency is achieved with ΔT_{in}. Air flow ratio (φ) changes both efficiency and temperature gradient. Higher φ leads to a lower temperature gradient and efficiency, and vice versa. We plotted these changes by varying φ from 10 to 17.5, but for two values of ΔT_{in} (i.e., 0 and 100K) as presented in Figure 3.4 (c). The target is to show how a higher ΔT_{in} can moderate the efficiency reduction when a specific value of temperature gradient is targeted. From another viewpoint, one may say how temperature gradient can be improved by ΔT_{in} while a specific value is targeted for the efficiency. The graph shows that efficiency versus temperature gradient profile is positively shifted towards better performance by increasing ΔT_{in}. Lower air flow rate will be needed to achieve a certain temperature gradient at a given efficiency or vice versa. Lower preheating duty may be mentioned as another benefit of this strategy. Since air flowrate is much larger than the fuel flowrate, providing air and fuel with lower and higher temperatures, respectively, could result in energy saving in the preheating processes.

3.3.2.3 Strategy #3: utilization of the oxygen-enriched air

The oxygen concentration in cathode gas is investigated as another opportunity that could be effective for the stack's thermal management purposes. The idea is to reduce the negative effect of excess air flow used for cooling on the total efficiency by enhancing the reaction progress and also minimizing the voltage losses via supplying the operation with the enriched air. In order to comprehensively assess this strategy, its technical and economic aspects must be well thought-out through the quantitative measures. The cost concerns are mainly attributed to the extra expenses imposed by the air conditioning process. The model developed in this work was applied to figure out how the adjustment of the oxygen fraction in air may alter the temperature profiles and efficiency. Moreover, a basic economic analysis was carried out, as presented in the economic analysis in section 3.4, to evaluate the commercial applicability of the tactic in practice. Stack's performances within a range of air flow rates and with various compositions were compared (Figure 3.5). As was expected the higher air flows in cathode side leads to smoother temperature profile and a simultaneous efficiency drop. However, utilization of oxygen-enriched air, with 25% oxygen, rather than 21% used for the basis case, enhances the efficiency and

undesirably increases the temperature gradients. Relative metrics indicate that the efficiency improvement is more considerable. For instance, for φ = 12, approximately 9% (from 0.33 to 0.36) efficiency increase was achieved. While at this air flowrate ratio, temperature gradients increase was around 3% (from 1.50 to 1.55 K/mm). These observations are more prominent by comparing the results presented for the case with 40% oxygen.

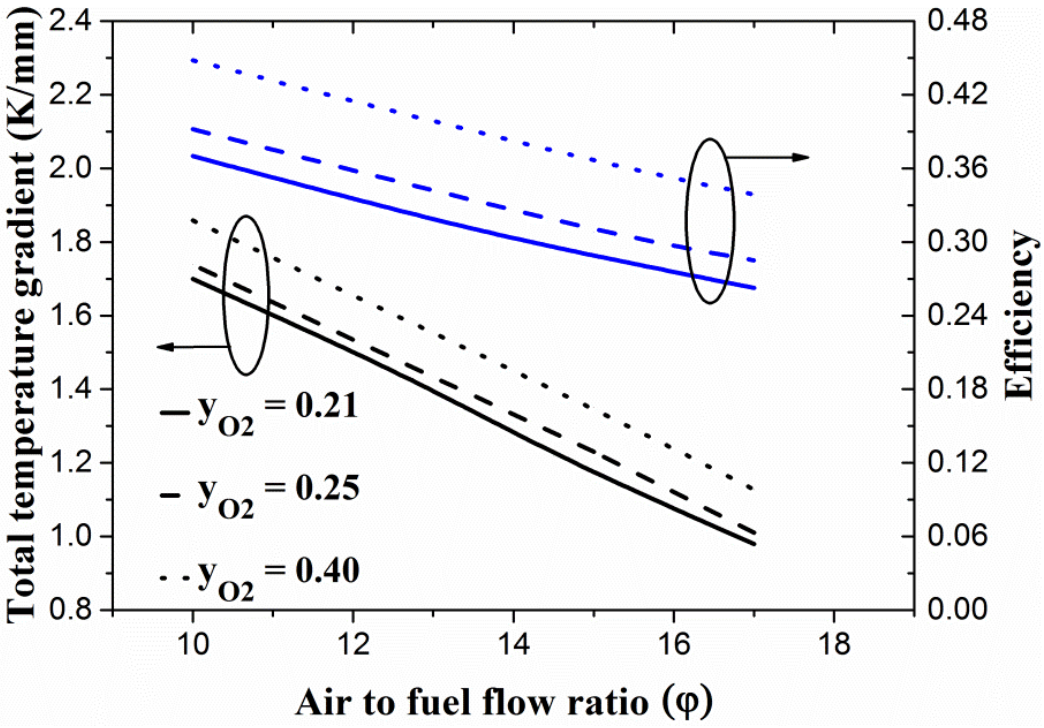

Figure 3. 5: Stack temperature gradient and efficiency achieved under different cathode flowrates with different oxygen concentration applied in cathode gas ($F_{H_2} = 900 ml/\min$)

The stack's current generation, is principally dominated by the open circuit voltage and also the voltage losses (Equation 3.1). The activation loss at the cathode side is a significant term in the estimation of total over-potentials. This term declines with the oxygen concentration [36]. The higher oxygen partial pressure (or mole fraction) results in a higher exchange current density value. This, subsequently, reduces the activation loss at the cathode. As a result, the current generation (or the exothermic electrochemical reaction) would be improved subsequently increasing the stack's temperature. Moreover, at higher temperatures, the cell also operates with a reduced Ohmic resistance. Note that oxygen fraction and temperature influence the OCV in

different ways. Whilst the former improves the OCV, the latter negatively influences it. Our numerical results, however, shows that the latter is dominant in this case study. The variations of the aforementioned variables with oxygen concentration are tabulated in Table 3.3. As can be seen in this table, the stack's current productivity is enhanced by using the oxygen-enriched air. Furthermore, the fuel utilization values also support this conclusion.

Table 3. 3: Stack performance fed with different oxygen concentration cathode

	$y_{O_2} = 0.21$	$y_{O_2} = 0.25$	$y_{O_2} = 0.40$
OCV, V	0.899	0.889	0.874
Activation overpotential, V	7.81×10^{-2}	6.87×10^{-2}	5.55×10^{-2}
Ohmic resistance, Ω	4.12×10^{-6}	3.59×10^{-6}	2.82×10^{-6}
Fuel utilization, %	58	62	71
Average temperature, K	1230	1249	1282
Average current density, A/m^2	5245	5685	6308

The temperature gradient was also increased with the improved oxygen concentration since the increase of current density will result in the higher reaction heat release. However, the increase of temperature gradient was slighter compared with the gain in efficiency. For example, as Figure 3.5 shows, for a target of total temperature gradient at 1.5 K/mm, cathode to anode ratio of 12 is required to be applied for the basis case (natural air). The stack efficiency is 33% at this operating point. When oxygen portion rises to 0.25 in the cathode stream, the stack must be supplied with an excess air ratio of 12.3 to achieve the same total temperature gradient (1.5 K/mm). However, at this operating point, the total stack's efficiency is improved to 35%. The efficiency improvement is attributed to the enhanced current generation. Similar analysis reveals an efficiency of up to 39% when the employed air is enriched up to 40% of oxygen. It can be concluded that the system fed by oxygen-enriched air has the capability to be operated at higher coolant rates without sacrificing the overall efficiency. The application of this, however, would be subject to cost justification, as is demonstrated in the next section.

3.4 Economic Analysis for the budget with different SOFC operation strategy

A basic cost analysis was conducted to assess the economic aspects of strategies aforementioned in this chapter. The basis of cost estimation was 1kWh power generation and subject to a total temperature gradient of 1.15K/mm. Both of the preheating cost and price of gases were taken into account. The gases' prices were quoted from the gas supplier BOC Australia. For of the all cases, the same fuel flow rates were introduced. The air flow rates, however, were adjusted depending on the strategy that applied as different air flow rates will be needed to attain a targeted temperature gradient through different strategies.

For a particular designed electrical energy to be produced, time required with different strategy is calculated as:

$$t^{strategy,i} = \frac{E^{design}}{P_{net}^{strategy,i}} \tag{3.11}$$

The amount of gases inserted in anode and cathode sides during this time can be calculated by Equations 3.12 and 3.13, respectively.

$$m_A^{strategy,i} = F_A t^{strategy,i} \tag{3.12}$$

$$m_C^{strategy,i} = \varphi^{strategy,i} F_A t^{strategy,i} \tag{3.13}$$

F_A stands for fuel flow rate that is constant. Also φ is the cathode to anode ratio.

The oxygen-enriched stream is assumed to be attained by mixing of pure oxygen and natural air. The cost of the final mixture can be estimated by using the second term of RHS of Equation S4 while the first term evaluates the hydrogen cost;

$$\mathrm{Pr}_{total}^{gas} = m_A y_{H_2} U_f \mathrm{Pr}_{H_2} + m_C \left(y_a \mathrm{Pr}_a + (1 - y_a) \mathrm{Pr}_{O_2} \right) \tag{3.14}$$

The preheating energy demand was assumed to be supplied via combustion of the depleted fuel. The remaining hydrogen in the anode exhaust will be combusted to supply a part of the heating duty. For the cases studied here, the demand fuel for combustion is larger than the exhaust fuel that can be provided, while the remaining will be supplied by combustion of methane. The amount of hydrogen remained for post combustion was calculated as per Equations 3.15;

$$m_{H_2}^{combus} = m_A y_{H_2} (1 - U_f) \quad (3.15)$$

The amount of methane needed for the preheating duty is calculated as Equation 3.16:

$$m_{CH_4}^{combus} = \frac{\Delta H_{ph}^{A} + \Delta H_{ph}^{C} - m_{H_2}^{combus} LHV_{H_2}}{LHV_{CH_4}} \quad (3.16)$$

Given the price of the hydrogen and methane, the total cost of the preheating process can be estimated through Equation 3.17;

$$Cost_{ph} = m_{H_2}^{combus} \Pr_{H_2} + m_{CH_4}^{combus} \Pr_{CH_4} \quad (3.17)$$

Table 3.4: Economic calculation results

	Preheating cost, $	Gas cost, $	Cost saving, $
Strategy #1			
Basis case	31.7	116.03	0
Strategy #2			
ΔT_{in}=100K	27.57	107.71	12.45
Strategy #3			
y_{O2}=0.25	29.16	113.87	4.72
y_{O2}=0.28	28.72	119.76	–0.75
y_{O2}=0.4	23.10	136.72	–12.01

As shown in Table 3.4, for the stack with ΔT_{in}=100K the costs associated with both gases consumption and preheating process were decreased in contrast to the basis case. Less amount of air is needed to gain the same temperature gradient while the efficiency is improved. Besides, the efficiency enhancement also results in reactants saving to gain 1kWh electricity. In contrast to the basis case, the total preheating duty decreases by using Strategy #2. For heating up the anode stream, extra energy is needed. However, energy is also saved by using cooler stream at cathode inlet. Because of the larger amount of material that flows through the cathode channel's inlet compared with anode side the net energy saving will be positive.

Application of Strategy #3 initially shows reduction in the total cost, compared to the basis case, for oxygen fraction up to 25%. However, the cost effectiveness of the strategy becomes questionable once the oxygen concentration proceeds to 28%. The cost saving is mainly due to the improvement in efficiency (enhanced electrochemical reaction as discussed in Section 3.3.2.3), that is less amount of reactants material needs to be supplied accordingly. However, larger φ becomes necessary to keep the temperature gradient within the acceptable range. And more importantly, oxygen price dominates the economical aspect of this approach which especially becomes more obvious at higher oxygen concentration. Therefore, Strategy #3 could become costly when the grade of the utilized coolant is too high.

3.5 Multi-objective optimization

Due to the crucial importance of efficiency and thermal homogeneity in fuel cell operation, a multi-objective optimization was implemented to address both requirements simultaneously. It should be noted that in this kind of optimization problems, where the conflicting targets must be met, it is not possible to conclude with a unique optimum point. Instead, a set of the so-called "effective solutions" would be achieved that can be presented as Pareto points (front) [37].

A weighted objective function was used, for the optimization as in Equation (3.18). In this function, $F_{\Delta T}$ and F_{Eff} stand for the total temperature gradient and inverse-of-

efficiency, $1/Eff_{el}$, respectively and s represents the manipulating variable(s). The weight factor values, $\omega \in [0,1]$, were used to adjust the importance of each criterion in achieving the objective function. Accordingly, minimization of the objective function based on each value of the weight factor generates a point of the Pareto front and, ultimately, provides the optimum operation guideline for the whole ω spectrum.

$$F_{ob} = \omega F_{\Delta T}(s) + (1-\omega) F_{Eff}(s) \qquad (3.18)$$

The normalized values of $F_{\Delta T}$ and F_{Eff} were used for reasonable comparability[37] ;

$$F^{Nomalised} = \frac{F(x) - F^{o}}{F^{\max} - F^{o}} \qquad (3.19)$$

F^{o}, F^{max} represents the optimum function value and maximum function value, respectively, within the calculation range.

Based on the sensitivity analysis outcomes (Section 3.3.2 of this chapter) the appropriate operating variables were identified. Table 3.5 shows the operating variables and their variation ranges. Based on the manipulating variables the various cases were classified, as presented in Table 3.6. In order to solve the optimization problem, the nonlinear optimization solver tool in MATLAB, *fmincon*, was 90tilized. This numerical tool can be used to find the minimum of a constrained nonlinear multi-variable function. The final results achieved as the optimum value may be influenced by the selection of the variable's initial guess. This also has effect on the calculation times. Different initial values for design variables were compared. The initial values used for each design variables include the middle value (MV) of the range, an upper value (125% MV), and a lower value (75% MV). Even though final results were slightly different for each initial values set, we used the minimum value that is attained for the objective function.

Table 3. 5: Mmanipulating variables and their ranges

Operating variables		Range/Values
1	φ	10 to 20
2	ΔT_{in}(K)	70 to 120
3	y_{O_2}	0.21 and 0.25

Table 3. 6: Optimization designed with different schemes

Optimization case (OC)	Operating variables
OC 1	1, 2
OC 2	1, 2, 3

The results of two optimization schemes are presented in Figure 3.6 where they are also compared with the basis case. The basis case is the gradient-efficiency profile for different air flowrates as was described in Section 3.3.2.1.

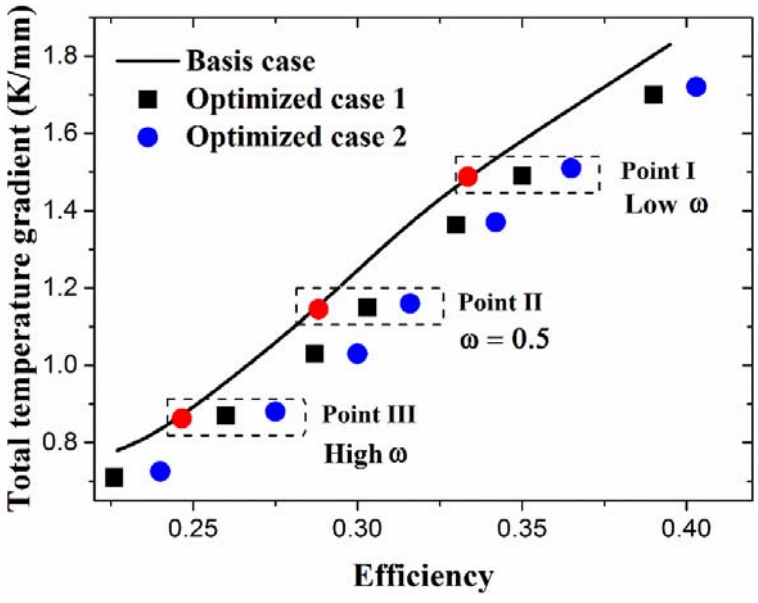

Figure 3. 6: Trade–off between efficiency and temperature gradient; Pareto points for basis case and optimization trials ($F_{H_2} = 900 ml/\min$).

Pareto fronts were improved in both optimization trials even though the improvement is more remarkable for Case 2. This indicates that the best performances might be

attained by combining all of the three tactics aforementioned.

Depending on the weight of each target on the optimum operation, decision can be made for the selection of the optimum variables. For example, if the temperature gradient minimization receives high attention, the system would be operated according to the conditions labelled as Point (III) in Figure 3.6. Under such a condition temperature gradient is reasonably minimized even though the efficiency is not at its maximum, i.e., efficiency would be higher if higher temperature gradient is allowed. Moreover, at this particular operating point one may improve the efficiency by applying optimization cases 1 and 2. For an operation that achieves both efficiency and temperature gradient goals with equal importance, one may select Point (II) and with the appropriate optimization opportunities. Finally, Point (I) corresponds to an operation in which the operators put more emphasis on the efficiency rather than the temperature gradient. The optimization results associated with these three operating points are tabulated in Table 3.7.

Table 3.7: Optimization results for different points of the Pareto front, labelled in Figure 3.6, for basis case (Basis), optimized case 1 (OC 1) and optimized case 2 (OC 2)

	Point (I)			**Point (III)**			**Point (III)**		
	Basis	**OC 1**	**OC 2**	**Basis**	**OC 1**	**OC 2**	**Basis**	**OC 1**	**OC 2**
dT, K/mm	1.47	1.50	1.51	1.15	1.15	1.16	0.88	0.87	0.88
Efficiency	0.33	0.35	0.37	0.28	0.30	0.32	0.25	0.26	0.28
ΔT_{in}, K	0	102	101	0	101	100	0	101	100
φ	12.4	11.3	12.1	15.7	13.7	15.2	17.8	16.2	17.2
y_{O2} in cathode	.21	0.21	0.25	0.21	0.21	0.25	0.21	0.21	0.25

3.6 Conclusions

Thermal management of SOFC stack plays a leading role in determining its durability and reliability. This is intrinsically a complicated concept mainly because of the various interactive phenomena that dominate the temperature profile inside a reactive stack. Due to this complexity, high fidelity numerical tools are inevitable to effectively simulate the stack's thermal behavior. Any promising strategy for temperature gradient reduction must be critically evaluated for its practical application. This is of crucial importance as some of these methods might sacrifice the efficiency and/or economy of system. A stack level model was developed and employed in this article aiming to account for temperature gradients in both flow course and stacking dimensions. Subsequently, model-based technical and economic assessments for three promising strategies for reduction of the temperature gradient inside SOFC stack were carried out in this study. Utilization of excess air, as a preliminary strategy, was evaluated individually and also in comparison with other typical tactics, including adjustment of the inlet gas temperature differences and also air enrichment. The results reveal the advantages and disadvantages relevant to each approach and potential features achieved by combining them. Evaluations cover technical and economic aspects of each strategy. A multi-objective optimization was also presented in this study in order to seek appropriate operating conditions that address the thermal and efficiency requirements and support a compromised decision-making process. The results reveal that the negative consequences that each strategy intrinsically causes can be moderated by combination of diverse strategies. In order to limit the excess air utilization, for instance, adjustment of ΔT_{in} about 110K and enrichment of air up to 25% oxygen were justified in this study. It was shown that higher ΔT_{in} can become ineffective or even harmful, and further air enrichment, beyond 25% of oxygen, might result in exceeding the justifiable operation cost margin due to the price of pure oxygen.

Nomenclature

C_p	Specific heat (J $mol^{-1}K^{-1}$)
Cost	Budget cost ($)
E	Voltage (V)
E^{design}	Designed energy (kWh)
Eff_{el}	Electrical net efficiency
Eff_{isen}	Isentropic efficiency
F	Molar flow rate (mol s^{-1})
F_{ob}	Objective function
$F_{\Delta T}$	Temperature gradient function
F_{Eff}	Efficiency function
LHV	Lower heating value (J mol^{-1})
ΔH	Heat (J)
I	Current (A)
i	Current density (A m^{-2})
L	Distances (m)
m	Total amount of substance (mole)
n	Calculated numbers of tanks in model
P	Pressure (Pa)
P_{net}	Net power (W)
P_{bl}	Blower power (W)
Pr	Price ($)
R^{ohmic}	Ohmic resistance (Ω)
t	Time (s)
T	Temperature (K)
$\overline{T}$	Average temperature (K)
ΔT	Temperature differences (K)
U_f	Fuel utilization
y	Species mole fraction
Greek Letters	
φ	Air to fuel flow ratio
ω	Weighting coefficient

$\boldsymbol{\eta}$	Overpotential (V)
κ	Specific heating ratio (=1.4) [23]

sub-/ superscripts

A	Anode
a	Air
act	Activation
C	Cathode
combus	Combustion
cell	SOFC cell
in	Inlet
max	maximum value
Normalised	Normalised function value
o	Optimum
out	Outlet
ph	Preheating
stack	SOFC stack
x	x direction
z	z direction
0	Ambient

Acronym:

MOO:	Multiple-Objective Optimization
MV:	Middle Value
OCV:	Open Circuit Voltage
OC:	Optimization Case
PEN:	Positive Electrode–Electrolyte–Negative Electrode
SOFC:	Solid Oxide Fuel Cell

References:

[1] P. Aguiar, C.S. Adjiman, N.P. Brandon, Anode-supported intermediate temperature direct internal reforming solid oxide fuel cell. I: model-based steady-state performance, Journal of Power Sources 138 (2004) 120-136.

[2] S. Park, J.M. Vohs, R.J. Gorte, Direct oxidation of hydrocarbons in a solid-oxide fuel cell, Nature 404 (2000) 265-267.

[3] S.C. Singhal, Advances in solid oxide fuel cell technology, Solid State Ionics 135 (2000) 305-313.

[4] J. Palsson, A. Selimovic, L. Sjunnesson, Combined solid oxide fuel cell and gas turbine systems for efficient power and heat generation, Journal of Power Sources 86 (2000) 442-448.

[5] L.-K. Chiang, H.-C. Liu, Y.-H. Shiu, C.-H. Lee, R.-Y. Lee, Thermo-electrochemical and thermal stress analysis for an anode-supported SOFC cell, Renewable Energy 33 (2008) 2580-2588.

[6] Y. Wang, F. Yoshiba, T. Watanabe, S. Weng, Numerical analysis of electrochemical characteristics and heat/species transport for planar porous-electrode-supported SOFC, Journal of Power Sources 170 (2007) 101-110.

[7] C.M. Huang, S.S. Shy, C.H. Lee, On flow uniformity in various interconnects and its influence to cell performance of planar SOFC, Journal of Power Sources 183 (2008) 205-213.

[8] D. Grondin, J. Deseure, M. Zahid, M.J. Garcia, Y. Bultel, Optimization of SOFC interconnect design using Multiphysic computation, in: B. Bertrand, J. Xavier (Eds.) Computer Aided Chemical Engineering, Elsevier2008, pp. 841-846.

[9] Y. Wang, J. Yu, X. Cao, Numerical analysis of optimal performance of planar electrode supported solid oxide fuel cell at various syngas flow rates, Energy Conversion and Management 77 (2014) 637-642.

[10] M. Iwata, T. Hikosaka, M. Morita, T. Iwanari, K. Ito, K. Onda, Y. Esaki, Y. Sakaki, S. Nagata, Performance analysis of planar-type unit SOFC considering current and temperature distributions, Solid State Ionics 132 (2000) 297-308.

[11] Y. Yang, G. Wang, H. Zhang, W. Xia, Computational analysis of thermo-fluid and electrochemical characteristics of MOLB-type SOFC stacks, Journal of Power Sources 173 (2007) 233-239.

[12] A. Amiri, P. Vijay, M.O. Tadé, K. Ahmed, G.D. Ingram, V. Pareek, R. Utikar, Solid oxide fuel cell reactor analysis and optimisation through a novel multi-scale modelling strategy, Computers & Chemical Engineering 78 (2015) 10-23.

[13] E. Achenbach, Three-dimensional and time-dependent simulation of a planar solid oxide fuel cell stack, Journal of Power Sources 49 (1994) 333-348.

[14] K. Sudaprasert, R.P. Travis, R.F. Martinez-Botas, A Study of Temperature Distribution Across a Solid Oxide Fuel Cell Stack, Journal of Fuel Cell Science and Technology 7 (2009) 011002-011002.

[15] A.C. Burt, I.B. Celik, R.S. Gemmen, A.V. Smirnov, A numerical study of cell-to-cell variations in a SOFC stack, Journal of Power Sources 126 (2004) 76-87.

[16] S.M.C. Ang, E.S. Fraga, N.P. Brandon, N.J. Samsatli, D.J.L. Brett, Fuel cell systems optimisation – Methods and strategies, International Journal Of Hydrogen Energy 36 (2011) 14678-14703.

[17] Larrain, D. Solid Oxide Fuel Cell Stack Simulation and Optimization, including Experimental Validation and Transient Behavior. Ph.D Dissertation, Swiss Federal Institute of Technology, Lausanne, 2005.

[18] F. Palazzi, N. Autissier, F.M.A. Marechal, D. Favrat, A methodology for thermo-economic modeling and optimization of solid oxide fuel cell systems, Applied Thermal Engineering 27 (2007) 2703-2712.

[19] C.I. Weber, F. Maréchal, D. Favrat, S. Kraines, Optimization of an SOFC-based decentralized polygeneration system for providing energy services in an office-building in Tokyo, Applied Thermal Engineering 26 (2006) 1409-1419.

[20] D. Xue, Z. Dong, Optimal fuel cell system design considering functional performance and production costs, Journal of Power Sources 76 (1998) 69-80.

[21] S.M.C. Ang, D.J.L. Brett, E.S. Fraga, A multi-objective optimisation model for a general polymer electrolyte membrane fuel cell system, Journal of Power Sources 195 (2010) 2754-2763.

[22] S. Tang, A. Amiri, P. Vijay, M.O. Tadé, Development and validation of a computationally epicient pseudo 3D model for planar SOFC integrated with a heating furnace, Chemical Engineering Journal 290 (2016) 252-262.

[23] L. Zhang, X. Li, J. Jiang, S. Li, J. Yang, J. Li, Dynamic modeling and analysis of a 5-kW solid oxide fuel cell system from the perspectives of cooperative control of thermal safety and high efficiency, International Journal Of Hydrogen Energy 40 (2015) 456-476.

[24] Blum, L.; Riensche, E. Systems. In *Encyclopaedia of electrochemical power sources Series 3;* Juergen, G., Chris D., Patrick M., Zempachi O., David R., Bruno S., Eds.; Elsevier: Amsterdam, 2009; pp 99-119.

[25] R. Peters, R. Deja, L. Blum, J. Pennanen, J. Kiviaho, T. Hakala, Analysis of solid oxide fuel cell system concepts with anode recycling, International Journal Of Hydrogen Energy 38 (2013) 6809-6820.

[26] D. Georgis, S.S. Jogwar, A.S. Almansoori, P. Daoutidis, Control of an energy integrated solid oxide fuel cell system, American Control Conference (ACC), 2011, 2011, pp. 1518-1523.

[27] A. Kawakami, S. Matsuoka, N. Watanbe, T. Saito, A. Ueno, T. Ishihara, N. Sakai, H. Yokokawa, Development of Two Types of Tubular SOFCS at TOTO, Advances in Solid Oxide Fuel Cells II: Ceramic Engineering and Science Proceedings, John Wiley & Sons, Inc.2008, pp. 3-12.

[28] A. Amiri, P. Vijay, M.O. Tadé, K. Ahmed, G.D. Ingram, V. Pareek, R. Utikar, Planar SOFC system modelling and simulation including a 3D stack module, International Journal of Hydrogen Energy 41 (2016) 2919-2930.

[29] W.B. Guan, H.J. Zhai, L. Jin, C. Xu, W.G. Wang, Temperature Measurement and Distribution Inside Planar SOFC Stacks, Fuel Cells 12 (2012) 24-31.

[30] D. Larrain, J. Van herle, D. Favrat, Simulation of SOFC stack and repeat elements including interconnect degradation and anode reoxidation risk, Journal of Power Sources 161 (2006) 392-403.

[31] V.M. Janardhanan, V. Heuveline, O. Deutschmann, Performance analysis of a SOFC under direct internal reforming conditions, Journal of Power Sources 172 (2007) 296-307.

[32] Y. Zhu, W. Cai, Y. Li, C. Wen, Anode gas recirculation behavior of a fuel ejector in hybrid solid oxide fuel cell systems: Performance evaluation in three operational modes, Journal of Power Sources 185 (2008) 1122-1130.

[33] X. Zhang, J. Li, G. Li, Z. Feng, Numerical study on the thermal charteristics in a tubular solid oxide fuel cell with indirect internal reformer, International Journal of Thermal Sciences 48 (2009) 805-814.

[34] S. Kakaç, A. Pramuanjaroenkij, X.Y. Zhou, A review of numerical modeling of solid oxide fuel cells, International Journal of Hydrogen Energy 32 (2007) 761-786.

[35] Gurbinder K. *Solid Oxide Fuel Cell Components: Interfacial Compatibility of SOFC Glass Seals*; Springer International Publishing: Switzerland, 2016

[36] Kaur, G. *Solid Oxide Fuel Cell Components*; Springer International Publishing, 2015.

[37] R.T. Marler, J.S. Arora Survey of multi-objective optimization methods for engineering, Structural and Multidisciplinary Optimization 26 (2004) 369-395.

Chapter 4

Exergy Analysis and Thermal Management at System Scale

4.1 Introduction

As a high temperature fuel cell, SOFC thermal management is a key issue in its design and application. For a cell or stack, avoiding the steep temperature gradient is the core of thermal management with necessity of satisfying its working temperature [1]. While in a system design, the first purpose of thermal management is to ensure the cell/stack is working within the required temperature range. Furthermore, by-products and heat sources/sinks are required to be well organized to make maximum use of energy. For the heat energy inside the system, the cell/stack is one of the major sources as thermal energy is released from the electrochemical reactions accompanied with Joule heating. In afterburner unit heat could also be generated by the combustion of fuel exhausts, since fuel will not be consumed completely in the stack. Additionally, the heat exchange will also occur in the gas pre-heater. Therefore, it is also essential to use the heat appropriately by the optimal thermal management for the purpose of improving the overall efficiency of system [1]. Above all, the thermal management for the operating of a SOFC system would impose requirements on both the SOFC design and defining of the operating conditions.

Energy or exergy analysis could be the means for analysing and improving the thermal management of a SOFC system. Energy analysis is estimated on First Law of Thermodynamics, which would involve the evaluation of the energy conversion, utilization. It can be helpful in analysing the energy distribution in the system and tracing the source of energy lost in system that can be potentially used. On the other hand, exergy is defined on Second Law of Thermodynamics which calculates the irreversibility. By the exergy analysis, the efficiency of the available work from the sources can be calculated, in which, the wasted work potential is estimated. It is useful to specify the responsible link in the system for the lost work. It is believed that exergy analysis is more realistic for the system operating design in practical than the results from conventional energy analysis [2].

Several exergy studies have been conducted for the SOFC from different viewpoints. For instance, Chan. et al. [3] conducted energy/ exergy analysis for two SOFC systems, one fed with pure hydrogen and the other one fed with methane in their

research. Their study indicated that the afterburner occupies the largest share of energy lost in system. Granovskij. et al. [4] performed exergy analysis on a SOFC-GT hybrid system and the results of their study indicated that the depletion number that reflects the efficiency of energy and fuel consumption of SOFC or GT system were much higher than the one of hybrid system. Some studies agreed that combustion chamber and SOFC stack were components with highest exergy destruction rate with their proposed systems and operating points [5] and [6]. Ali et al. [7] analyse the hydrogen fed system in their study based the criterion named exegetic performance coefficient (EPC). They also claimed that the system working with certain operating conditions which achieve higher EPC will result in a better performance that considered both power and environmental issues. Suranat et al. [8] analysed the thermodynamic performance of a direct internal reforming planar SOFC with co- and counter- configuration through the energy/exergy efficiency evaluations to propose a suitable operating conditions.

Table 4.1 compares some of the recent SOFC exergy studies with the current work. These works are compared based on the scales and features of SOFC that are considered. Most of the system investigations are based on a system model with a simple built-in fuel cell module, focusing on the system performance, while the detailed cell/stack level thermal information is ignored. Calise et al. [15] conducted the exergy analysis with considering the stack performance based on the tubular stack model. However, the studies for a planar SOFC so far are very limited but necessary, since the tubular stack thermal behaviours could vary greatly from the ones of planar. Additionally, the operating conditions benefit for the criteria in cell/stack level may influence the system performance, and on the other side, system processing condition will also affect the characters of cell/ stack level. Sometimes they may even have adverse effects. The influence of process operating conditions on the thermal behaviours of cell/ stack and system in parallel needs to be further studied.

In this chapter, an exergy analysis is firstly presented based on a simple SOFC system model. Since multi criteria with different levels of SOFC system is required to be satisfied simultaneously, a more comprehensive SOFC system model [21] and [22] is then introduced in this study, with which the properties of all levels can be

obtained, and more importantly, the interactions between these properties can be captured. Based on this model, the assessment for a SOFC system thermal behavior in all levels is presented, accounting for the cell temperature gradient, utilization of heat resource within whole system, system efficiency, etc. Moreover, sensitive analysis with different operating scenarios is conducted, based on which, the direction of improved thermal management of a SOFC can be proposed.

Table 4.1: Comparison of recent studies for SOFC system concerning exergy analysis and detailed stack characters

Study characteristics	**Recent studies**																		
	[3]	[4]	[5]	[6]	[7]	[8]	[9]	[10]	[11]	[12]	[13]	[14]	[15]	[16]	[17]	[18]	[19]	[20]	This work
A. Exergy evaluation for SOFC system level	*	*	*	*	*	-	*	*	*	*	*	*	*	*	*	*	*	*	*
B. Exergy evaluation for variation flowsheets	-	-	-	-	-	-	-	*	-	-	-	*	-	-	*	*	-	-	*
C. Sensitive analysis of SOFC system in exergy	-	-	-	-	-	-	-	*	-	*	-	-	*	*	*	-	-	-	*
D. SOFC exergy evaluation along with detailed planar SOFC thermal features	-	-	-	-	-	*	-	-	-	-	-	-	-	-	-	-	-	-	*
E. Operating direction proposal for better thermal management based on both SOFC system and stack levels	-	-	-	-	-	*	-	-	-	-	-	-	-	-	-	-	-	-	*

*: considered; -: not considered;

4.2 Energy and exergy estimation

The energy and exergy analysis for SOFC system is carried out based on the fundamental equations as follows.

Energy for each stream is calculated based on the enthalpy estimation:

$$E_n = \sum c_{p\ i,n}\, \dot{m}_{i,n} (T_n - T_0) \tag{4.1}$$

in which, n refers to the steam's number in the system, i refers to the species in the stream, $\dot{m}$ is the molar flowrates, T_0 is the standard temperature

The net electrical efficiency in energy respect is calculated as [23]:

$$\eta_{el}^{en} = \frac{P_{el} - P_{consum}}{\dot{m}_{fuel}^{input}\ LHV_{fuel}} \tag{4.2}$$

The power consumed for the air compressor, however, is not considerable compared to the input energy in the case of this study, that less than 1.5% power of the total input fuel energy required by the air blower. The electrical efficiency for the analysis in this study is simplified as:

$$\eta_{el}^{en} = \frac{P_{el}}{\dot{m}_{fuel}^{input}\ LHV_{fuel}} \tag{4.3}$$

The waste heat energy of the system is estimated as the enthalpy of the exhaust gas stream.

$$E_{th} = E_{hot\_exahust} \tag{4.4}$$

For the SOFC system in this study, the hot exhaust gas temperature is usually around 400 K, and it could be utilized for low-temperature heating, such as the room and water heating [23]. Therefore, in order to better utilize the energy in plant and improve the total system efficiency, the heat exhaust energy can be utilized to make use of this waste of heat. The portion of the exhaust heat can be recovered can vary from 38% ~ 70% [10], [24] and [25], according to the way of heat exhaust utilization, such as converting into mechanical work, or heating the water. The thermal efficiency of the system in this case study is defined as the recoverable

thermal energy share of the system input energy.

$$\eta_{th}^{en} = \frac{\varepsilon E_{th}}{\dot{m}_{fuel}^{input} \; LHV_{fuel}} \quad (4.5)$$

where, ε is the heat recovery ratio, and 60% is used for this study.

The exergy analysis is based on the exergy estimation for each stream, and it is calculated for the sum of physical and chemical exergy [6] and [12]:

$$Ex_n = Ex_n^{chem} + Ex_n^{ph} \quad (4.6)$$

Chemical exergy [8]:

$$Ex_n^{chem} = \sum_i \dot{m}_i Ex_i^0 + RT_0 \sum_i \dot{m}_i \ln y_i \quad (4.7)$$

where, i refers to the species in the stream, Ex^0 is the reference chemical exergy of species, $\dot{m}$ is the flow rates and y denotes the species molar fraction in stream.

Physical exergy can be estimated through equation 4.8 [6] and [12]:

$$Ex_n^{ph} = [(h - h_0)_n - T_0(s - s_0)_n] \quad (4.8)$$

in which, h is the specific enthalpy and s is the entropy

The electrical efficiency in respected to exergy value can be estimated as:

$$\eta_{el}^{ex} = \frac{P_{el}}{Ex^{input}} \quad (4.9)$$

Thermal efficiency with respect to exergy calculation is estimated as Equation 4.10. The thermal exergy is estimated by the physical exergy of the hot exhaust steam of the system.

$$\eta_{th}^{ex} = \frac{\varepsilon Ex_{th}}{Ex^{input}} \quad (4.10)$$

$$Ex_{th} = Ex_{hot\_exhaust}^{ph} \quad (4.11)$$

The total efficiency with respect to exergy calculation in this study is defined as in Equation 4.12:

$$\eta_{total}^{ex} = \frac{P_{el} + Ex_{th}}{Ex^{input}} \quad (4.12)$$

Since with the exergy analysis, the destroyed exergy that is so called as irreversibility during the process is considered, and this part of exergy for each process of the system is calculated as:

$$Irr = Ex_{provided} - Ex_{utilized} \quad (4.13)$$

The share of irreversibility of the exergy input is calculated as:

$$\mu_{Irr}^{Ex} = \frac{Irr}{Ex^{input}}$$

Taking the key component of the system, SOFC stack, as an example, the process is presented as below.

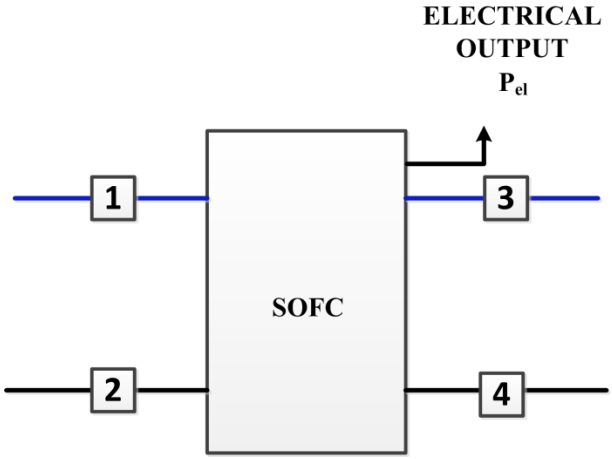

Figure 4.1: Schematic illustration of process unit in plant

With this process, input streams are 1 and 2 which will denote the anode and cathode input gases, and the output streams 3 and 4 will refer to the anode and cathode exhaust respectively. The electrical output is the electrical power gained by this process which is calculated by the inbuilt SOFC stack module in the model.

The provided exergy is calculated as:

$$Ex_{provided}^{SOFC} = Ex_1 + Ex_2 \quad (4.14)$$

The utilized exergy concludes the produced electrical power and the remaining exergy in the output streams:

$$Ex_{utilized}^{SOFC} = Ex_3 + Ex_4 + P_{el} \quad (4.15)$$

The destroyed exergy by this process is defined as:

$$Irr^{SOFC} = Ex_1 + Ex_2 - (Ex_3 + Ex_4 + P_{el}) \quad (4.16)$$

4.3 Exergy analysis for a SOFC system with a simple model

4.3.1 Model description and flowsheet

In order to study the system scale performance, a plant-wide model is used proposed by Zhang et al. [26]. This model is utilized for its simplicity and its capability for the analysis of thermodynamics for balance of plant. A SOFC system model is developed in AspenPlus environment, for which the flowsheet is shown in Figure 4.2. In additional to the core module (SOFC anode and cathode), the other components of the plant include the pre-reformer, after burner, and heat exchanger, etc..

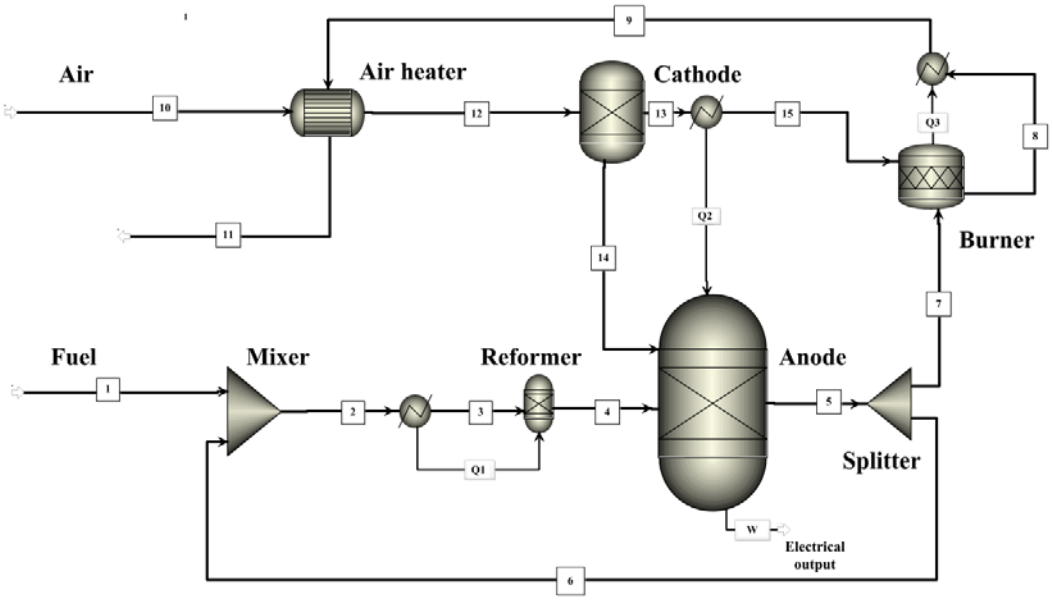

Figure 4.2: AspenPlus simple SOFC system model flowsheet (adapted from Ref. 26)

All the system's components, including the fuel cell, are simulated by applying the existing AspenPlus operation blocks. The fresh fuel is mixed with the anode recycle gas (reaction products and some unreacted fuel) before feeding into the pre-reformer, The ratio of recycling gases in anode exhausts can be controlled. This process is

simulated by using *Mixer* and *Fslipt* blocks from AspenPlus modelling library. This stream of fuel is then introduced to the pre-reformer for the reformation reaction. Due to the endothermic nature of this reaction, the module of Rgibbs connected with Heater are used to simulate this process. The former is used for the reforming reaction modelling inside the pre-reformer, while the latter simulates the temperature decrease brought by the endothermic reaction. Air stream is firstly preheated with the heat generated from afterburner, and then separated into two streams that fed into afterburner and anode respectively. These two processes are simulated by *Heatx* and *Sep* blocks respectively. Since the air will also be heated through the exothermic reaction in anode, *Heater* module is also used for this temperature increases. For the anode, where the electrochemical reaction occurs, the module *Rgibbs* is utilized. All the cathode exhausts and partial of anode exhausts are then introduced into afterburner for combustion. The reactor module *Rstoic* is chosen for this process simulation, with the assumption of 100% conversion occurring in this module. The temperature increase of the gases after combustion is predicted by *Heater* block.

For electrical features calculations, the voltage is estimated based on equations as blow. The cell voltage was calculated by subtracting the losses from the Nernst voltage. And they are calculated as below in Equations 4.17~4.21.

Nernst equations:

$$E_{Nernst} = E^0 + \frac{RT}{2F}\ln\frac{p_{H_2}\,p_{O_2}^{0.5}}{p_{H_2O}} \tag{4.17}$$

Activation loss is calculated as:

$$V_{act} = \left(\frac{RT}{n_e F\alpha_A}\right)\ln\left(\frac{i}{i_{0,A}}\right) - \left(\frac{RT}{n_e F\alpha_C}\right)\ln\left(\frac{i}{i_{0,C}}\right) \tag{4.18}$$

in which,

$$i_0^A = K_0^A (y^{H_2})^{\gamma_{H_2}} (y^{H_2O})^{\gamma_{H2O}} \exp\left(-\frac{E_{act}^A}{RT}\right) \tag{4.19}$$

$$i_0^C = K_0^C (y^{O_2})^{\gamma_{O_2}} \exp(-\frac{E_{act}^C}{RT}) \quad (4.20)$$

Ohmic loss is calculated as:

$$V_{Ohmic} = IR^{Ohmic} \quad (4.21)$$

4.3.2 Simulation results

4.3.2.1 Model validation

The calculation results are compared with the published data [26], as shown in Table 4.2, with the simulation setting listed in Table4.3. Results show good agreement with the published data.

Table 4.2: Calculated results compared with published data.

Parameters	**Published data [26]**	**Current model**
Current density (mA/cm^2)	178	187
Operating Voltage (V)	0.70	0.68
Pre-reformer CH_4 conversion fraction	0.259	0.250
Anode exhaust composition (mol %)		
H_2O	50.9	50.7
CO_2	24.9	24.9
H_2	11.6	11.6
CO	7.4	7.4
N_2	5.1	5.1
O_2	0	0
Stack exhaust composition (mol %)		
H_2O	4.5	4.5
CO_2	2.3	2.3
H_2	0	0
CO	0	0
N_2	77.3	77.3
O_2	15.9	15.9

Table 4.3: Simulation input parameters [26]

Parameters	Values
Fresh fuel composition	CH_4 81.3%, $C_2H_6N_2$ 2.9%, C_3H_8 0.4%, N_2 14.3%, CO_2 0.9%
Operation temperature, K	1183
Fuel inlet temperature, K	473
Air inlet temperature, K	973
Fuel utilization	0.85
Air Utilization	0.19
Electrical power, kW	120

4.3.2.2 Exergy analysis

In order to study the system performance by considering of utilization of energy in system, exergy analysis is carried out, with the results shown in Figure 4.3. Based on this flowsheet, analysis results show that almost 30% of input exergy in system are destroyed during the processes in the plant, with is a considerable loss. It is to be noticed that, the hot waste in this cases is extremely high, as a relatively high temperature (around 900 K) was set for the fresh air that the heat generated by the burner is not completely utilized, leading to a high temperature for the exhaust gas of the system. This also indicates that the system needs improved flowsheet arrangement for the better utilization of the hot exhaust. For the total irreversibility generated in the whole plant, the exergy loss in burner constitutes the largest share, followed by the one in air heater. The main reason for exergy destruction is the mixing of gases with temperature differences. For the combustion chamber, large heat generated with air exhausts and anode exhausts with unreacted fuel leading to high temperature for the burner outlet stream, and large exergy loss is therefore generated during this process. High exergy loss occurred in air heater due to large temperature differences and the high air flow rates as well. Some researchers showed that the gas preheaters and the combustion chamber are the most and second exergy destruction in system [6] and [12]. However for the cases study here, a relatively small temperature differences are induced for the air heater as inlet air temperature is set high, and therefore, the exergy loss is not as obvious as in burner. The SOFC unit is third largest exergy loss unit in this system, as internal reforming and electrochemical reaction occurring here, that some of the chemical exergy of fuel are

consumed for heating the gas, resulting in the generation of exergy loss in this process. The exergy loss in the other units is relatively small compared to air heater and burner.

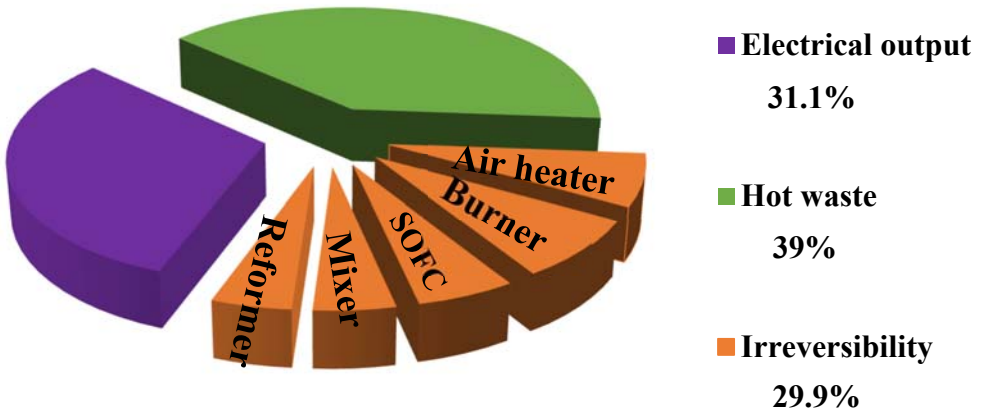

Figure 4.3: Exergy share of the input for the plant

This simulation is carried out using the simplified model presented in Ref.24. The estimations, however, was based on some simplification assumptions, which may be inaccurate in predictions. For example, some operating parameters are set based on specific experimental conditions. Accordingly, errors may occur when different conditions are set to simulate various scenarios. Moreover, these variables will also affect the prediction of system performance in turn. The above drawbacks that concerned would lead to the barriers for the parameter sensitive analysis of the system. Most importantly, the stack detailed performance, such as the temperature distribution cannot be captured. However, the operating conditions that benefit the system performance may even have opposite effects on the stack. All these information are important for evaluating the thermal performance of a SOFC, and defining operating conditions that aims for an improved thermal management of a SOFC system in multi-scale. Therefore, a more comprehensive model that can compute the behaviours of SOFC at different levels in parallel is required.

4.4 Thermal management study on SOFC system with a comprehensive model.

Due to the limitations of evaluating the thermal behaviors for a SOFC system by using the simple model, a more detailed model that offers a parallel computing of stack and system levels' performances is introduced. Furthermore, thermal management studies including sensitivity analyses are conducted through the demonstrated model.

4.4.1 Model description and flowsheet

Figure 4.4 displays the schematic of a SOFC system, containing a pseudo 3D SOFC stack module, developed by Amiri et al. [21] and [22]. The stack includes 4 cells, which are approximated by the network of repeating compartment units. The governing equations covering the mass balance, energy balance, and electric balance are employed on each compartment, so that fuel cell unit in the system is capable of calculating the distributed electrochemical and thermal fields inside the SOFC stack. For the whole system simulation, in addition to the fuel cell unit, other unit operations including the preheaters for air, water, and fuel/pre-reformer as well the burner for combustion of anode exhausts, and the anode exhausts cycling are also considered. This multi-scale model is capable of capturing the detailed information at cell, stack, and system levels at the same time.

.

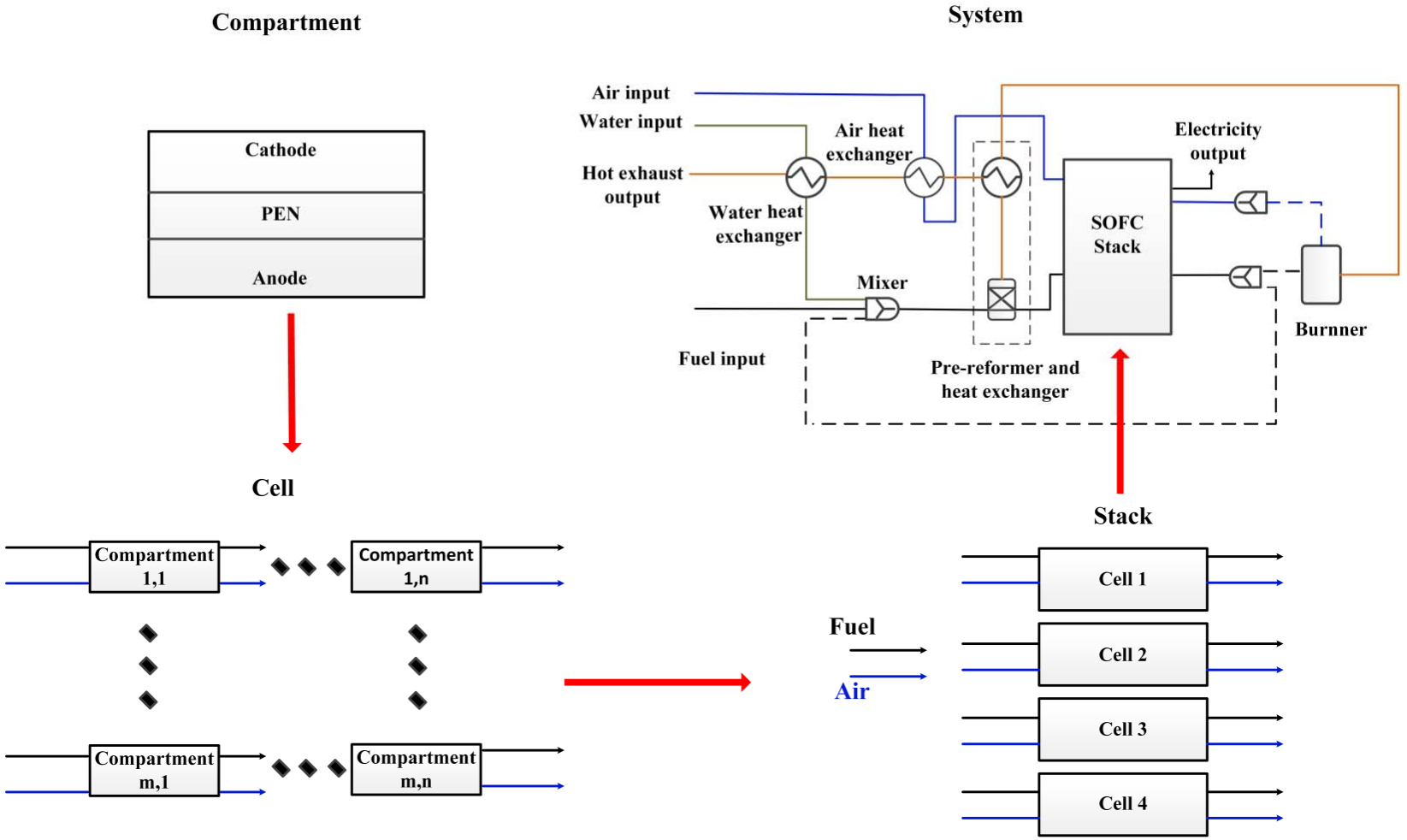

Figure 4.4: schematic multi-scale model structure (adapted from [21] and [22])

4.4.2 Simulation Results

4.4.2.1 System performance evaluation for a basis case

Based on the multi-scale mode, an evaluation of the system performance for a basis case is firstly carried out, with the operating condition listed in Table 4.4. It is to be noted that, the external reforming is applied for this system, while a full reforming is carried out such that the fraction of CH_4 in the inlet stream to the SOFC is not larger than 0.5% for all the simulations. The energy and exergy distribution for the system is illustrated as in Figure 4.5

Table 4.4: Operating conditions for the basis case

Parameters	**Values**
Fresh fuel composition	CH_4 87%, N_2 13%
Fuel flow rate, mol/s	3.3×10^{-5}
Fuel inlet temperature, K	1073
Operation pressure, bar	1
Air inlet temperature, K	1073
Air to fuel flow rate ratio	10
Anode recycling ratio	0.5
Pre-reformer temperature, K	1073

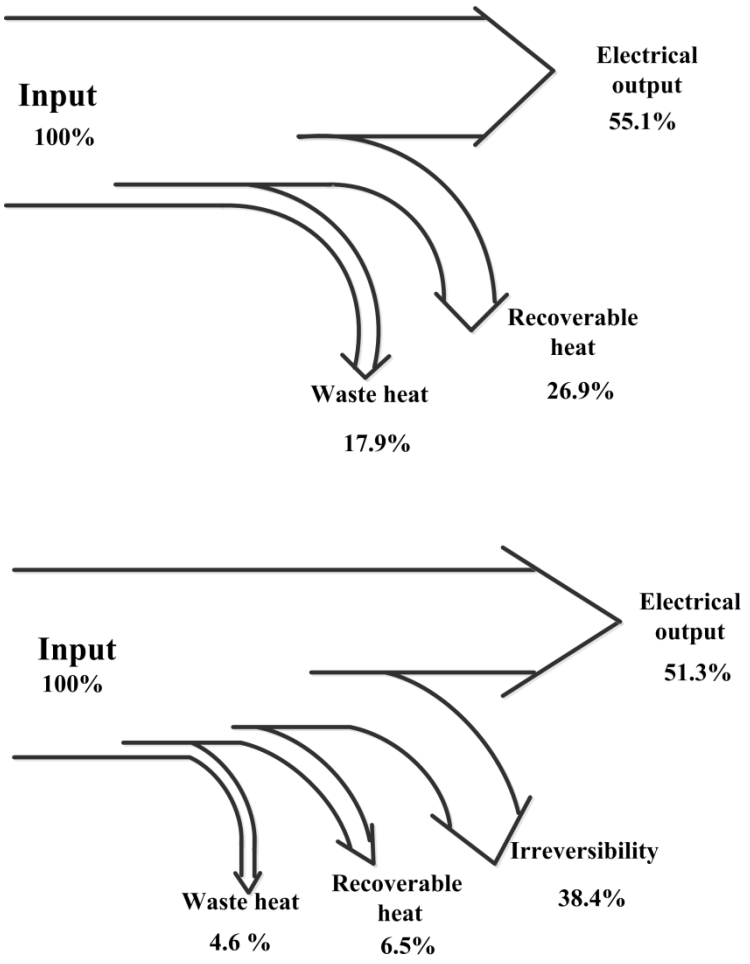

Figure 4.5: Energy balance of the system calculated in energy (top) and exergy (bottom).

Compared to the exergy analysis, the share of the electrical output with respect to energy is a slightly higher. It is because the exergy for input fuel is slightly higher than the value of lower heating value of the fuel based on the Equations 4.3 and 4.9. However, the share of heat recovery and the wasted heat in system with respect to energy analysis performs much higher than the one estimated by exergy analysis. It is known that energy is never destroyed during a process that it changes from one form to another according to First Law of Thermodynamics. For the case of this study, electrical power and heat waste construct the input energy. Conversely, different from energy analysis, exergy is always destroyed when a process involves a temperature change, which is defined based on Second Law of Thermodynamics. The transfers invariably bring about spread, dispersal, or dissipation of matter or energy, or both amongst the bodies. Therefore, for the current study as showed in

Figure 4.5, some of the exergy is destroyed through the processes of whole system, and the available exergy for work remained in the heat waste is much less compared with the values estimated from energy analysis.

As a consequence, the performance of this part of lost exergy within the system is necessary to be studied. Accordingly, the distribution of irreversibility for each process within the system is further studied as presented in Figure 4.6. With an equally 100 W input for fuel, the electrical output is 51.3 W, the achieved heat resources which can be utilized is 10.3 W, while the total lost exergy is 38.4 W. Two components in system that consume the exergy most are air heat exchanger and combustion, causing 61.2% and 15.3% of total irreversibility respectively. Similar observation can also be found in the works [10] and [23]. And SOFC stack imposes approximately 10.7% of the total irreversibility. Among all components in the system, the attention should be paid on the air heat exchanger as it occupies more than half of the total irreversibility. According to the Equations 4.6 to 4.8, exergy will be destroyed when entropy rises. Hence, large exergy is destroyed through the air heater since the air flowrates are large, and more importantly, large temperature difference exists in this process under the requirement of heat exchange. The second exergy dissipated unit in the plant is the burner, which occupies 15.3% of the total exergy loss, while the amount of exergy loss caused by other units is much smaller. Accordingly, the air heater and burner will mainly be the focus of the exergy analysis in the next sections.

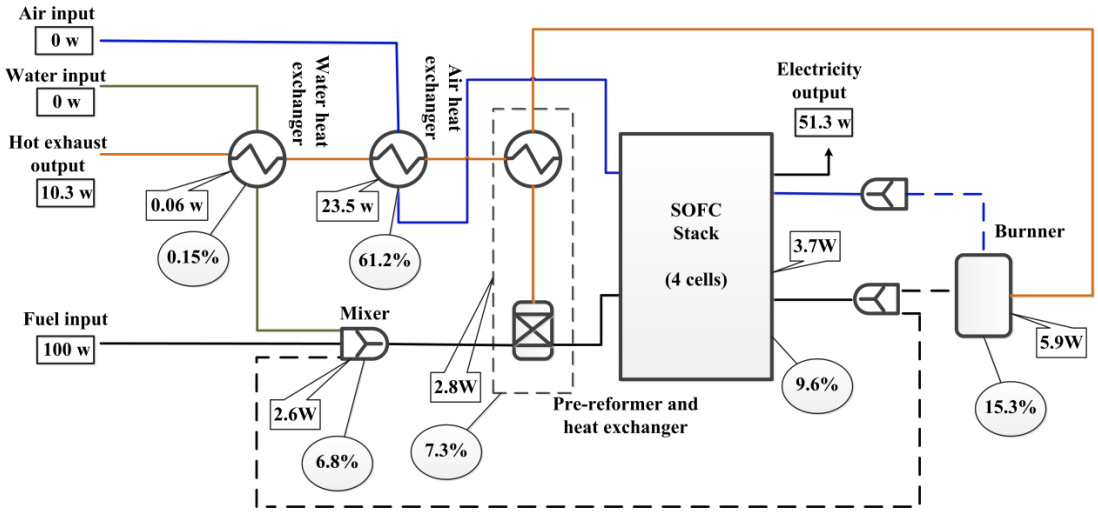

Figure 4.6: Process flowsheet for a SOFC stack system. The rectangular boxes with arrows show the exergy loss in each process, the oval boxes with arrows show the ratio of exergy loss and the input exergy into the system, the rectangular boxes without arrows show the system input and output.

4.4.2.2 Parameter studies of the thermal behaviours

As discussed in the previous sections, several criteria should be satisfied simultaneously for a SOFC system to claim a reliable, durable, and efficient operation. The operation of SOFC system can be complicated, as large number of parameters is involved and they may influence different criteria of the system diversely. As the thermal management of a SOFC system is the focus for the current study, the thermal behaviors are the main focus of this study. Characteristics such as the temperature gradient, electrical efficiency, thermal efficiency, total efficiency, and irreversibility are examined.

Four scenarios including the air flowrates, oxygen concentration in cathode, anode recycling ratio, and modified flowsheet with cathode recycling loop will be assessed. The sensitive analysis is conducted in order to understand the influences on the system performance by the different operating scenarios.

4.4.2.2.1 Air flow rates (Scenario #1)

As the most common strategy for regulating the temperature of the SOFC stack, the scenario of variation of air flowrate is firstly examined. An air flowrate of M is applied for the basis case. The simulation is carried out with different air flowrates from 0.5 M ~ 2.5 M while the fuel flowrates was kept constant. The calculated results for the thermal behaviors of the SOFC system are presented in Table 4.5.

Table 4.5: Simulation results for the system thermal behaviors with application of different air flowrates

$\dot{m}_{air}$	dT_x, K/mm	η_{total}^{ex}, %	η_{el}^{ex}, %	η_{th}^{ex}, %	μ_{Irr}^{Ex}, %
0.5 M	1.72	65.0	58.0	7.0	30.4
M (Basis Case)	1.20	57.5	51.3	6.2	38.4
1.5 M	0.93	50.7	46.0	4.7	47.2
1.8 M	0.82	48.4	44.2	4.2	48.8

The results show that the increase of air flowrates is very effective in reducing temperature gradient (dT_x) of SOFC stack. The stack temperature is quite sensitive to the air flowrates. This conclusion was also obtained from the study in Chapter 3 and many other studies. The larger air flowrates will improves the cooling in the stack and induce the reduction of the operating temperature as well as the temperature gradient [27], [28] and [29]. Accordingly, the electrical efficiency is reduced as current density is decreased caused by operating temperature reduction. Around 23% of electrical efficiency is reduced when air flowrates increase from 0.5 M ~ 1.8 M. It is should be noticed that, the total efficiency and thermal efficiency are reduced more severely, approximately 26% and 39%, respectively. This is attributed to the increase of irreversibility in system when air flowrates increase. As for this system, the input exergy of fuel (Ex_{in}) are transferred into output exergy in several forms including electrical power (P_{el}), heat in hot exhaust (Ex_{th}), and irreversibility (Irr) that is generated in all units of the system (Equation 4.16 [3] and [24]). Having a fixed input exergy, the reduction of thermal efficiency indicates that the raise in irreversibility is more considerable than the decrease of electrical power reduction by air flowrates increase.

$$Ex_{input} = Ex_{th} + P_{el} + Irr \qquad (4.16)$$

Two mechanisms can be detected that dominate the system performance's matrix containing those thermal behaviors that are inspected in this study. The stack level performance, such as temperature gradient and electrical efficiency are influenced by stack operating temperature that is controlled by air flowrates. However, the total efficiency associated with the thermal efficiency is affected by the irreversibility in system under the variation of the air flowrate. Therefore, it is necessary to examine the mechanism of the exergy losses during the operation of the system.

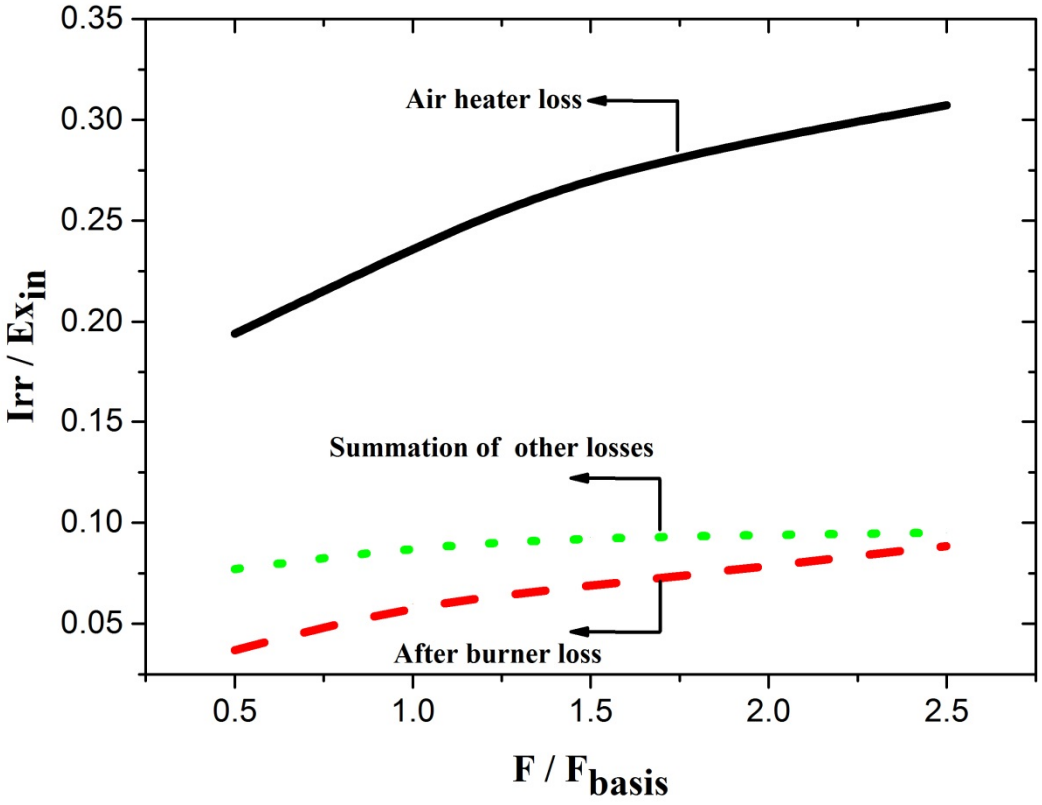

Figure 4.7: Ratio of the exergy losses to the total exergy input for different air flow rates

With a fixed fuel flowrates at inlet, the share of exergy losses in different process of the exergy input is presented in Figure 4.7. From the results, it can be observed that the air heater occupies the largest portion, which is approximately 3 times higher than the others. All the exergy losses are increased by the increase of air flowrates. However, the losses in air heater has the most rapid increasing rate, followed by the burner, while the other losses exhibit much slower increasing rate, especially when air flowrates are beyond 1.7. Based on the exergy analysis principles that described in section 4.2, the main source for the increase of exergy losses in air heater is the

increase of air flowrates. And besides, since the inlet / outlet temperature for cold stream in this process (air) is fixed, the exergy losses can also be traced to the increase in temperature differences of hot stream. As increase of air flowrates will result in decrease of current density, and therefore more unreacted hydrogen exists in the fuel exhaust. Accordingly, more fuel would enter the after burner, and higher temperature of outlet stream from burner, which is the inlet of hot stream in air heater, will be achieved. On the other hand, the temperature of outlet of hot stream in this process is even lower as more heat resources are consumed in the heater. Under all these interactive effects, the exergy losses in air heater increases rapidly due to the increase of air flowrates. The exergy loss will also be increased in the after burner because of the higher air flowrates and higher burner exhaust temperature with lower anode exhaust temperature. However, the temperature differences are much lower than the ones in the air heater. Thus, lower exergy losses are obtained and the slower increasing rate can be observed in the combustion process. As an effective strategy used for regulating SOFC stack temperature and temperature gradient, its disadvantage can be inferred from the analysis that exergy losses will be raised by the higher air flowrates. With a particular air flowrates required for the operation, reducing temperature differences in the process could be the possible solution for reducing the exergy losses and increasing system efficiency.

4.4.2.2.2 Oxygen concentration in fresh cathode gas (Scenario #2)

Increasing the oxygen concentration in cathode gas can enhance the stack electrical efficiency due to the improvement of oxygen partial pressure in cathode. In this section, this operation scenario will be examined for this system. The influences on the system behaviors are evaluated and presented in Table 4.6 and Figure 4.8.

Table 4.6: Simulation results for the system thermal behaviors at different oxygen concentration in fresh cathode gas

y_{O_2}	$dT_{x,}$ K/mm	η_{total}^{ex}, %	η_{el}^{ex}, %	η_{th}^{ex}, %	μ_{Irr}^{Ex}, %
0.21 (Basis Case)	1.20	57.5	51.3	6.2	38.4
0.25	1.21	58.3	52.4	5.9	37.7
0.4	1.25	60.3	54.8	5.5	36.2

Consistent results are achieved with the last chapter with increasing oxygen concentration in cathode, both electrical efficiency and temperature gradient increased, while more considerable enhancement is obtained for the electrical efficiency compared with the gain in temperature gradient. It is to be noticed for this scenario that, the increase in the total efficiency is not as considerable as in the electrical efficiency. The main reason can be attributed to the loss of thermal efficiency, which can be observed in Table 4.6. As with the enhancement of electrical performance, less unreacted fuel would remain in the anode exhausts. This will lead to the lower temperature of burner outlet stream, and subsequently result in lower hot exhaust temperature. However, slight increase of total efficiency is achieved such that irreversibility drops with the enriched air, and the behaviors of these exergy losses under this scenario are as presented in Figure 4.8. The results show that the slight drop in irreversibility in the system is mainly attributed to the decrease of exergy loss in the burner. Since the air flowrates and the temperature increase for the feeding air is the same in this case, the amount of heat transfer is the same for each condition. The influence of oxygen concentration in cathode on the exergy in pre-heater is minor. For the burner, since less amount of fuel is combusted with increasing of oxygen concentration, less exergy loss will result during this process. The effects of improving system performance can be observed, particularly in improving electrical efficiency by this scenario. However, as discussed in the last chapter, it will also cause problems in the economic aspects of the operation.

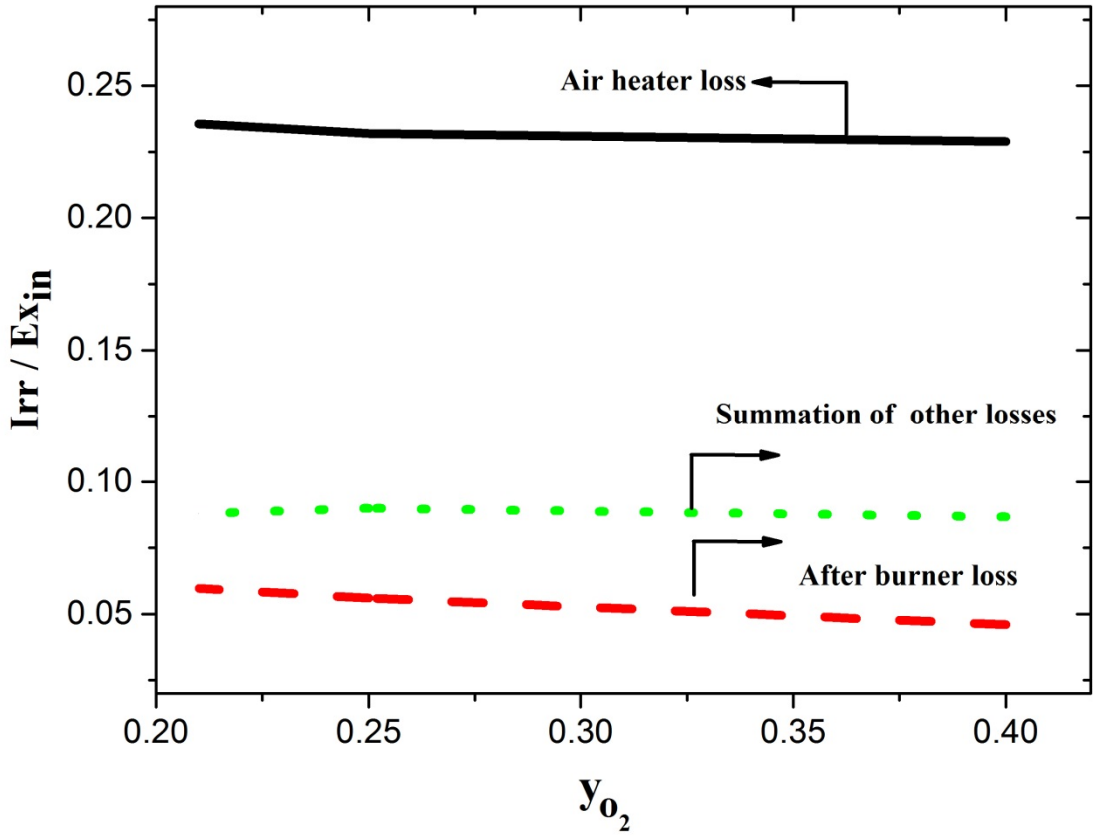

Figure 4.8: Ratio of the exergy losses to the total exergy input for different oxygen concentration in cathode

4.4.2.2.3 Anode recycling ratio (Scenario #3)

Another processing parameter examined is anode recycling ratio (R_A). Since it could affect the system performance in different ways, such as the fraction of reactants in streams, the enthalpy change associated with recycling gases and the feed gas to pre-reformer. All these could affect the electrochemical reaction and thermal exchange inside the cell, which may influence the temperature distribution accordingly. The calculated results are presented in Table 4.7. Unlike the analysis work by Nikooyeh et al. [30], where the temperature gradient of stack is examined with internal reforming, which has large impact on temperature due to endothermic reaction. In this case, the influence on temperature gradient from this parameter is not much in the large range of R_A (from 0.1 ~0.7). The electrical efficiency is increased along with the increase of R_A, since more fuel will be fed into the stack with higher R_A, and it would accordingly enhance the reaction inside the cell. The thermal efficiency

is reduced slightly with the increase of R_A, while the irreversibility is also reduced, and subsequently, the total efficiency will rise. As shown in Figure 4.9, the detailed exergy behaviors influenced by this parameter is illustrated. Similar to scenario 2, the influence on the air preheater is small. However, an exergy loss decline in the burner can be observed, because with the increase of R_A, less flowrates of fuel will be fed into burner. And besides, higher R_A will lead to higher electrical efficiency, which indicates higher anode exhaust temperature but lower temperature for the burner exhaust as less fuel can be combusted remained in the anode exhaust. Under these two effects of lower temperature differences and lower flowrates, the drop of exergy loss in burner performances is obvious. However, the other losses are increased with the rise in R_A. This can be mainly attributed to the increase of flowrates in the recycling stream, as the exergy loss will be increased in the anode mixer and pre-reformer as well. The results show that the influence of this parameter on thermal behaviors is small. However, some studies show that increase of R_A is helpful for the uniformity of hydrogen concentration distribution. [26]

Table 4. 7: Simulation results for the system thermal behaviors at anode recycling ratio

R_A	dT_x, K/mm	η_{total}^{ex}, %	η_{el}^{ex}, %	η_{th}^{ex}, %	μ_{Irr}^{Ex}, %
0.1	1.14	54.7	47.9	6.8	40.5
0.3	1.16	56.0	49.6	6.4	39.7
0.5 (Basis Case)	1.20	57.5	51.3	6.2	38.4
0.7	1.24	58.7	52.8	6.0	37.2

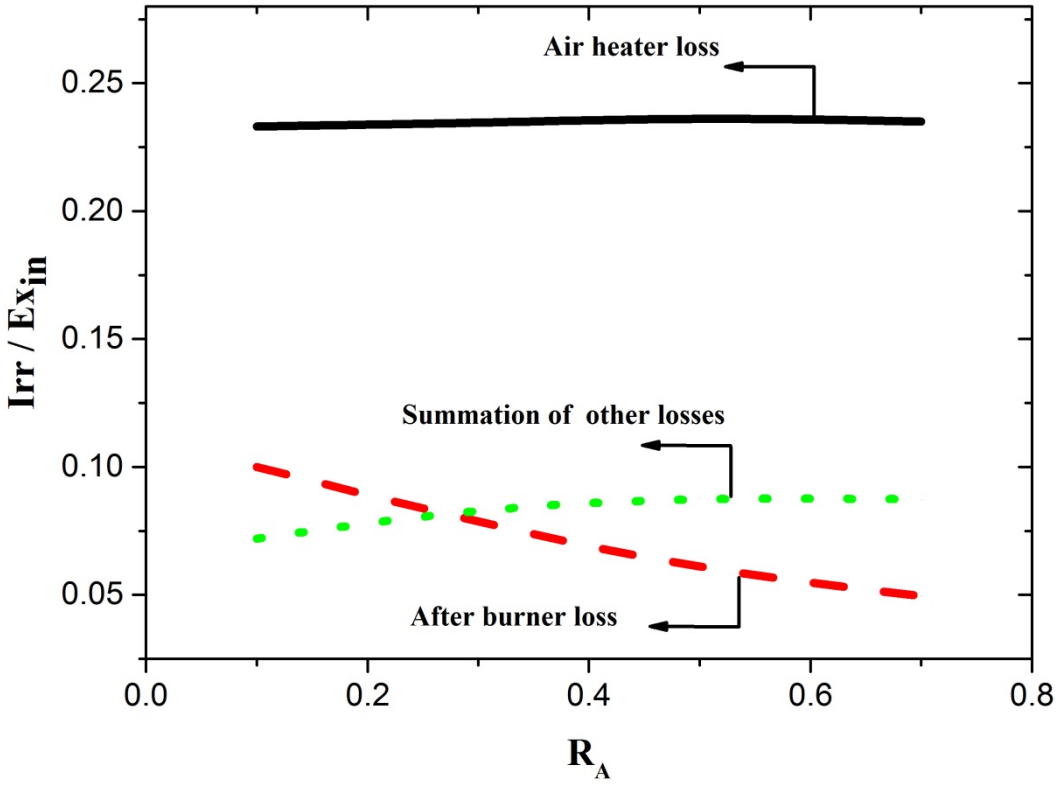

Figure 4. 9: Ratio of the exergy losses to the total exergy input for different anode recycling ratio

4.4.2.2.4 Cathode recycling (Scenario #4)

In order to evaluate this scenario, flowsheet amendment was carried out as shown in Figure 4.10, in which, a cathode exhaust recycle loop is added to the plant. In this case study, the air temperature and flowrate at the stack inlet are kept the constant, where the cathode recycle ratio is set equal to 0.2.

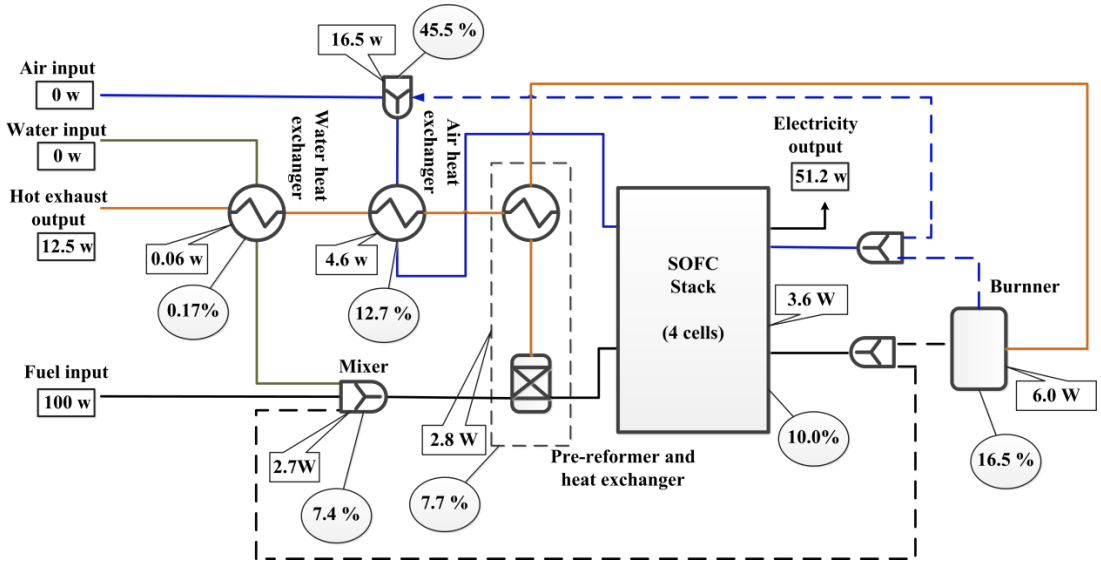

Figure 4.10: SOFC system flowsheet modification for simulation of cathode recycle stream. The rectangular boxes with arrows show the exergy loss in each process, the oval boxes with arrows show the ratio of exergy loss and the input exergy into the system, the rectangular boxes without arrows show the system input and output.

The results are as illustrated in Figure 4.10 and Table 4.8. Since the stack operating conditions, the inlet temperature and flowrates for the air and fuel, remain almost the same, very close stack performance is achieved. Consequently, the same temperature gradient with minor drop in electrical efficiency can be observed. The main reason for the electrical efficiency reduction can be attributed to the application of dilute air with smaller oxygen concentration. It is should be noticed that, a gain in total efficiency is resulted due to the obvious reduction in irreversibility. As it can be seen in Figure 4.10, the main exergy loss reduction occurs during the air heating process. Compared to the basis case without cathode recycling, exergy loss is reduced by 2.4W. Through recycling the cathode outlet, air pre-heating process will be completed firstly by mixing fresh and recycled air and subsequently through a heat exchanger. The heat exchanger outlet will be corresponding to the process requirement for the inlet air temperature. Compared with process in heat exchanger, the process of mixing will destroy less exergy. While for the heat exchanger, hotter air is introduced so that less heat exchange is required. Thus the irreversibility is reduced and more exergy can be achieved for the thermal recovery.

Table 4.8: Simulation results for the system thermal behaviors with cathode recycling

R_C	$dT_{x,}$ K/mm	η_{total}^{ex}, %	η_{el}^{ex}, %	η_{th}^{ex}, %	μ_{Irr}^{Ex}, %
0 (Basis Case)	1.20	57.5	51.3	6.2	38.4
0.2	1.20	58.9	51.2	7.7	36.3

4.5 Conclusions:

The thermal analysis of the SOFC plant is conducted in this chapter for the purpose of thermal management for system level. The system level performance was firstly assessed by a simple model through exergy analysis. As the thermal management of SOFC can be a complicated issue since requirements for all levels should be satisfied simultaneously, a more detailed multi-scale SOFC system model is utilized, so that the thermal behaviors of SOFC in different levels can be examined in parallel. The comparison of energy and exergy evaluation in system show that, the exergy analysis is more realistic for the practical system design, as it is evaluated based on the available work. Furthermore, four different system operating scenarios are examined for SOFC thermal behaviors in multi-scales. Each scenario demonstrates different features of advantages and disadvantages associated with various aspects of thermal characteristics. The air flowrates are the most efficient way for regulating the temperature gradient of SOFC. However, the disadvantages in the aspect of system performance brought by the increasing air flowrates are quite obvious, since considerable exergy loss will be induced by the increase of air flowrates, which significantly lower the total efficiency of system. Enriching the air with higher oxygen concentration is effective in increasing electrical efficiency, while less effect is found in total efficiency improvement. However, an increase of temperature gradient will also be experienced by this scenario. With the current flowsheet of plant, anode recycling ratio has limited effects on the thermal behaviors of SOFC, since the temperature gradient, electrical efficiency and total efficiency increased slightly with the increasing of anode recycling ratio. The last scenario, inserting the system with a cathode recycling loop, indicates obvious effects on reducing exergy loss in the process of air heating, which lead to the higher total efficiency of the whole system without sacrificing the thermal performance in stack level.

Nomenclature

C_p	Specific heat (J $mol^{-1}K^{-1}$)
dT_x	Temperature gradient in flowing direction (K mm^{-1})
E_{Nernst}	Nernst voltage (V)
E^0	Equilibrium potential (V)
E	Energy (W)
Ex	Exergy (W)
E_{act}	Activation energy (J mol^{-1})
Ex^0	Standard exergy (W)
F	Faraday's constant (96485 C mol^{-1})
h	Enthalpy (J mol^{-1})
I	Current (A)
i	Current density (A m^{-2})
i_0	Exchange current density (A m^{-2})
Irr	Irreversibility (W)
i	Current density (A m^{-2})
K_0	Pre-exponential factor (A m^{-2})
LHV	Lower heating value (J mol^{-1})
M	Molar flowrates of air for basis case (mol s^{-1})
$\dot{m}$	Molar flowrates (mol s^{-1})
n_e	Number of electrons
P_{el}	Electrical power (W)
P_{consum}	Consumption power (W)
R	Ideal gas constant (J mol^{-1} k^{-1})
R_A	Anode recycling ratio
R_C	Cathode recycling ratio
R^{ohmic}	Ohmic resistance (Ω)
s	Entropy (W)
T	Temperature (K)

ΔT	Temperature differences (K)
V	Voltage (V)
y	Species mole fraction

Greek Letters

α	Charge transfer coefficient
γ	Reaction orders
$\boldsymbol{\eta}$	Efficiency
ε	Heat recovery ratio
μ	Exergy portion of the input

sub-/ superscripts

A	Anode
act	Activation
C	Cathode
chem	Chemical
el	Electrical
en	Energy
ex	Exergy
th	Thermal
i	Specie in stream
n	Stream number
ph	Physical
0	Ambient

References:

[1] A. Faghri, Z. Guo, Challenges and opportunities of thermal management issues related to fuel cell technology and modeling, International Journal of Heat and Mass Transfer 48 (2005) 3891-3920.

[2] N. Hotz, S.M. Senn, D. Poulikakos, Exergy analysis of a solid oxide fuel cell micropowerplant, Journal of Power Sources 158 (2006) 333-347.

[3] S.H. Chan, C.F. Low, O.L. Ding, Energy and exergy analysis of simple solid-oxide fuel-cell power systems, Journal of Power Sources 103 (2002) 188-200.

[4] M. Granovskii, I. Dincer, M. A. Rosen., Exergy and industrial ecology: an application to an integrated energy system. International Journal Exergy (2008) 5: 52–63

[5] I. Dincer, M.A. Rosen, C. Zamfirescu, Exergetic Performance Analysis of a Gas Turbine Cycle Integrated With Solid Oxide Fuel Cells, Journal of Energy Resources Technology 131 (2009) 032001-032001.

[6] F. Calise, A. Palombo, L. Vanoli, Design and partial load exergy analysis of hybrid SOFC–GT power plant, Journal of Power Sources 158 (2006) 225-244.

[7] A.V. Akkaya, B. Sahin, H. Huseyin Erdem, Exergetic performance coefficient analysis of a simple fuel cell system, International Journal Of Hydrogen Energy 32 (2007) 4600-4609.

[8] S. Wongchanapai, H. Iwai, M. Saito, H. Yoshida, Selection of suitable operating conditions for planar anode-supported direct-internal-reforming solid-oxide fuel cell, Journal of Power Sources 204 (2012) 14-24.

[9] N. Hotz, S.M. Senn, D. Poulikakos, Exergy analysis of a solid oxide fuel cell micropowerplant, Journal of Power Sources 158 (2006) 333-347.

[10] R.J. Braun, S.A. Klein, D.T. Reindl, Evaluation of system configurations for solid oxide fuel cell-based micro-combined heat and power generators in residential applications, Journal of Power Sources 158 (2006) 1290-1305

[11] I. Dincer, M.A. Rosen, C. Zamfirescu, Exergetic Performance Analysis of a Gas Turbine Cycle Integrated With Solid Oxide Fuel Cells, Journal of Energy Resources Technology 131 (2009) 032001-032001.

[12] Y. Wu, W. Yang, W. Blasiak, Energy and Exergy Analysis of High Temperature Agent Gasification of Biomass, Energies 7 (2014) 2107.

[13] A. Stamatis, C. Vinni, D. Bakalis, F. Tzorbatzoglou, P. Tsiakaras, Exergy Analysis of an Intermediate Temperature Solid Oxide Fuel Cell-Gas Turbine Hybrid System Fed with Ethanol, Energies 5 (2012) 4268.

[14] C. Bang-Møller, M. Rokni, B. Elmegaard, Exergy analysis and optimization of a biomass gasification, solid oxide fuel cell and micro gas turbine hybrid system, Energy 36 (2011) 4740-4752

[15] F. Calise, G. Ferruzzi, L. Vanoli, Parametric exergy analysis of a tubular Solid Oxide Fuel Cell (SOFC) stack through finite-volume model, Applied Energy 86 (2009) 2401-2410

[16] Liqiang Duan, Xiaoyuan Zhang and Yongping Yang (2011). Exergy Analysis of a Novel SOFC Hybrid System with Zero-CO2 Emission, Advances in Gas Turbine Technology, Dr. Ernesto Benini (Ed.), InTech, DOI: 10.5772/21342

[17] S. Motahar, A.A. Alemrajabi, Exergy based performance analysis of a solid oxide fuel cell and steam injected gas turbine hybrid power system, International Journal of Hydrogen Energy 34 (2009) 2396-2407

[18] H.A. Reyhani, M. Meratizaman, A. Ebrahimi, O. Pourali, M. Amidpour, Thermodynamic and economic optimization of SOFC-GT and its cogeneration opportunities using generated syngas from heavy fuel oil gasification, Energy

107 (2016) 141-164

[19] L. Fryda, K.D. Panopoulos, J. Karl, E. Kakaras, Exergetic analysis of solid oxide fuel cell and biomass gasification integration with heat pipes, Energy 33 (2008) 292-299

[20] A. Odukoya, I. Dincer, G.F. Naterer, Exergy Analysis of a Gasification-Based Combined Cycle with Solid Oxide Fuel Cells for Cogeneration, International Journal of Green Energy 8 (2011) 834-856

[21] A. Amiri, P. Vijay, M.O. Tadé, K. Ahmed, G.D. Ingram, V. Pareek, R. Utikar, Solid oxide fuel cell reactor analysis and optimisation through a novel multi-scale modelling strategy, Computers & Chemical Engineering 78 (2015) 10-23.

[22] A. Amiri, P. Vijay, M.O. Tadé, K. Ahmed, G.D. Ingram, V. Pareek, R. Utikar, Planar SOFC system modelling and simulation including a 3D stack module, International Journal of Hydrogen Energy 41 (2016) 2919-2930.

[23] K.W. Bedringås, I.S. Ertesvåg, S. Byggstøyl, B.F. Magnussen, Exergy analysis of solid-oxide fuel-cell (SOFC) systems, Energy 22 (1997) 403-412.

[24] M.H. Nehrir, C. Wang, Modeling and control of fuel cells: Distributed generation applications, Wiley-IEEE Press 2009.

[25] E.J. Naimaster Iv, A.K. Sleiti, Potential of SOFC CHP systems for energy-efficient commercial buildings, Energy and Buildings 61 (2013) 153-160.

[26] W. Zhang, E. Croiset, P.L. Douglas, M.W. Fowler, E. Entchev, Simulation of a tubular solid oxide fuel cell stack using AspenPlusTM unit operation models, Energy Conversion and Management 46 (2005) 181-196.

[27] Y. Yang, G. Wang, H. Zhang, W. Xia, Computational analysis of thermo-fluid and electrochemical characteristics of MOLB-type SOFC stacks, Journal of Power Sources 173 (2007) 233-239.

[28]V.M. Janardhanan, V. Heuveline, O. Deutschmann, Performance analysis of a SOFC under direct internal reforming conditions, Journal of Power Sources 172 (2007) 296-307.

[29] A. Amiri, S. Tang, P. Vijay, M.O. Tadé, Planar Solid Oxide Fuel Cell Modeling and Optimization Targeting the Stack's Temperature Gradient Minimization, Industrial & Engineering Chemistry Research 55 (2016) 7446-7455.

[30]K. Nikooyeh, A.A. Jeje, J.M. Hill, 3D modeling of anode-supported planar SOFC with internal reforming of methane, Journal of Power Sources 171 (2007) 601-609

Chapter 5

Conclusions and Recommendations

The main purpose of this study is to improve the thermal management for the SOFC. A multi-layer planar SOFC model has been developed and validated against the experimental rig, based on which, a stack model was built up. Due to the limitation of a simple system model, a comprehensive multi-scale system model was introduced that is capable of predicting the cell/stack and system level performances in parallel. The studies of thermal behaviors, which involve optimization studies, were carried out based on the above computational models according to different research targets. The main conclusions drawn from the present study are listed as below.

5.1 Conclusions

A multi-layer model for a SOFC was established according to the realistic experimental rig scales, with model parameter adjustments carried out based on the practical data. The validation results and model improvement analysis indicate the improved perdition of the current model compared to the previous work. More accurate temperature prediction can be achieved since the thermal environment of the cell has significant effects on the cell's performance, especially in the higher current range. The model presents the capability for simulating the distributed thermal performances inside the cell structure. The distribution of different types of heat transfer in the cell are presented and compared between different models and thermal conditions, which give better insight of the cooling mechanism occurring inside the cell. For the model without the interconnects in adiabatic condition, a 'simple model' is presented in the study. In this, the effects of conduction are ignored, which can play important role in heat transport in the structure. The convection heat transfer is more dominant than the conduction heat transfer in adiabatic condition as shown by the 'improved model'. The significant role of conduction is more obvious in the non-adiabatic condition indicated by the 'comprehensive model' presented, and it outweighs the convection's role around the outlet range of cell. All these variations of heat exchange mechanisms inside the cell affect the cell's temperature and temperature profile, which can be found from the cell spatial temperature distribution analysis in different thermal conditions that are provided by this study. Additionally, the PEN temperature estimation under the test

rig parameter adjustment is also provided through the operational map of the cell. An insight of the thermal behaviors of SOFC cell is provided in this study. However, the cell performance cannot be instead of the stack level behavior of SOFC, therefore, the thermal management study on a stack SOFC is focused on the next chapter, and the solutions of improved thermal management of SOFC stack is proposed.

The stack level study is carried out based on the stack model which is developed and extended from the reliable cell level model. Three operating strategies, including the utilization of excess air, inlet gas temperature differences, and the air enrichment, were examined for the temperature gradient in both flowing directing and stacking direction as well as the stack efficiency. The advantages and disadvantages were discussed for each approach. Using excess amount of air is an effective way of reducing temperature gradient of the stack. However, it also results in the sacrifice of efficiency. Operating with the inlet gas temperature differences is helpful in decreasing temperature gradient in flowing direction without reducing the stack efficiency, while the increase of temperature gradient in z direction will be accompanied. The range of temperature difference of inlet gases should be proper calculated and selected accordingly. The effect of improving stack efficiency by enriching the air is obvious, although a relatively slight increase in temperature gradient will be achieved. However, the increase of budget cost by this strategy cannot be ignored. The economic analysis in this study provided the optimum oxygen concentration that can be applied for operation. The results show the controversial feature of temperature gradient and efficiency, indicating the necessity of multi-objective optimization, as both stack reliability and productivity are important for the SOFC operation. The multi-objective optimization is conducted combining those strategies, through which, effective solutions are provided and improved SOFC performance is achieved. So far, SOFC on cell and stack level are modeled and studied, however, the SOFC is a commercial product to be operated in the integrated plant and its thermal behaviors in a system is required to be further studied to achieve the final goal of thermal management of SOFC.

The operation of the SOFC in a system can face complicated issues and criteria for all levels, the cell, stack, and system level, should be satisfied simultaneously. Due to the limitation of common simple model, the multi-scale system model was

introduced to study the thermal behaviors of SOFC in all levels under different scenarios. The thermal performance of system level was assessed through exergy analysis since it is more realistic compared to the energy analysis for the practical system design. Different scenarios examined in this study include air flowrates, oxygen concentration in cathode, anode recycling ratio, and the different flowsheets with cathode recycling. They present different effects on thermal behaviors of the SOFC. Large irreversibility will be generated by increasing of air flowrates that is harmful for the total system efficiency, although it is helpful in reducing temperature gradient. Increasing of oxygen concentration is very effective in enhancing the stack efficiency; however slightly positive effect will be achieved for the total efficiency of the system as it reduces the thermal exhaust exergy. With the external reforming system, the anode recycling ratio influence on the thermal behaviors of SOFC is limited, that the temperature gradient and total efficiency are increased slightly with higher anode recycling ratio. Adding the cathode recycling in the system is an effective strategy in enhancing the total system efficiency without increasing the temperature gradient of the stack, since the recycle loop can effectively reduce the irreversibility generated in the air heater.

5.2 Recommendations

Thermal management studies are conducted on SOFC in the cell, stack and system levels in this study. The following recommendations are suggested for future research in related areas.

- The V-I data was used for the model training and validation in this study. The distributed profiles, such as temperature profiles can be applied for the model verification and validation to achieve more accurate and reliable computational model.

- For the current study, pure hydrogen is used for the cell and stack model. For the system simulation, external reforming is considered while pure hydrogen as fuel for the SOFC unit in the plant. The models can be further extended for

the methane or syngas fueled SOFC with internal reforming. The thermal behaviors of internal reforming SOFC can be varied significantly from the one with external reforming, due to the features of the reforming reaction. Hence, more parameter and optimization studies can be conducted for the thermal management on the syngas fueled SOFC.

- To achieve the optimum operating condition for a SOFC system, a multi-objective optimization can be conducted with objectives of optimizing thermal management on both system level and stack level.

- The current studies conducted in this thesis are all based on the steady-state operation of SOFC. Further thermal management studies regarding the SOFC dynamic performances can be carried out.

Appendix I

Permission of Reproduction from the Copyright Owner

ELSEVIER LICENSE
TERMS AND CONDITIONS

Jul 28, 2016

This Agreement between Shi Tang ("You") and Elsevier ("Elsevier") consists of your license details and the terms and conditions provided by Elsevier and Copyright Clearance Center.

License Number	3917691046876
License date	Jul 28, 2016
Licensed Content Publisher	Elsevier
Licensed Content Publication	Chemical Engineering Journal
Licensed Content Title	Development and validation of a computationally efficient pseudo 3D model for planar SOFC integrated with a heating furnace
Licensed Content Author	Shi Tang,Amirpiran Amiri,Periasamy Vijay,Moses O. Tadé
Licensed Content Date	15 April 2016
Licensed Content Volume Number	290
Licensed Content Issue Number	n/a
Licensed Content Pages	11
Start Page	252
End Page	262
Type of Use	reuse in a thesis/dissertation
Portion	full article
Format	both print and electronic
Are you the author of this Elsevier article?	Yes
Will you be translating?	No
Order reference number	
Title of your thesis/dissertation	Multi-scale Modelling and Optimization Study on the Thermal Management of SOFC
Expected completion date	Aug 2016
Estimated size (number of pages)	160
Elsevier VAT number	GB 494 6272 12
Requestor Location	Shi Tang 15 Burren Gate Willetton Perth, 6155 Australia Attn: Shi Tang
Total	0.00 USD
Terms and Conditions	

INTRODUCTION

RightsLink®

Home | Create Account | Help | Live Chat

Title: Planar Solid Oxide Fuel Cell Modeling and Optimization Targeting the Stack's Temperature Gradient Minimization

Author: Amirpiran Amiri, Shi Tang, Periasamy Vijay, et al

Publication: Industrial & Engineering Chemistry Research

Publisher: American Chemical Society

Date: Jul 1, 2016

LOGIN

If you're a copyright.com user, you can login to RightsLink using your copyright.com credentials. Already **a RightsLink user** or want to learn more?

PERMISSION/LICENSE IS GRANTED FOR YOUR ORDER AT NO CHARGE

This type of permission/license, instead of the standard Terms & Conditions, is sent to you because no fee is being charged for your order. Please note the following:

- Permission is granted for your request in both print and electronic formats, and translations.
- If figures and/or tables were requested, they may be adapted or used in part.
- Please print this page for your records and send a copy of it to your publisher/graduate school.
- Appropriate credit for the requested material should be given as follows: "Reprinted (adapted) with permission from (COMPLETE REFERENCE CITATION). Copyright (YEAR) American Chemical Society." Insert appropriate information in place of the capitalized words.
- One-time permission is granted only for the use specified in your request. No additional uses are granted (such as derivative works or other editions). For any other uses, please submit a new request.

BACK | CLOSE WINDOW